RM E57E16

NACA RM E57E16

NACA

RESEARCH MEMORANDUM

EXPLORATORY INVESTIGATION OF AERODYNAMIC EFFECTS OF EXTERNAL COMBUSTION OF ALUMINUM BOROHYDRIDE IN AIRSTREAM ADJACENT TO FLAT PLATE IN MACH 2.46 TUNNEL

By Robert G. Dorsch, John S. Serafini,
and Edward A. Fletcher

Lewis Flight Propulsion Laboratory
Cleveland, Ohio

NATIONAL ADVISORY COMMITTEE
FOR AERONAUTICS

WASHINGTON

July 29, 1957

NATIONAL ADVISORY COMMITTEE FOR AERONAUTICS

RESEARCH MEMORANDUM

EXPLORATORY INVESTIGATION OF AERODYNAMIC EFFECTS OF EXTERNAL COMBUSTION OF ALUMINUM BOROHYDRIDE IN AIRSTREAM ADJACENT TO FLAT PLATE IN MACH 2.46 TUNNEL

By Robert G. Dorsch, John S. Serafini,

and Edward A. Fletcher

SUMMARY

Pressure distributions associated with stable combustion of aluminum borohydride in the supersonic stream adjacent to a short, 13-inch chord, and an extended, 25-inch chord, flat-plate model were determined experimentally. The models were mounted in the center of the test section of a 1- by 1-foot Mach 2.46 wind tunnel. High-speed direct and schlieren motion pictures of the flame and associated shock waves were taken, and selected photographs are presented.

Static-pressure increases measured during combustion at selected chordwise, spanwise, and base static taps are presented. The increase in static pressure averaged about 60 percent of the nonburning value. The resultant lift force on the flat-plate surface during combustion was of the order of 100 pounds per square foot at a pressure altitude of about 52,000 feet.

In addition to the static-pressure changes, total temperatures and pressures were measured at three chordwise stations within the flame adjacent to the extended flat plate. The approximate local Mach numbers at points in the flame were computed from the measured data.

Because the combustion took place in a small tunnel, the measurements were subject to quantitatively unknown tunnel effects, which can best be determined by performing a similar large-tunnel or free-flight test for comparison.

INTRODUCTION

Theoretical studies of aerodynamic effects associated with heat addition to supersonic flow are reported by a number of authors

(refs. 1 to 3). In addition, several authors have made analytical predictions of practical benefits to be achieved by heat addition to the supersonic stream adjacent to an aerodynamic body (refs. 4 and 5). For example, reference 4 shows that the lift of a wing in supersonic flight should be significantly increased by the direct addition of heat to the stream beneath the wing. It also indicates reduction in drag will occur when the heat addition takes place adjacent to the rearward-facing surfaces.

Experimental research has been hampered by the difficulty of finding a practical method of adding heat directly to a supersonic stream. Combustion of fuel in the stream has been considered for some time as a possible method of adding heat. In the past, it had not been possible to stabilize a flame in such a stream. Recent research has shown that combustion can be stabilized in regions having high stream velocities.

In reference 6, for example, it is shown that aluminum borohydride could be burned stably in the stream below the top wall of a supersonic wind tunnel without employing any flameholders other than the wall and its associated boundary layer. The tests of reference 6 were conducted at Mach numbers of 1.5, 2, and 3. In addition, it is shown in reference 7 that the static-pressure rise along the top wall of the supersonic tunnel caused by the combustion in the stream below was of the order of 20 to 40 percent of the stream static pressure prior to combustion.

The preliminary work reported in references 6 and 7 showed the feasibility of establishing external combustion below a flat-plate model located in the test section of a supersonic tunnel. An exploratory investigation was therefore undertaken to determine the aerodynamic effects of adding heat to the supersonic stream adjacent to a flat-plate model by external combustion. The goal of the investigation was to obtain a set of aerodynamic measurements during heat addition by utilizing the basic combustion methods already developed in the preliminary investigation. No attempt was made to find the most efficient method of combustion in a high-velocity stream or the best fuel for the purpose. The choice of aluminum borohydride as a fuel was, therefore, dictated.

This report outlines the techniques used to obtain combustion of aluminum borohydride in the airstream below a flat plate in a 1- by 1-foot Mach 2.46 wind tunnel and the methods employed to measure the resulting changes in aerodynamic parameters. Static-pressure changes measured at the model surface and total-temperature and -pressure changes measured in the stream during a total of 50 combustion runs are presented, and their implications are discussed. Because this investigation was in an area in which much theoretical and experimental work still remains to be done, it was difficult to interpret much of the measured data. Therefore, the data are presented in this report in such a way as to allow the reader to made a separate theoretical interpretation of the measurements where differences in interpretation are possible.

APPARATUS AND PROCEDURE

Wind Tunnel and Model

The experiments were conducted in the 1- by 1-foot wind tunnel at the NACA Lewis laboratory. The tunnel is a nonreturn type and has a test-section Mach number of 2.46.

The flat plate was mounted at zero angle of attack in a vertical plane, as illustrated in figure 1, with the reference surface adjacent to which combustion took place 0.31 inch from the centerline of the tunnel.

The flat plate was made in two sections, which were constructed so that they could be used in one of two ways: (1) The upstream section could be used independently as a short flat-plate model; (2) the two sections could be fastened together to form an extended flat-plate model.

A photograph of the extended flat-plate model is shown in figure 2. The reference surface adjacent to which combustion took place is shown in figure 2(a). The back (nonburning) side of the model with its removable cover plates which permitted access to the internal plumbing and instrumentation is shown in figure 2(b).

The pertinent dimensions of the models are as follows:

Short-flat-plate length, in.	13
Extended-flat-plate length, in.	25
Width, in.	$11\frac{15}{16}$
Thickness, in.	5/8
Leading-edge half-wedge angle, deg	12
Blunt trailing-edge thickness, in.	5/8
Distance from leading edge to fuel orifices, in.	$3\frac{1}{2}$

The locations of the static-pressure taps, the fuel orifices, and the surface thermocouples are shown in figure 3. Rather large static orifice diameters (0.0400 to 0.0465 in.) were used in order to reduce plugging by the ash deposits resulting from the combustion.

The Mach number of the stream between the reference surface of the flat-plate models and the tunnel wall was 2.46 with a maximum spacewise variation of ±0.05. The average Mach number of the stream adjacent to the model reference surface was 2.45 for the short flat plate and 2.46 for the extended flat plate. Nonburning aerodynamic measurements were taken to define the flow field existing adjacent to the flat-plate model

as installed and to ensure that all runs were made under essentially similar conditions. The average Reynolds number per foot during the nonburning flow measurements was 4.6×10^6. Nominal total pressure, total temperature, and dew point were 48 inches of mercury, 560° R, and -50° F, respectively. The nonburning aerodynamic data are summarized in table I in terms of the ratio of local static to free-stream total pressure p/P_0 at each surface tap.

Prior to and following each combustion run, the static pressure was measured at the tunnel nozzle and test-section walls and at those model taps which were not connected to the pressure-change measuring instruments. These measurements provided a check on the nonburning flow conditions. The tunnel-inlet conditions were held as nearly constant as possible during the combustion period.

Fuel

The fuel used in this investigation, aluminum borohydride, is a volatile colorless liquid at the temperature at which it was injected. Because it ignites spontaneously in air, the fuel was transferred either by vacuum distillation or directly as a liquid in an inert atmosphere of dry helium.

The pertinent physical properties of aluminum borohydride $Al(BH_4)_3$ obtained from references 8, 9, and 10 are:

Melting point, °C	-64.5
Normal boiling point, °C	44.5
Vapor pressure at 20° C, mm Hg	295
Density at 20° C, g/cc	0.554
Viscosity at 20° C, centipoise	0.216
Heat of combustion, j/cc (24,800 Btu/lb)	32,000

The temperature dependence of vapor pressure and density is as follows:

$$\log p = 7.808 - \frac{1565}{T}$$

where the vapor pressure p is in millimeters of mercury and the temperature T is in °K, and

$$\rho = 0.7866 - 0.000793\ T$$

where the density ρ is in grams per cubic centimeter and T is in °K.

Fuel Injection

The method of injecting the liquid aluminum borohydride into the supersonic stream adjacent to the flat plate was similar to that of references 6 and 7. The fuel-injection system is shown in figure 4. Figure 4(a) is a schematic sketch of the fuel system. A closeup of the valve-type fuel injector which contained the $Al(BH_4)_3$ is shown in figure 4(b). The injector was coupled to a 1/8-inch copper tube connected to a fuel manifold inside the model. From the fuel manifold, three 1/16-inch tubes of approximately equal flow resistance were connected to three fuel orifices drilled in the reference surface. The fuel orifices were 0.016-inch in diameter and were located as shown in figure 3.

The fuel-injection procedure was as follows: The injector was charged with approximately 25 cubic centimeters of $Al(BH_4)_3$ through the upper valve by distillation to the condensation arm from a conventional vacuum-transfer line. It was then mounted on the remote-controlled injection system on top of the tunnel. The injector was next pressurized with dry helium through the upper valve to about 50 pounds per square inch gage. Then, the fuel lines below the lower valve of the injector were flushed by a continuous stream of low-pressure helium (20 lb/sq in. gage) which flowed out the three fuel orifices. The helium was turned off by a solenoid-operated valve just before the lower valve of the fuel injector was opened by the drive motor. The fuel was injected through the three orifices for a 1- to 5-second period until it was all expelled from the injector. The liquid was atomized by the high-velocity airstream. Following fuel injection, the injector and the lines were flushed with helium to remove the residual fuel.

The amount of fuel, the helium injection pressure, the injection duration, and the fuel-flow rate (total through the three orifices) used for each combustion run are given in table II. The fuel-flow rate (approx. 11 cc/sec) was selected on the basis of the experience gained in the work reported in references 6 and 7. The runs were limited to less than 5 seconds in order to avoid overheating the tunnel windows and to economize on fuel. The fuel-flow rates given in table II were determined from the volume of fuel contained in the injector and the duration of fuel flow. The duration of fuel flow for each run was determined by measuring the average width, in seconds, of the pressure-change traces and adding 0.2 second to this period to allow for the period prior to ignition and for the post-flame period.

Ignition

It is shown in reference 6 that, although aluminum borohydride could ignite spontaneously when injected into the airstream of a supersonic wind tunnel, it was desirable to ensure prompt ignition by employing an ignitor. An electric-spark-type ignitor was therefore used. The ignitor

was a 1/4-inch rod which extended from the tunnel wall to within spark-gap distance (of the order of 3/16 in.) of the plate surface. The tip of the rod was so placed that it was in line with the fuel stream from the lower fuel orifice and was about 3/8 to 5/8 inch upstream of the blunt trailing edge of the model. The ignitor was connected to a 1-joule, repeating, capacitance-type power supply which provided a spark from the rod to the model surface five times a second.

Three differently shaped ignitor rods were employed along with different tunnel-entrance port locations. The ignitor shape and tunnel-entrance port locations were varied as necessary in order to accommodate the long and short models and the various stream probes employed.

Figure 5 shows the three configurations employed and identifies them with the number referred to in tables I and III and other sections of this report.

Photography

The tunnel was equipped with a schlieren system for flow visualization and photography. The model was mounted across the schlieren windows, as shown in figure 1, so that most of the short-flat-plate model and the adjacent supersonic stream could be photographed. A photograph of the short-flat-plate model attached to the upper schlieren window retaining ring is shown in figure 6. When the extended-flat-plate model was used, only the upstream half of the model was visible as the extension plate was joined to the short plate just downstream of the window retaining ring.

During many of the combustion runs, two high-speed (1000 to 4000 frames/sec) motion-picture cameras were employed simultaneously. One camera took direct motion pictures of the flame in the stream, and the other was used with the schlieren optical system to obtain schlieren motion pictures. Timing markers at the edge of the films allowed the events on both films to be correlated. The direct motion-picture camera was focused on the image of the model in the top 45° flat mirror of the schlieren system with the aid of a long-focal-length lens. Because the flame was bright, it was possible to take either black and white or color motion pictures at frame speeds between 1000 and 4000 frames per second.

During some runs, an 8- by 10-inch still camera on the schlieren system was employed instead of the high-speed motion-picture camera to get a combination open-shutter photograph of the flame and a flash photograph of the shock waves accompanying the combustion on the same film. This was done by opening the 8- by 10-inch camera shutter just before the run and then flashing the mercury-bulb-type light source for the schlieren system when the flame was well established. The shutter was closed at the completion of the flash.

Method of Measuring Model Static-Pressure Changes Resulting from Combustion

Static-pressure changes at the model surface and in the base region were made during each combustion run. The change in pressure resulting from combustion was measured at selected locations by either a Statham strain-gage-type differential pressure transducer or by an NACA standard base six-capsule differential pressure manometer.

Ten channels of amplification and recording were available for the strain-gage pressure transducers. These along with two six-capsule manometers provided a total of 22 channels for measuring static-pressure changes.

A fixed reference pressure for the 22 differential pressure transducers was provided by a vacuum pump continuously removing air from a reference tank provided with an adjustable air bleed to the atmosphere.

The strain-gage pressure transducers had a range of either ±4 inches of mercury or ±10 inches of mercury differential pressure. The six-capsule manometers had a range of -0.5 to 3 inches of mercury differential pressure. In order to avoid exceeding the range of the pressure transducers, they were isolated from the model orifices and both sides of the sensing elements were kept at reference pressure while test conditions were being established or terminated.

As shown in reference 7, the pressure change at any point due to combustion of $Al(BH_4)_3$ in a supersonic tunnel was essentially rectangular in form with respect to time for constant fuel flow over the combustion interval. On the basis of that experience and a contemplated 1- to 5-second combustion period, the time response characteristics of the components of the pressure-change measuring systems (orifices, tubing, pressure transducers, chart recorders, etc.) were selected and matched to provide an over-all response of 98 percent of the steady-state value in 1 second or less. Since the typical run was of the order of 2 seconds, approximately half the pressure-change trace was at the steady-state level.

Sample pressure-change traces for the strain-gage instrument and for the six-capsule instrument are shown in figure 7. These traces show the typical exponential rise during the first half of the trace. The traces then flatten out to an approximate plateau, which is the steady-state value. On most traces, just at the end of the combustion period, there is a small bump of increased pressure change followed by an exponential decay in pressure to approximately the original level.

The calibrations of both types of instruments were periodically checked in place against a butyl phthalate manometer. In addition to the static calibration check, the use of two different types of pressure

transducers allowed a consistency check on the response of each type of instrument to the pressure changes caused by combustion. The intermixed pressure-change values measured along the plate usually fell on a reasonably smooth curve when plotted.

Because of the formation of ash on the surface of the model during combustion (see fig. 6, e.g.), there was a tendency for the static orifices to plug or partially plug. Complete plugging could easily be detected by an obvious flattening of the pulse and failure to return to the original level at the end of the combustion period. In the case of partial plugging of the static orifices, it was not always possible to say with certainty whether or not the time constants of the measuring system were changed enough to affect the indicated pressure change. For this reason, some of the measured pressure-change values included in the data may be conservative.

Method of Measuring Stream Temperature and Pressure Changes Resulting from Combustion

In addition to measurements of static-pressure changes along the plate, a series of measurements in the stream itself was made. Changes in local total pressure, total temperature, and stream static pressure were measured during combustion at several stations. These measurements were made along the lines perpendicular to the surface of the flat plate at three chordwise stations located along the centerline of the model surface. As shown in figure 8, these stations were 5.25, 15.5, and 20.0 inches from the fuel orifice. Because of the effect of a probe on the stream flow and on combustion, particularly downstream of the probe, a single station was surveyed during each run. Static-pressure changes along the plate upstream of the probe station were also measured during each run. These were made so that the relative intensity of the combustion runs could be compared and any effect of the probes on the upstream static profiles could be determined.

In addition to the measurements in the heated stream adjacent to the flat plate, some total-pressure and -temperature measurements were made in the wake region. The measurements were made 7 inches downstream of the base of the extended-flat-plate model in a plane perpendicular to the surface of the plate at its centerline, as shown in figure 8.

Total pressure. - The total-pressure probe was a seven-tube rake. The rake tubes were spaced 1/2 inch apart with the first tube usually located 1/4 inch from the flat-plate surface. The tubes were made of Inconel and had an outside diameter of 0.090 inch and a thickness of 0.020 inch. They extended 3/4 inch upstream of the centerline of the rake stem. A schlieren photograph (fig. 9) of the rake at the upstream station shows the shock waves associated with it.

The change in total tube pressures were measured with ±10-pound-per-square-inch or ±20-pound-per-square-inch Statham strain-gage-type pressure transducers. An independent reference pressure system was employed.

A typical set of indicated pressure-change pulses measured with the total-pressure rake is shown in figure 10. They are similar in shape to the static-pressure-change traces of figure 7.

Total temperature. - The local stream total temperature was measured with seven thermocouple rakes, which were similar in external dimensions to the total-pressure rakes. The junctions were 1/2 inch apart with the first couple usually located 1/4 inch from the flat-plate surface. The junctions were 3/4 inch upstream of the centerline of the rake stem. Two different thermocouple types were employed. For one series of measurements, 28-gage (0.013-in. diam) chromel-alumel thermocouple wire with a transverse butt-welded junction was employed. The measurements were then repeated with rakes using 30-gage (0.010-in. diam) platinum - platinum plus 13 percent rhodium thermocouple wire with spike-type junctions. The measurements were made with the two different types of thermocouples because the higher temperatures were above the usable steady-state range for the chromel-alumel thermocouples and because there was a greater possibility of catalytic action of the platinum thermocouple on the combustion at the lower temperatures. A schlieren photograph of a thermocouple rake in the stream is shown in figure 11.

The reference junctions were at room temperature. The output of each thermocouple was amplified by a Brush d-c amplifier, which was connected to a strip-chart recorder. A sample thermocouple output trace obtained from the strip-chart recorder during a combustion run is shown in figure 12. The calibration of the amplifier and recorder was accomplished by employing a potentiometer and standard electromotive-force charts for each type of thermocouple.

Stream static pressure. - Static-pressure changes in the stream were measured with a three-prong rake. A schlieren photograph of this rake is shown in figure 13. The needle-like prongs had a cylindrical outside diameter of 0.090 inch and were alined with the nonburning flow. Four static orifices (no. 69 drill) were drilled in each prong at right angles to each other 1.17 inches downstream of the nose. The prongs were spaced so that the two closest to the flat plate were 1 inch apart and the third was 2 inches from the second. The first prong was located 0.75 inch from the plate surface when at station I and 1.00 inch from the surface at stations II and III.

The change in stream static pressure due to combustion, which was sensed by the rake, was measured by employing three of the 10 strain-gage pressure-transducer channels previously described for measuring static-pressure changes on the surface.

Surface Temperature Measurements During Combustion

The temperature of the flat-plate reference surface was measured during some of the combustion runs. This was done by mounting the bare ends of 0.010-inch-diameter chromel-alumel thermocouple wire in milled grooves in the surface so that the top of the wire formed part of the surface itself. The portions of the wires leading into the inside of the model were insulated so that the only electric contact was along the 0.010-inch deep grooves. The surface thermocouple locations are shown in figure 3.

The output of the surface thermocouples was amplified and recorded by using the d-c amplifiers and chart recorders described for the stream measurements.

RESULTS AND DISCUSSION

Description of Combustion and Associated Stream Disturbances

Fifty combustion runs were made with the flat-plate models. These runs are numbered and summarized in tables II and III. The first five runs of table II were taken with the short flat plate. The remaining 45 runs were made with the extended flat plate. The type of spark-ignitor configuration employed in each run is given in table III.

Description of flame. - The combustion of the aluminum borohydride in the airstream adjacent to the flat-plate models during these runs appeared to the naked eye as a very steady, smooth, bright-green or yellow-green flame. There was no apparent difference in the general appearance of the flame adjacent to the short flat plate and that observed adjacent to the forward half of the extended flat-plate model. Similar impressions were obtained from the 8- by 10-inch photographs taken by the combination open-shutter and schlieren flash technique. Figure 14 contains several such photographs. Figure 14(a) shows a schlieren flash photograph of the flow field just prior to combustion. Helium used to inert the fuel system is flowing from the orifices. The shock wave associated with the helium flow can be used to locate the approximate chordwise position of the fuel orifices. Figures 14(b) and (c) show typical combined open-shutter flame and schlieren flash photographs from two combustion runs (runs 31 and 32 of table II). These photographs show that in gross detail the combustion runs were similar and reproducible. Comparison of figure 14(a) with figures 14(b) and (c) shows that the flame advanced approximately 1 inch upstream of the fuel orifices.

The high-speed direct and schlieren motion pictures showed that each combustion run had three stages. The first stage (occurring within 0.1 to 0.2 sec from the start of the fuel injection) consisted of ignition

of the fuel from the lower orifice at the ignitor followed by a very rapid upstream travel of the flame to the injection region and simultaneous lateral spreading to the fuel streams from the middle and top fuel orifices. The second stage (lasting on the order of 80 to 90 percent of the injection period) consisted of stable combustion with the flame seated in the vicinity of the injection region and extending downstream into the wake. The third stage was a period of unstable combustion (lasting about 0.2 sec) which took place as the last portions of the fuel were being expelled from the orifices. Stages II and III are illustrated by figure 15. Figure 15 contains selected direct and schlieren motion-picture frames from the middle and end portions of run 18 of table II. Figure 15(a) contains direct photographs of the flame. Frames 1 to 4 are from stage II of the runs while frames 5 to 10 show the end oscillations of the flame (stage III). Figure 15(b) consists of selected frames from the schlieren motion pictures. Frames 1 and 2 were selected from the middle portion of the run (stage II) and frames 3 to 8 were selected to illustrate the end oscillations of stage III.

These photographs show that the flame adjacent to the surface consisted of three tongues of flame associated with the three fuel orifices. During the main portion of the run (stage II), the three tongues of flame merged into approximately a single slab of flame a few inches downstream of the fuel orifices. Although the flame had a very definite average configuration (fig. 14) and appeared steady to the eye, the high-speed movies show that at least the upstream portions of these flame tongues were often oscillating in the chordwise direction with a high-frequency low-amplitude motion. During the last part of the run (stage III) as the fuel flow declined and the fuel injection became erratic, the slab of flame broke up into definite individual flame tongues of diminished intensity which oscillated up and downstream individually with increasing amplitude while gradually retreating downstream toward the base of the model. The retreating tongues of the flame can be seen in frames 5 to 10 of figure 15(a) and frames 3 to 8 of figure 15(b).

The second or steady stage of combustion is of major interest in this investigation as the aerodynamic variables were measured during this stage only. The starting and end transients in the pressure field during stages I and III were not measured as the frequency response of the pressure-measuring equipment was not adequate for this purpose.

Although the flame appeared to the eye as bright green or yellow-green in color, the high-speed (1000 to 4000 frames/sec) color motion pictures of the flame recorded three predominant colors in the flame. There was a pale-blue region in the upstream area, particularly in the region where the flame was strongly expanding outward. This was followed in the outer downstream regions of the flame by a more extensive area with the typical green color associated with the combustion of boron compounds, which is so noticeable to the naked eye. Adjacent to the surface of the flat plate was a layer which was quite orange in color and which extended along a large part of the plate.

[redacted]

An evaluation of the degree of spanwise spreading and other structural details of the flame region was obtained by supplementing visual and photographic observation of the flame with measurements of the geometry of the ash pattern formed on the surface during each run. A typical ash deposit on the short flat plate is shown in figure 6. In the particular run, it can be seen from the ash pattern that the upstream portion of the tongue of flame associated with the center fuel orifice was located somewhat downstream with respect to the outer-flame tongues. The relative upstream advancement of the flame tongue from each orifice varied from run to run with approximately equal advancement occurring quite often. The distance that the flame traveled upstream of the fuel orifices was recorded by ash patterns similar to that of figure 6 as well as by the flame photographs for each run. The maximum upstream travel beyond the fuel orifices was about $1\frac{1}{2}$ inches. The ash pattern on the extension plate was much more uniform than on the upstream section. The sharp gradations in ash color and the complex patterns evident in the upstream sections of the short flat plate were not usually present on the extension plate. The extension plate was usually covered with an almost rectangular ash pattern extending out to within about 1 inch of the tunnel walls on each side of the plate. Thus, as the flame extended downstream, it appeared to become more homogeneous and behave more as a single slab. The base region of the extension plate was also covered with a fairly uniform layer of ash.

Description of flame shock system. - A complex three-dimensional system of shock waves was associated with the combustion in the stream adjacent to the flat plate. These disturbances are visible in the schlieren photographs of combustion in figures 14(b), 14(c), and 15(b). These photographs show that the stream disturbances originate from several sources. Associated with the upstream portions of the flame tongue from the fuel orifices were a series of shocks which united to form the main shock system caused by the flame. When a flame tongue advanced upstream or retreated downstream, these shocks moved with it, as shown in figure 15. Throughout the runs, there was a shock which originated in each flame tongue at the point where fuel was injected and which remained relatively motionless during most of stage II, while the other flame shocks oscillated with high-frequency and low-amplitude motion. Upstream of the main flame shocks, there were weaker disturbances probably associated with the ash deposits at the far upstream edges of the flame. As the flame retreated downstream, these weak disturbances often remained.

Static-Pressure Change at Model Reference Surface Caused by Combustion

The static-pressure increases measured at the surface of the flat-plate model during the combustion runs are summarized in table II. The

static pressure prior to combustion at each surface tap can be obtained from the data of tables III and I, which give the total pressure for each run and the nonburning ratios of static to total pressure for each surface tap, respectively. The static pressure during combustion at each surface tap, if desired, can be obtained by adding the pressure change from table II to the corresponding nonburning pressure for the run. The first 21 runs listed in table II were primarily for the purpose of measuring static-pressure changes at the model surface. During these 21 runs, there were no probes in the stream adjacent to the flat-plate reference surface. Table II does not include pressure-change data for a static tap when definite plugging of the orifice by ash deposits occurred during a run. Pressure-change measurements where partial plugging was suspected but not definitely established were included in the table. These values would be somewhat smaller than the actual pressure changes which occurred in the stream.

4138

Static-pressure measurements were made first with the short-flat-plate model to ensure that the model would be well within the test rhombus formed by the shock-wave system associated with the flame. However, inasmuch as flame was still visible a considerable distance downstream of the base and because there was no apparent way to scale down the flame, it was necessary to lengthen the chord of the model to better fit the size of the heated region. Therefore, the remaining runs were made with the extended flat plate, which matched the length of the heated region much better. However, the disadvantage of the extension was that the flame shock-wave system reflected from the tunnel wall and struck the heated region of the stream forward of its base.

Short flat plate. - The chordwise distribution of the increase in static pressure $p_c - p$ along the centerline of the model surface caused by combustion in the stream is shown in figure 16 for two runs (runs 1 and 5, table II). In each run the pressure increase rose to a peak value of a little over 2 inches of mercury at a distance of 1 inch downstream of the fuel orifice and then decreased rapidly to a minimum value of less than 0.5 inch of mercury at about 5 inches downstream of the fuel orifice. Downstream of this minimum, there was a modest trend toward increased pressure change with distance.

Chordwise and spanwise plots of the individual pressure-change values measured at the model surface during the five short-flat-plate combustion runs listed in table II are presented in figure 17. The average chordwise and spanwise pressure changes are also given in figure 17 by the curves faired through the average pressure change at each tap. The data of figure 17 show that, although the runs were of different intensities (fuel-injection rates, 5 to 14 cc/sec), the same general pressure-change pattern occurred in all runs.

In order to be certain that the pressure-change pattern observed was not caused simply by the shock waves associated with the injection

of a liquid into the supersonic stream, two types of nonburning checks were made. In one, the fuel injector was loaded with acetone, and a nonburning run was made under the usual operating conditions. The second type was obtained with aluminum borohydride, which was injected as usual but was not ignited. The pressure changes caused by the liquid injection during these check runs were small (a maximum of 0.15 in. Hg) compared with the ones occurring during combustion. It was, therefore, concluded that the disturbances caused by the liquid injection had very little effect on the measurements made during combustion.

Because the peak and minimum pressure-change regions measured during combustion occupied such a large fraction of the chord of the short-flat-plate model, apparently because of the poor matching of the heat-addition region with model length, only five runs were made prior to adding the extension plate. On the basis of the preliminary work of reference 7, it was expected that adding the extension to the flat plate would permit measuring an additional pressure increase farther downstream which was beginning to appear on the last few inches of the plate.

Extended flat plate. - Chordwise static-pressure changes from two typical extended-flat-plate combustion runs (runs 12 and 13, table II) are presented in figure 18. Comparison of runs 12 and 13 with the short-flat-plate data shows that the general pattern was similar. That is, there was a maximum increase in pressure about 1 inch downstream of the fuel orifice followed by a minimum 4 to 5 inches downstream of the fuel orifice. Because of the extra 12 inches of chord length provided by the extension plate, the pressure-change curve downstream of the minimum rose to much higher values (of the order of 2 in. Hg) before the end of the plate was reached than were measured with the short flat plate. This trend is consistent with the data of reference 7. In reference 7, the pressure change along the top wall of a 4- by 10-inch supersonic wind tunnel during combustion of $Al(BH_4)_3$ in the stream below increased with distance downstream of the fuel orifice up to about 20 inches, where it became relatively more constant with increasing distance. In figure 18, the strain-gage data (solid circles) and pressure-capsule data (open symbols) are designated differently in order to illustrate the degree of quantitative agreement usually experienced with the two types of pressure-measuring instruments during a given run.

Because the intensity of combustion varied from run to run, there were marked differences in the static-pressure increases measured at a given tap. To illustrate this variance, the curves showing the maximum (run 15, table II) and the minimum (run 6, table II) chordwise changes in pressure are shown in figure 19 along with the average chordwise pressure-change curve for runs 6 to 21 of table II (runs 10 and 14 were not included because the center fuel orifice plugged early in each run).

Figure 19 shows that, in general, there was a rough correlation of pressure change with fuel-flow rate. The maximum- and minimum-change

runs had, respectively, the highest and lowest fuel-flow rate of the group of runs. The data of table II show, however, that because of the lack of control of all variables (the individual flow from each fuel orifice, e.g.) and because of inaccuracies in the measurement of fuel-flow rate the magnitude of the pressure-change effect correlates with the fuel-flow rate only in a gross sense.

Although the pressure effects varied considerably between some of the runs, the flame shape and shock configurations were qualitatively similar for all runs. This can be seen by comparing the photographs of the flame and shock waves shown in figure 20 for the maximum-change run (run 15) with those previously shown for a more average run (fig. 15).

If the higher- and lower-fuel-flow-rate runs are excluded, there was considerably less variation in pressure change at any given tap measured from run to run. This is shown in figure 21, where only data from runs with fuel-flow rates of 9.6 to 11.8 cubic centimeters per second are plotted. The average chordwise and spanwise pressure-change curves for these runs are also given in the figure. The spanwise data of figure 21 show that the flame spread out laterally in such a manner that the pressure was reasonably constant across the span. The slightly unsymmetrical deviations of the data from the constant pressure-change line drawn through the average value at each spanwise station are probably caused by small differences in average fuel-flow rates through the three orifices. The lower fuel orifice (-2 in. from centerline) apparently had the highest average fuel-flow rate of the three.

It was necessary to ascertain that the static pressures measured on the flat-plate surface were the result of the adjacent combustion zone and its associated shock system rather than the result of any change in the gross flow through the tunnel which might be caused by combustion. In reference 6, it is demonstrated (as predicted by theory) that for sufficiently high fuel-flow rates it was possible by the combustion of aluminum borohydride in the stream to choke the flow of the entire test section of a 4- by 10-inch supersonic tunnel causing the normal shock to "pop" upstream.

In order to be certain that the free-stream flow of the 1- by 1-foot tunnel was not disturbed by the combustion, the angle of the shock off the leading-edge wedge on the nonburning side of the flat plate was checked for constancy before and during combustion with the aid of the high-speed schlieren motion pictures. No measurable change in the shock angle occurred during any of the runs. In addition, for some runs strain-gage-type pressure transducers were connected to the plenum-chamber static orifice and to several test-section wall static taps on the nonburning side of the model. These measurements indicated that no significant change occurred in the plenum or test-section pressure levels.

Lift Forces Resulting from Combustion

The static-pressure increases at the flat-plate surface caused by combustion in the adjacent supersonic stream resulted in lift forces on the surface. The lift forces obtained in the tunnel (and not corrected for tunnel effects) can be calculated from the pressure-change data of table II.

Representative values of lift for the extended-flat-plate surface were obtained by integrating several chordwise static-pressure-change profiles. It was assumed that the pressure during combustion was constant across the entire foot of the span at each chordwise position. The spanwise data of figure 21 indicate that this is a good assumption at chordwise distances greater than 5 inches downstream of the fuel orifices. In the vicinity of the fuel orifices this assumption is, of course, not true because the flame and pressure fields vary spanwise between orifice locations.

The lift on the flat-plate surface during combustion was calculated for the average, maximum, and minimum chordwise pressure-change profiles given in figure 19. The resultant lift forces obtained were 209, 283, and 120 pounds, respectively. Since the flame was adjacent to about 23 inches of chord (assuming a $1\frac{1}{2}$-in. advance upstream of the fuel orifices), this represents an average lift force of the order of 100 pounds per square foot. Inasmuch as the free-stream static pressure corresponded to a pressure altitude of about 52,000 feet, the lift obtained in the tunnel would be of practical magnitude if it can be realized in free flight.

Base Pressure Change Caused by Combustion

Although the models and installation were designed primarily for flat-plate aerodynamic studies, the pressure changes measured at the base static taps are of qualitative interest because of their effect on base drag. The pressure-change data measured during the combustion runs at the base static taps are therefore included in table II.

The base pressure changes $p_{b,c} - p_b$ are summarized in figure 22 for both the short and the extended flat plates. A constant pressure-change line is drawn through the average base-pressure change for each model. Inasmuch as the average base pressure prior to combustion was less than 1 inch of mercury, these changes represent 270- to 400-percent increases in base static pressure.

The interpretation of the base-pressure-increase data is complicated by the poor aerodynamic flow on the nonburning side of the model and by tunnel effects, such as the effect of reflected shocks in the wake region.

However, the large magnitude of these base-pressure increases offers promise of obtaining base-drag reduction by external combustion. In fact, pressure increases will probably occur on all rearward-facing surfaces adjacent to the combustion region in an external stream. Thus, some reduction in pressure drag and base drag can be expected from properly distributed external combustion about an aerodynamic body.

4138

Stream-Parameter Measurements During Combustion

Various stream parameters were measured during combustion in order to determine the temperature and the Mach number levels within the flame. Runs 22 to 50 of table II were for the purpose of making total-temperature, total-pressure, and stream-static-pressure measurements. Photographs of the total-temperature and -pressure probes in the stream at station I (fig. 8) during combustion are shown in figure 23. Figure 23(a) shows a direct and a schlieren frame of one of the thermocouple rakes in the stream. The total-pressure rake is shown in figure 23(b).

Because of the many uncertainties which exist with regard to the composition, kinetics, thermodynamics, and aerodynamics of the system, it is not possible at this time to determine accurately the Mach number within a flame in a high-velocity stream. Therefore, the actual indicated data are given in tables for the stream measurements with no correction for local Mach number or heat-transfer effects. This will allow the reader to make an independent evaluation of the conditions within the flame if he so desires. In addition, the data, converted to stream values by using the approximate local Mach number as determined from the stream measurements assuming simple stream-tube flow, are summarized and discussed in this section. The methods and assumptions used to determine local Mach numbers from the stream data and to correct the indicated data to local stream values are given in appendix A.

Total temperature. - Temperatures indicated by the thermocouple rakes located at chordwise stations I, II, and III and at the wake station are given in table IV. Many of the indicated temperatures (not corrected for radiation or recovery-ratio losses) reached the 2500° to 3500° R range. The indicated wake temperatures were about one-half as high.

The indicated total-temperature data of table IV were converted to local stream values by the methods of appendix A and are shown in figure 24. The total temperatures shown in figure 24 are average values for each thermocouple location. These data show that the flame extended out from the model surface a distance of 1 to $1\frac{1}{4}$ inches at station 1, $2\frac{3}{4}$ inches at station II, and about $2\frac{1}{2}$ inches at station III. Because of the physical properties of the thermocouple material, the platinum thermocouple data are probably more accurate than the chromel-alumel

thermocouple data at temperatures above 2500° R. At lower temperatures, the chromel-alumel data are probably more accurate because of their greater electromotive-force output. The faired curves through the average data points were drawn accordingly. Part of the temperature differences between thermocouple types and between chordwise station locations evident in table IV and in the average values of figure 24 may have been caused by differences in combustion intensity from run to run, by the lack of precision of the temperature measurements, or both. The data of figure 24 are, therefore, primarily indicative of the general temperature level of the flame in the stream adjacent to the model.

Total pressure. - The indicated total-pressure changes due to combustion are summarized in table V. Within the flame region, the combustion caused a large decrease in indicated pressure at each total tube. This decrease was as much as 18 to 20 inches of mercury. Outside the flame region, the total tubes apparently were affected primarily by the change in strength of the local shock wave ahead of each tube caused by the reduction in Mach number behind the shock-wave system associated with the flame. In this region, therefore, the total tubes indicated an increase in pressure of the order of 6 to 8 inches of mercury.

The average local total pressures at rake stations I, II, and III during combustion were calculation from the indicated total-pressure-change data of table V by employing the assumptions of appendix A. The results are shown in figure 25. Figure 25 shows that the total pressure dropped to very low values within the flame region at the three rake stations. At several points in the flame, it was within 1 inch of mercury of the static pressure during combustion. The total-pressure profiles and the corresponding total-temperature profiles (fig. 24) yield the same values for the thickness of the heated region at each rake station, i.e. $1\frac{1}{4}$, $2\frac{3}{4}$, and $2\frac{1}{2}$ inches at stations I, II, and III, respectively. At the stream boundary of the flame, two values of average total pressure are given at stations I and II. One value is representative of total pressure measured in the first part of the runs, and the other value (indicated by a tailed symbol) is for the pressure during the last half of the runs. The flame apparently expanded out slightly into the stream late in each run. This put the pressure tube at the edge of the flame region a little deeper into the flame region, thus accounting for the greater decrease in pressure.

The differences shown in figure 25 between total pressures in the heart of the flame at the three rake stations may not be significant because of the previously discussed variations in the runs and because the differences are of the same order as the possible error in measurement for the pressures lower than 7 inches of mercury.

Stream static pressure. - It is reasonable to assume that within the flame region the static-pressure gradient is approximately zero normal to the flat plate. A few static-pressure-change measurements were made within the flame and adjacent stream with the three-prong static rake to check the validity of this assumption.

In figure 26 data from a stream static-pressure-change measurement at each of the three chordwise rake stations are shown. These data show that the static-pressure change within the flame and the adjacent nonburning stream behind the flame shock system can be regarded as approximately constant (allowing for secondary disturbances in the stream) along a line perpendicular to the surface. The surface values of static pressure during combustion are therefore representative of the static pressure in the flame region adjacent to the plate. Figure 26 shows that at station I the static pressure 3.75 inches from the surface showed no significant change (within the accuracy of measurement). The static probe at this position was in the undisturbed stream outside of the flame and the main flame shock system. As the point of measurement was quite close to the main flame shock system, the small pressure increase may have been due to a weak shock originating at the farthest upstream edge of the flame or the ash deposit. It should be noted that the pressure changes presented for station III were not typical in magnitude for the corresponding chordwise position. The unusually small pressure increases measured during this run (run 49) were due to a low fuel-flow rate (6.1 cc/sec). However, the pressure change was nearly constant along a line perpendicular to the surface, as it was in the stronger runs.

Local Mach number during combustion. - An estimate of the local Mach number at the three chordwise stations in the flame and adjacent stream can be obtained from the stream measurements. The method and the assumptions used to calculate the Mach number from the stream data are given in appendix A.

Figure 27 shows the Mach numbers obtained at distances between 1/4 and $3\frac{1}{4}$ inches from the flat-plate surface at the three rake stations. The data for rake station I are included, although they are probably the least reliable in view of the assumptions used in the calculations because of their upstream location. Because, as discussed in appendix B, the rakes affected the static-pressure profiles during combustion, the local Mach number was determined at each station from both the value of the average local static pressure measured with rakes present (solid symbols) and the average value with no rakes in the stream (open symbols).

The data of figure 27 show that at the three rake stations the Mach number was subsonic throughout much of the depth of the flame, becoming sonic and low supersonic only at the outer edges. The Mach number values of this figure should be interpreted as indicative of the estimated general Mach number regime prevailing in the flame rather than providing a detailed profile at each station.

Surface Temperature Changes During Combustion

Surface temperature measurements during some of the combustion runs were made with the six surface thermocouples located as shown in figure 3. Although the model surface had a rather thick skin for transient heat-transfer measurements, it was anticipated that a measurable increase in surface temperature would occur because of the high temperatures expected in the stream. Actually, the increase in surface temperature was so small that it was barely measurable with the instrumentation used. The maximum temperature measured at any point on the plate surface was 150° F (about a 70° F change). This change was measured during the longest run (run 49, table II). A typical rate of temperature increase was about 10° F per second, with the highest rates about 18° F per second.

GENERAL DISCUSSION

It was relatively easy to sustain external combustion of aluminum borohydride in the airstream adjacent to a 25-inch-chord two-dimensional flat-plate model in a Mach 2.46 wind tunnel. The runs showed good general reproducibility and were quite trouble free.

The chordwise pressure-increase profile that was measured over the downstream portion of the extended-flat-plate model was qualitatively similar to that caused by a flame beneath the top wall of a supersonic wind tunnel in the preliminary investigation reported in reference 7. The magnitude of the pressure change was greater, however, of the order of 60 percent of the static pressure prior to combustion compared with the 20- to 40-percent change of reference 7.

In reference 7 pressure changes along the top wall of the tunnel during combustion were not measured for the first few inches downstream of the fuel orifice, so that no hint of the sharp rise in static pressure immediately behind the fuel orifices was found. This peak region of static-pressure change just downstream of the flat-plate fuel orifices was apparently associated with the oblique three-dimensional shock system caused by the combustion.

Figure 28 shows a two-dimensional sketch of the upstream portions of a typical flame and associated shock waves in the plane perpendicular to the model surface through the centerline. Superimposed on this sketch is a plot of the corresponding chordwise static-pressure-change profile in this region. The upstream portions of the flame apparently affected the external stream flow aerodynamically much like a solid half-wedge of about 10°. This concept is supported by the low mass flows calculated (appendix C) for the flame region from the stream-parameter measurements in the flame, which indicate that much of the air is deflected around the flame zone.

The series of shock waves indicated in the sketch, which are generated by the flow compression and which combine to form a single wave (in this plane) at about a 32.5° angle, were clearly seen in the schlieren photographs. The occurrence of a sharp drop in pressure along the model surface just downstream of the peak region indicates that this strong aerodynamic compression was apparently immediately followed by a strong aerodynamic expansion region in the stream external to the flame (provided the pressure gradients perpendicular to the model surface in the flame are small in this region). The pressure reaches a minimum at a distance of 4 to 5 inches downstream of the fuel orifice. The actual cause of this pressure decrease within the flame region is not clear. It is probably associated with a low rate of combustion in this area, or possibly it is associated with the spanwise expansion of the heated region in this area (see ash pattern of fig. 6).

4138

Figure 28 shows that both the peak and the region of decreasing pressure occurred in a region of the flame which is physically expanding in the direction perpendicular to the plate surface. Comparison of the flame photographs with the chordwise-pressure-change curves indicates that the position of the peak pressure may coincide with the inflection point of the curve bounding the upstream portion of the flame and the external stream. The minimum pressure occurred at the first plateau of the flame boundary. Following the minimum there was an increase in pressure with increasing distance downstream, and the flame and pressure fields became more uniform. In this region the flame expanded out gradually from a thickness of $1\frac{1}{4}$ inches to a maximum thickness of $2\frac{3}{4}$ inches at rake station II and then contracted slightly between rake station II and the end of the plate. Comparison of the stream measurements (figs. 24 and 25) at rake station I with those at rake station II shows that further combustion of fuel probably occurred in this region with additional air entering the flame.

The increase in pressure with increasing distance downstream noted along the downstream half of the extended flat plate may have been caused by tunnel effects. Because of the short distance between the model and the tunnel walls compared with the length of the plate, the flame shock-wave system was reflected from the tunnel wall and impinged on the flame boundary at a point upstream of the base of the model. This, in itself, might be expected to cause an increase in pressure with increasing distance downstream if the shock waves remain strong. The presence of a thick layer of subsonic flow in the flame (indicated by the stream data) would permit the pressure disturbances to propagate upstream. In fact, it is possible that the reflected shock wave may have caused extensive flow separation (as suggested by the strong adverse chordwise pressure gradient downstream of the minimum) similar to that caused on a smaller scale when a shock wave of sufficient strength impinges on a boundary layer. It should be noted, however, that further combustion in this

region might, in itself, cause flow separation. In addition, channel effects on the nonheated flow between the flame zone and the tunnel wall may be important in this investigation because part of the pressure increase accompanying a reduction in Mach number could be transmitted upstream through the subsonic heated region and thereby change the shape of the pressure profile. Because of the quasi-conical nature of the shock system, and because of possible canceling action of the expansion waves which originate in the decreasing pressure region, the Mach number reduction caused by the reflected shock waves may not be large. It is not possible with the present data to determine what part of the Mach number reduction in the unheated stream is due to reflected waves and what part is due to further compression of the stream caused by combustion in the downstream portions of the flame region.

Thus, if the tunnel effects just described are of primary rather than of secondary importance, then the increase in pressure downstream of the minimum might be considerably less or might not occur at all in free flight. In this case the increase in lift and the reduction in drag realizable from external combustion for a given expenditure of fuel would be sizably less than indicated by the data of this report. In this connection it should be noted that the short-flat-plate data also show a trend toward increasing pressure with distance downstream of the minimum, even though the reflected flame shock system intersected the heated region at a point in the wake which was well downstream of the base of the model. However, as this region of the heated wake was probably subsonic, it is possible that even here tunnel effects may have caused the pressure rise downstream of the minimum. The magnitude of the tunnel effects can best be determined by performing a similar experiment in a large tunnel or with a free-flight model.

The analysis of the stream-parameter measurements during combustion was complicated by the lack of a proven model for the air flow in the heated region. In fact, even the locus of the heat addition was not known with certainty. Several flow models are suggested by the data. As mentioned previously, it is possible that the combustion occurred in a region of separated flow in which large-scale vortices existed. Another possibility is that a wave phenomenon, such as a standing detonation wave, occurred. Inasmuch as the measurements do not clearly establish the presence of either of these flow types, a simplified flow model was chosen for the stream calculations of appendixes A and C. In this model it was assumed that any reverse or vorticular flow which might have existed occurred only in a shallow layer next to the plate surface or at the boundary of the flame and nonburning flow. The rest of the flow in the heated region was assumed to be stream-tube flow at small angles to the free-stream flow.

The analysis of the stream-parameter measurements made at rake stations I, II, and III during combustion runs indicated that the local

stream velocities were subsonic over much of the depth of the flame. Figure 27 shows that only in the outer portions of the flame zone was the flow sonic or low supersonic at these stations. Because of the existing uncertainties in the determination of the local Mach number in the flame, it is interesting to consider the effect of the weight-flow rate of air through the flame on the total temperature. In appendix C it is shown that, if the calculated Mach numbers of figure 27 are employed to determine the average air weight-flow rate through the flame from the stream data at rake station III, a value is obtained which is about one-ninth of the rate through the same region prior to combustion. The corresponding average fuel-air equivalence ratio in the flame was calculated in the appendix to be 0.34.

In appendix D a relation between equivalence ratio and flame temperature is calculated. The results are given in figure 29, in which total temperature in the flame zone is plotted as a function of the fuel-air equivalence ratio. The curve is approximate to the extent that the chemical enthalpy actually released to the airstream depends on the static temperature. This point is discussed further in appendix C. From figure 29 it can be seen that an equivalence ratio of 0.34 corresponds to a theoretical total temperature in the flame (assuming the reaction is completed) of 2800° R. This temperature is in good agreement with the magnitude of the total temperatures measured in the flame at rake station III, as can be seen from figure 24. Thus, the high total temperatures measured in the stream are consistent with the subsonic and transonic Mach numbers calculated from the stream data.

If, on the other hand, the average Mach number in the flame zone is assumed to be supersonic, the fuel-air equivalence ratio would have been too low to explain the high measured total temperatures. For example, if the flow in the flame zone is assumed to be at a Mach number of 2.0, the value of the equivalence ratio calculated from the data at rake station III and the fuel-injection rate would be 0.06. From figure 29 it is apparent that the total temperature expected would be much less than the averaged measured value at station III. If the Mach number is assumed to be sonic throughout the flame, the calculated total temperatures would, of course, be much closer to the measured values than for the Mach 2 assumption.

In view of the various approximations made in the Mach number calculations and the inherent inaccuracies in the stream measurements, it cannot be established with certainty that the flame zone was not sonic throughout. However, the results of figure 27, which shows a large portion of the flame region to be subsonic, are most consistent with the measured values of the stream parameters obtained.

Thus, it appears that much of the heat addition due to external combustion occurred in a flow which was locally subsonic in the flame. Only

at the boundaries of the flame region did heat addition occur in regions which were sonic or supersonic. The sizable pressure increases measured on the flat-plate surface resulting from the external combustion of aluminum borohydride are in qualitative agreement with the results of various theoretical investigations. These investigations predicted that appreciable lift would result from external combustion below a wing in a supersonic stream whether or not the theoretical model assumed that the heat addition occurred in a locally supersonic (ref. 4) or a locally subsonic (ref. 5) region. The combustion and flow fields present in this experiment do not correspond in detail to the theoretical models of either reference 4 or 5. It is not possible, therefore, to make detailed quantitative comparisons of the experimental data with the theoretical results without modifying the theoretical models to correspond more closely to the conditions of this experiment.

The short duration of the combustion runs of this experiment introduces some additional difficulties in interpreting the results. Although the measurements indicated that the combustion and flow fields rapidly reached a steady state in the stream, the model surface temperature increased only slightly during the short runs. Since an equilibrium surface temperature was obviously not reached, a considerable amount of heat transfer from the stream to the model occurred. It is, therefore, not certain what effect prolonged combustion, which would allow the surface to reach thermal equilibrium, might have on the pressure field. It appears likely that the pressure field would not be changed much, but the viscous forces on the surface may very well be changed. It therefore appears important in future experiments to measure the viscous forces on the surface during both short and long combustion runs.

SUMMARY OF RESULTS

An exploratory experimental investigation of the aerodynamic effects of burning aluminum borohydride in a Mach 2.46 airstream adjacent to the surface of a flat-plate model was conducted in a 1- by 1-foot supersonic wind tunnel. Measurements of surface static and base pressures, stream total temperatures, and stream total pressures during combustion were made along with direct and schlieren photographic observation of the flame and associated stream disturbances. The aerodynamic measurements were subject to presently undetermined tunnel effects, the magnitude of which can best be found by making a similar large-tunnel or free-flight investigation. The following results were obtained in this investigation:

1. Liquid aluminum borohydride injected (approx. 11 cc/sec) into the stream adjacent to the flat-plate-model surface burned with a stable steady flame after ignition.

2. Static-pressure increases averaging about 60 percent were measured at the flat-plate surface as a result of the external combustion. The average static pressure during combustion reached a maximum value (2.7 in. Hg change, or a 90-percent increase) just downstream of the fuel orifices. Following this, the pressure decreased sharply, reaching a minimum (0.7 in. Hg change, or a 23-percent increase) at a distance of 4 to 5 inches downstream of the fuel orifices. Downstream of the minimum value, the pressure increased with distance, reaching a level corresponding to a change in pressure of about 2.1 inches of mercury (a 70-percent increase) near the end of the extended flat plate.

3. The lift forces on the flat-plate surface resulting from external combustion in the tunnel airstream at a pressure altitude of about 52,000 feet were calculated from the static-pressure-change data. The lift force on the extended flat plate varied from 120 pounds for the weakest run to 283 pounds for the strongest run. The average value for all runs was 209 pounds, which was of the order of 100 pounds per square foot.

4. Large increases (up to 400 percent) in the base pressure of the flat-plate models were measured during combustion. These pressure increases were of sufficient magnitude to offer promise of sizable base-drag reduction during external combustion.

5. Stream total temperatures were determined from measured rake data in the flame region at three chordwise stations. The total temperature was between 2400° and 3800° R in the hottest part of the flame (the layer between $\frac{1}{4}$ and $1\frac{1}{2}$ in. below the plate surface).

6. Large changes in total pressure occurred in the flame region. Total pressures in the flame as low as 5 or 6 inches of mercury were obtained from the total rake data. The corresponding nonburning values were approximately 48 inches of mercury.

7. The local Mach number in the flame region was estimated from the stream rake data. The calculations indicated that the Mach number was subsonic in much of the flame zone, becoming sonic and low supersonic in the outer portions of the flame adjacent to the nonburning stream.

Lewis Flight Propulsion Laboratory
National Advisory Committee for Aeronautics
Cleveland, Ohio, May 29, 1957

APPENDIX A

CALCULATION OF TOTAL TEMPERATURE, TOTAL PRESSURE, AND MACH NUMBER OF HEATED STREAM FROM INDICATED RAKE DATA

Several factors made the conversion of indicated stream data to local stream values difficult. They are a lack of a clearly established model for the flow field in the heated region; a lack of understanding of the type of combustion occurring; and the many uncertainties with regard to the composition, kinetics, and thermodynamics of the system. For example, it was not known a priori whether the combustion caused the heated region of the supersonic stream to become sonic, subsonic, or merely low supersonic. In addition, because of the adverse pressure gradients present along portions of the flat-plate surface during combustion and because of the very large decrease in total pressure, flow separation may have occurred. If extensive flow separation took place, it is possible, although not conclusively indicated by the stream data, that large-scale vorticular flow may have occurred throughout much of the heated region.

For these reasons it is necessary to make quite a few simplifying physical assumptions in order to determine local total temperatures, total pressures, and Mach numbers from the indicated stream data. For example, it is convenient to assume that the isentropic exponent γ depends only on the temperature of the stream and not on the composition. Actually, since the composition of the airstream changes with introduction of the fuel, and because dissociation and phase changes of the combustion products occur in the flame, the effective local value of γ in some portions of the stream may differ from that calculated for air at the same temperature.

For the purpose of calculating the stream parameters in the heated region, it was assumed that the flow behaved aerodynamically as if it were heated air. Since 80 percent of the air (N_2) was unchanged by the combustion, this appears to be a reasonable assumption. In addition, it was assumed that large-scale vorticular flow was not occurring in the heated region, that is, the air flow was parallel to or at small angles to the flat plate. Furthermore, the heat added (or lost) by chemical reaction or phase change in the stagnation regions of the stream probes was assumed to be small compared with the total heat added to the stream upstream of the measuring station. That is, the reaction was assumed to be essentially completed. In some regions of the flame this may have been a poor assumption as the reaction may have been incomplete and the unburned fuel may have burned locally in the stagnation region of the probes. The assumption of complete reaction is probably much better at rake stations II and III than at station I since the data indicate that additional combustion probably occurred between stations I and II. If the local flow was

supersonic within the flame region, then the problem is further complicated by similar difficulties in calculating the total-pressure loss across the normal shock wave ahead of a total tube.

With the preceding assumptions, the local total temperatures, total pressures, and Mach numbers were obtained from the indicated data by an iterative calculation employing the usual equations for compressible flow of a perfect gas (ref. 11). One of these equations gives Mach number as a function of static pressure, total pressure, and γ. The static pressure at a point in the flame was obtained from the measured static pressure at the corresponding point on the plate surface during combustion. Because of the effect of the rakes on static pressure discussed in appendix B, dual calculations were made employing static pressures with and without the presence of rakes in the flame. The local values of total pressure were obtained from the indicated total pressures during the iterative calculation. The indicated total pressure at each total tube location was obtained by adding the change in indicated total pressure (table V) caused by combustion to the local nonburning indicated pressure P_1 for the run (table I gives measured ratios of P_1/P_0). The local values of γ were determined from the local stream temperatures by employing the relation between γ and temperature given in reference 11 for heated air. This gave values of γ as low as 1.30 in the hottest regions of the stream.

In order to obtain the local stream temperatures and therefore appropriate local values of γ, the indicated total-temperature data of table IV were corrected for radiation and recovery losses during the process of iteration. Heat-transfer data for thermocouples in high-temperature high-velocity streams are, however, very limited. Therefore, the conversion of the indicated temperatures of table IV to local stream total temperatures required some extrapolation of the available heat-transfer data. The methods and heat-transfer data given in references 12 to 14 were employed in the calculations.

With conduction losses (which are small) neglected, the total temperature is given by

$$T_t = T_\omega + (\Delta T)_{rad} + (\Delta T)_{rec} \qquad (A1)$$

where

T_t local total temperature of stream, $^\circ R$

T_ω temperature of thermocouple wire, $^\circ R$

$(\Delta T)_{rad}$ correction for radiation losses, $^\circ R$

$(\Delta T)_{rec}$ correction for recovery losses, $^\circ R$

For the range of Mach numbers present in this experiment, the radiation correction for a bare wire in subsonic cross flow is given by the relation

$$(\Delta T)_{rad} = \frac{27\varepsilon_\omega \sqrt{d}}{\sqrt{Mp}} \left(\frac{T_\omega}{1000}\right)^{-0.18} \left[\left(\frac{T_\omega}{1000}\right)^4 - \left(\frac{T_0}{1000}\right)^4\right]$$

where

ε_ω emissivity of wire

d wire diameter, in.

M Mach number

p static pressure, atm (1 atm = 29.92 in. Hg)

T_0 wall and plate temperature, $^\circ R$

Because the wind-tunnel walls and the flat-plate surface do not heat up in the short runs of this experiment,

$$\left(\frac{T_0}{1000}\right)^4 << \left(\frac{T_\omega}{1000}\right)^4$$

Therefore,

$$(\Delta T)_{rad} = \frac{27\varepsilon_\omega \sqrt{d}}{\sqrt{Mp}} \left(\frac{T_\omega}{1000}\right)^{3.82} \tag{A2}$$

The spike-type junction used for the platinum - platinum plus 13 percent rhodium thermocouples and the transverse butt-welded type junction used for the chromel-alumel thermocouples have approximately similar heat-transfer characteristics but differ somewhat from the bare wire in cross flow previously discussed. Therefore, equation (A2) must be modified as suggested in reference 12 to account for the heat-transfer difference. For the spike-type junction,

$$(\Delta T)_{rad} = \frac{1.3\times 27\varepsilon_\omega \sqrt{d}}{\sqrt{Mp}} \left(\frac{T_\omega}{1000}\right)^{3.82}$$

The quantity $1.3\times 27\varepsilon_\omega \sqrt{d}$ can be treated as a constant for each particular thermocouple and will be denoted as K^*_{rad}. For the thermocouples employed in this investigation,

$K^*_{rad} = 3$ for the chromel-alumel thermocouples

$= 0.9$ for the platinum - platinum plus 13 percent rhodium thermocouples

Then,

$$(\Delta T)_{rad} = \frac{K^*_{rad}}{\sqrt{M_p}} \left(\frac{T_\omega}{1000}\right)^{3.82}$$

Thus, with the use of the radiation constant K^*_{rad}, the radiation correction was computed from the indicated temperature, the static pressure during combustion, and the local Mach number obtained from the calculations.

4138

With the radiation correction calculated, the recovery correction was obtained from the approximation

$$(\Delta T)_{rec} \approx (1 - R_O)[T_\omega + (\Delta T)_{rad}]$$

where R_O is the recovery ratio for the spike-type junction at the calculated Mach number. The factor $1 - R_O$ is small in magnitude, being below 0.02 for subsonic Mach numbers and equal to 0.055 at a Mach number of 2.46. Values of R_O or $1 - R_O$ as a function of Mach number are given in references 12 to 14.

Upon completion of the iteration process, local values of total temperature, total pressure, and Mach number were obtained. Plots of average values of the stream parameters are given in figures 24, 25, and 27, respectively.

APPENDIX B

EFFECT OF STREAM PROBES ON LOCAL STATIC PRESSURE DURING COMBUSTION

Inasmuch as the rakes disturbed the stream and the flat-plate boundary layer, and because they may have altered the combustion, static pressures upstream of the selected probe positions were measured at the model surface taps during each run. These static-pressure profiles were compared with the static-pressure profiles measured during combustion without the presence of rakes in the stream. In addition, the direct motion pictures of the upstream half of the extended flat plate were examined for evidence of intensification of the flame in the vicinity of the rake. There was no conclusive evidence in the photographs that the rake in the number I position (the only one that could be photographed) acted as a flameholder or altered the combustion in any way. The static-pressure profiles, on the other hand, indicated some differences. The static-pressure-data upstream of the rakes are summarized in table II (runs 22 to 50). In figure 30 the averages of all the static pressures measured during the combustion runs in which a rake was present are compared with the averages of all no-rake runs. The average curve does not include data from runs 48 to 50 because the static rake was of considerably different shape than the total-pressure and -temperature rakes, which were similar in construction. In addition, the static rake runs were not typical in that the fuel-flow rates were below average. Figure 30 shows that the general shapes of the two average chordwise static-pressure-change curves are similar. Two main differences are apparent, however. The rake runs indicated a smaller increase in static pressure over the downstream half of the flat plate and a small upstream shift of the peak-value position. The reduction in pressure increase over the downstream half of the plate in the rake runs may have been due to an average difference in intensity of the combustion during the rake runs in comparison with the no-rake runs. However, the average fuel-flow rates computed for the two sets of runs were approximately the same (10.9 and 11.1 cc/sec). Inasmuch as the downstream half of the extended flat plate was not directly observable, there may have been unobserved differences in the combustion in this region which may have affected the pressure fields.

In figure 31 the average static-pressure change measured at the model static taps ahead of each rake station for all runs with a rake at the respective station is shown along with the average of all no-rake-run data for comparison. The averages for the rake-run data include the data for all runs using either one of the two total-temperature rakes or the total-pressure rake. In addition to the trends discussed in the previous paragraph, the most noticeable characteristic of the data of figure 31 is the disturbance of the pressure field immediately upstream of the rakes located at station I. Examination of the data of table I shows that this effect was experienced primarily when the total-pressure rake was in place at station I.

In order to examine further the effect of the total-pressure rake on the model static pressures upstream of a given rake station, the data for the total rake runs only are shown in figure 32. This figure shows the average chordwise model static-pressure change measured ahead of the total rake at the three stations. For comparison, the over-all average increase for all runs with the rakes in the stream is shown. Figure 32 shows that the total rake apparently considerably disturbed the pressure distribution during combustion for a short distance upstream of the end of the total tubes when the rake was located at rake station I. The static-pressure change with the total rake at stations II and III, on the other hand, did not differ significantly from the average for all three rakes.

In summary, it appears that the distribution of the static-pressure change (upstream of any given rake) during combustion with the rakes in the stream was generally similar to that for the no-rake data for runs with the rakes at stations II and III. The most important difference was that the pressure increase was somewhat smaller over the last half of the flat plate (fig. 30). At rake station I, the thermocouple rakes also apparently caused little disturbance to the upstream pressures during combustion. On the other hand, the total-pressure rake located at station I caused considerable disturbance upstream during combustion, with the static pressure just ahead of it being considerably higher than typical.

[redacted]

APPENDIX C

METHOD USED TO DETERMINE FUEL-AIR EQUIVALENCE RATIO

The approximate equivalence ratio of the aluminum borohydride - air mixture in the flame below the flat plate can be determined from the measured data. The weight fuel-air ratio can be determined from the measured fuel-injection rate and from the calculated air weight-flow rate through the flame. The air weight-flow rate $w_{a,c}$ through the flame can be determined from the stream-parameter measurements from the relation

$$w_{a,c} = \frac{v_c}{v_1} \frac{p_c}{p_1} \frac{t_1}{t_c} m_1 A_f \qquad (C1)$$

where

v_c average (over A_f) stream velocity in flame at measuring station

v_1 stream velocity prior to combustion at measuring station

p_c static pressure in flame at measuring station

p_1 static pressure prior to combustion at measuring station

t_c average (over A_f) static temperature of heated stream at measuring station

t_1 static temperature of stream prior to combustion at measuring station

m_1 weight flow per unit area prior to combustion

A_f cross-sectional area of flame at measuring station

In calculating the equivalence ratio, the data from rake station III (fig. 8) were employed. Station III was chosen because the combustion was more likely to have been completed than at the upstream stations. The value of A_f in equation (C1) will, therefore, be the cross-sectional area of the flame at rake station III. Based on visual observation of the flame and the surface ash deposits along with the rake measurements, A_f was estimated to be 20 square inches at station III. The original weight flow through this area prior to combustion $m_1 A_f$ can be calculated from the nonburning aerodynamic data for the tunnel. The values of p_1 and p_c were measured directly, and t_1 and v_1 were readily calculated from the nonburning aerodynamic data. The values of t_c and v_c were calculated from the measured total temperature and the local Mach number in the flame at station III (fig. 27). The average static temperature

over the 2.5-inch depth of the flame at station III obtained by this method is 2200° R. The average velocity is 1050 feet per second. Substituting these values in equation (C1) gives

$$w_{a,c} = \frac{1050 \text{ ft/sec}}{1914 \text{ ft/sec}} \times \frac{5.22 \text{ in. Hg}}{3.09 \text{ in. Hg}} \times \frac{257^\circ \text{ R}}{2200^\circ \text{ R}} (4.12 \text{ lb air/sec})$$

$$w_{a,c} = 0.11(4.12 \text{ lb air/sec}) = 0.453 \text{ lb air/sec}$$

That is, the mass flow of air through the cross-sectional area of the flame at station III is about one-ninth of the amount flowing through the same area prior to combustion. Knowing the air mass-flow rate and the average fuel-injection rate (11 cc/sec) along with the density of the fuel, the fuel-air ratio f/a is calculated to be

$$\frac{f}{a} = \frac{0.0133 \text{ lb fuel/sec}}{0.453 \text{ lb air/sec}} = 0.0294 \frac{\text{lb fuel}}{\text{lb air}}$$

Since the stoichiometric fuel-air ratio $(f/a)_{st}$ for aluminum borohydride - air mixtures is 0.0863 pound fuel per pound of air, the equivalence ratio φ is

$$\varphi = \frac{f/a}{(f/a)_{st}} = \frac{0.0294}{0.0863} = 0.34$$

In view of all the approximations involved in a calculation of this type, the value of equivalence ratio obtained is primarily indicative of the order of magnitude prevailing during the combustion runs.

APPENDIX D

CALCULATION OF FLAME TEMPERATURE

In order to compare measured flame temperatures and equivalence ratios with the theoretically expected values, the flame temperatures of aluminum borohydride - air mixtures were calculated.

Static Calculations

Since flow conditions after combustion could not be deduced a priori, it was found convenient to first treat the flowing system as if it were static. The average static air temperature of the Mach 2.46 stream prior to combustion (254° R) was used as the air temperature of the nonflowing mixture. The initial temperature of the aluminum borohydride in this experiment was approximately 536° R. The equilibrium flame temperatures calculated are, therefore, the temperatures to be expected in a static chamber when air at 254° R is allowed to react adiabatically at a constant pressure of 0.1641 atmosphere with aluminum borohydride initially at a temperature of 536° R. The pressure selected (0.1641 atm) was the average measured static pressure of the combustion zone during combustion.

The equilibrium flame temperatures were calculated for aluminum borohydride - air mixtures by a technique which is essentially that of reference 15. It was assumed that the only products of combustion are AlO, Al_2O_3(gas), BO, B_2O_3(gas), OH, H_2O, O_2, H_2, N_2, NO, Al_2O_3(condensed), B_2O_3(condensed), Al, B, H, and O. The equilibrium composition of the products was then calculated at four temperatures, 500°, 1000°, 2000°, and 2500° K, for each of four equivalence ratios, 0.1, 0.5, 0.8, and 1.0, at a pressure of 0.1641 atmosphere. With the product compositions known, the enthalpy of each of the mixtures at each temperature was calculated. The tabulated values of reference 15 were used, except that the values for B_2O_3 were corrected as suggested in reference 16 to make use of recent vapor-pressure data (refs. 17 and 18).

For each equivalence ratio, a plot was then made of enthalpy against temperature. Since conservation of energy requires that the enthalpy of the reactants equal the enthalpy of the products, the only remaining requirement for finding the flame temperatures was the enthalpy of the reactant. For oxygen and nitrogen, the values were obtained by linear interpolation of the values in reference 15. The enthalpy of the fuel was obtained on a base which is consistent with the other values by making use of the reported (ref. 19) 298° K heat of combustion of aluminum borohydride (984 kcal/mole) and the 298° K enthalpies of O_2, B_2O_3, Al_2O_3, and H_2O of reference 15. With the reactant enthalpy known, the equilibrium flame temperature for each equivalence ratio was obtained from the enthalpy-temperature plots.

Stream Temperature

The preceding calculation does not directly provide an indication of what the total temperature of the stream in the flame zone should be for a given equivalence ratio. In order to convert the preceding temperatures to stream temperatures, the change in temperature occurring in the static mixture was assumed equal to the change in total temperature of the flowing stream in the flame region. This is not strictly true as the heat capacity and the chemical composition of the products depend on the static temperature. Therefore, the amount of heat added to the stream depends on the final static temperature, which is, in turn, dependent on the final Mach number. In this temperature range, the heat capacities of the products do not vary greatly with temperature; furthermore, equilibrium calculations suggest that the composition does not vary appreciably with temperature. The assumption that the temperature rise (obtained under the conditions of the static chemical reaction) is equal to the change in total temperature of the stream therefore seems justified. Figure 29 shows the calculated total temperature (^{o}R) as a function of the fuel-air equivalence ratio. For a given equivalence ratio, there should be reasonable agreement between the temperature given by figure 29 and the measured total temperature at the downstream rake stations. In appendix C the average equivalence ratio of the flame was calculated from the stream measurements at rake station III. A value of $\varphi = 0.34$ was obtained. From figure 29 the calculated total temperature is 2800° R. This value is in good agreement with the magnitude of the measured values of total temperature shown in figure 24.

REFERENCES

1. Hicks, Bruce L., Montgomery, Donald J., and Wasserman, Robert H.: On the One-Dimensional Theory of Steady Compressible Fluid Flow in Ducts with Friction and Heat Addition. Jour. Appl. Phys., vol. 18, no. 10, Oct. 1947, pp. 891-903.

2. Shapiro, Ascher H., and Hawthorne, W. R.: The Mechanics and Thermodynamics of Steady One-Dimensional Gas Flow. Jour. Appl. Mech., vol. 14, no. 4, Dec. 1947, pp. A317-A336.

3. Pinkel, I. Irving, and Serafini, John S.: Graphical Method for Obtaining Flow Field in Two-Dimensional Supersonic Stream to Which Heat Is Added. NACA TN 2206, 1950.

4. Pinkel, I. Irving, Serafini, John S., and Gregg, John L.: Pressure Distribution and Aerodynamic Coefficients Associated with Heat Addition to Supersonic Air Stream Adjacent to Two-Dimensional Supersonic Wing. NACA RM E51K26, 1952.

5. Smith, E. H., and Davis, T.: The Creation of Thrust and Lift by Combustion on External Surfaces of Aerofoils. Smith and Davis, Physicists, Silver Spring (Md.), Sept. 1, 1952. (Bur. Ord., Dept. Navy Contract NOrd 12141.)

6. Fletcher, Edward A., Dorsch, Robert G., and Gerstein, Melvin: Combustion of Aluminum Borohydride in a Supersonic Wind Tunnel. NACA RM E55D07a, 1955.

7. Dorsch, Robert G., Serafini, John S., and Fletcher, Edward A.: A Preliminary Investigation of Static-Pressure Changes Associated with Combustion of Aluminum Borohydride in a Supersonic Wind Tunnel. NACA RM E55F07, 1955.

8. Schlesinger, H. I., Sanderson, R. Thomas, and Burg, A. B.: Metallo Borohydrides. I. Aluminum Borohydrides. Jour. Am. Chem. Soc., vol. 62, no. 12, Dec. 1940, pp. 3421-3425.

9. Smith, S. H., Jr., and Miller, R. R.: Some Physical Properties of Diborane, Pentaborane, and Aluminum Borohydride. Jour. Am. Chem. Soc., vol. 72, no. 4, Apr. 1950, pp. 1452-1458.

10. Brumfield, R. C.: Water Reactive Fuels for Undersea Warfare - Appendix E to Problems in Power for Propulsion Applying to Submarines, prepared for the Panel on Power for Propulsion of Nat. Res. Council, Comm. on Undersea Warfare, Sept. 1950. (Ser. No. NRC: CUW: 0075E.)

11. Ames Research Staff: Equations, Tables, and Charts for Compressible Flow. NACA Rep. 1135, 1953. (Supersedes NACA TN 1428.)

12. Glawe, George W., Simmons, Frederick S., and Stickney, Truman M.: Radiation and Recovery Corrections and Time Constants of Several Chromel-Alumel Thermocouple Probes in High-Temperature, High-Velocity Gas Streams. NACA TN 3766, 1956.

13. Stickney, Truman M.: Recovery and Time-Response Characteristics of Six Thermocouple Probes in Subsonic and Supersonic Flow. NACA TN 3455, 1955.

14. Scadron, Marvin D., and Warshawsky, Isidore: Experimental Determination of Time Constants and Nusselt Numbers for Bare-Wire Thermocouples in High-Velocity Air Streams and Analytic Approximation of Conduction and Radiation Errors. NACA TN 2599, 1952.

15. Huff, Vearl N., Gordon, Sanford S., and Morrell, Virginia E.: General Method and Thermodynamic Tables for Computations of Equilibrium Composition and Temperature of Chemical Reaction. NACA Rep. 1037, 1951. (Supersedes NACA TN's 2113 and 2161.)

4138

16. Tower, L. K.: Analytic Evaluation of Effect of Inlet-Air Temperature and Combustion Pressure on Combustion Performance of Boron Slurries and Blends of Pentaborane in Octene-1. NACA RM E55A31, 1955.

17. Speiser, Rudolph, Naiditch, Sam, and Johnston, Herrick L.: The Vapor Pressure of Inorganic Substances. II - B_2O_3. Jour. Am. Chem. Soc., vol. 72, no. 6, June 14, 1950, pp. 2578-2580.

18. Soulen, John R., Sthapitanonda, Prason, and Margrave, John L.: Vaporization of Inorganic Substances: B_2O_3, TeO_2, and Mg_3N_2. Jour. Phys. Chem., vol. 59, no. 2, Feb. 1955, pp. 132-136.

19. Rulon, Richard M., and Mason, L. S.: The Heat of Formation of Aluminum Borohydride. Jour. Am. Chem. Soc., vol. 73, no. 11, Nov. 1951, pp. 5491-5493.

TABLE I. - NONBURNING AERODYNAMIC DATA

(a) Average ratio of static pressure to free-stream total pressure p/P_0

	Static tap (fig. 3)	Short flat plate		Extended flat plate		
		No ignitor	Ignitor I	No ignitor	Ignitor II	Ignitor III
Chord-wise ↓	1	0.0620	0.0620	0.0625	0.0625	0.0623
	2	.0608	.0608	.0608	.0608	.0608
	3	.0588	.0588	.0575	.0574	.0573
	4	.0602	.0602	.0595	.0594	.0594
	5	.0635	.0635	.0625	.0629	.0623
	6	.0654	.0654	.0623	.0628	.0624
	7	.0654	.0654	.0619	.0618	.0616
	8	.0621	.0622	.0619	.0618	.0615
	9	.0628	.0628	.0625	.0624	.0623
	10	.0642	.0642	.0642	.0640	.0639
	11	.0647	.0647	.0629	.0630	.0628
	19	---	---	.0658	.0657	.0657
	20	---	---	.0630	.0631	.0628
	21	---	---	.0615	.0617	.0614
	22	---	---	.0625	.0623	.0621
	23	---	---	.0650	.0650	.0647
	24	---	---	.0658	.0777	.0656
Span-wise ↓	12	0.0643	0.0644	0.0615	0.0618	0.0612
	13	.0627	.0627	.0607	.0606	.0610
	14	.0637	.0637	.0625	.0629	.0625
	15	.0616	.0616	.0620	.0620	.0618
	25	---	---	.0640	.0640	.0640
	26	---	---	.0643	.0641	.0640
	27	---	---	.0617	.0619	.0617
	28	---	---	.0620	.0622	.0619
Base ↓	16	0.0170	0.0182	---	---	---
	17	.0169	.0185	---	---	---
	18	.0171	.0166	---	---	---
	29	---	---	0.0200	0.0219	0.0199
	30	---	---	.0200	.0218	.0200
	31	---	---	.0198	.0198	.0195

TABLE I. - Concluded. NONBURNING AERODYNAMIC DATA

(b) Average ratio of indicated total pressure to free-stream total pressure P_1/P_0

Distance from flat-plate surface, in.	Rake station (fig. 8)		
	I	II	III
1/4	0.5087	0.5148	0.5233
3/4	.5120	.5132	.5229
$1\frac{1}{4}$	.5087	.5153	.5286
$1\frac{3}{4}$	.5023	.5144	.5283
$2\frac{1}{4}$	.4987	.5272	.5204
$2\frac{3}{4}$	.5099	.5184	.5096
$3\frac{1}{4}$	.5120	.5228	.5142

[redacted]

TABLE II. - SUMMARY OF

Run	Model	Primary measurement	Helium injection pressure, lb/sq in. gage	Fuel in injector, cc	Fuel injection time (length of pulse +0.2 sec), sec	Fuel injection rate, cc/sec	Rake at station -	Static-pressure increase, in. Hg, at static pressure tap - 1	2	3	4	5	6	7	8	9	10
1	Short	Chordwise	80	21.3	2.3	9.3				2.08	[a]1.78		[a]0.50	0.48	[a]0.73	0.67	
2	flat	static-	50	15.0	2.9	5.2				2.24	[a]1.44		[a].23				
3	plate	pressure	80	14.0	1.0	14.0						0.87	[a].71	.69	[a].91	1.04	
4		change	50	15.0	1.6	9.4				2.01	[a]1.46	.78	[a].50	.32		.42	
5	↓	↓	50	15.0	1.3	11.5				2.17	[a]1.63	.91	[a].50	.37		.49	
6	Ex-	Chordwise	50	15.0	1.8	8.3	Wake	0	0	[a]0.83	1.48	1.20	0.68		0.23	0.07	0.15
7	tend-	static-	50	15.3	1.3	11.8	Wake	0	0	[a]3.85	1.74	.95	.67	[a]0.63	1.06	1.22	1.41
8	ed	pressure	50	23.7	2.4	9.9				[a]1.42		1.07	.66	[a].50	.95	1.17	1.39
9	flat	change	50	24.1	1.9	12.7								[a].93			
[b]10	plate		50	24.4	3.1	----		0	.04	[a].50	1.70	1.40	.94	[a].75	.41	.24	.36
11			50	25.6	2.6	9.9		0.07	0.05	[a]1.60		0.85	0.46	[a]0.38	0.40	0.68	0.95
12			50	25.0	2.3	10.9		0	0	[a]3.48	2.09	.99	.75	[a].82	1.09	1.31	1.52
13			50	25.0	2.6	9.6	Wake	.07	.04	[a]3.46	2.55	.98	.54		.35		1.02
[b]14			75	25.0	2.7	----		.04	.02	[a].88	1.82	1.48	1.11	[a].98	.93	1.11	1.34
15		↓	75	24.0	1.8	13.3		.05	.04	[a]3.90	2.71	1.28	1.00	[a]1.42	1.64	1.83	2.01
16		Spanwise	50	23.0	2.4	9.6	Wake										
17		static-	50	25.0	2.6	9.6									[a]0.94		
18		pressure	50	20.0	1.7	11.7	Wake							1.19	[a]1.38		
19		change	75	20.0	1.7	11.7	Wake							1.19			
20			50	20.0	1.6	12.5	Wake										
21		↓	50	21.0	1.9	11.0	Wake							.97			
22		Stream total-	50	20.0	1.6	12.5	I	0	0.52	[a]2.26	[a]1.98	[a]1.32	[a]1.38	[a]1.64			
23		pressure	50	20.0	1.6	12.5	I	0	.52	[a]2.26	[a]2.02	[a]1.32	[a]1.35				
24		change	50	17.0	1.4	12.1	I	0	.44	[a]2.48	[a]1.96	[a]1.41					
25			50	19.0	1.6	11.9	II	0	.66	[a]2.23	[a]1.94	[a]1.17		1.11	1.19		
26			50	20.0	1.6	12.5	II	0	.90	[a]2.10	[a]1.70	[a].98		.88	1.02	1.12	
27			50	20.0	1.8	11.1	II	0	0.90	[a]2.05		[a]1.06		0.88	1.02	1.12	
28			50	21.0	1.7	12.3	II	0	.61	[a]2.08		[a]1.08		.83	1.04	1.19	
29			50	20.0	1.8	11.1	III		1.33	[a]1.88				.83		1.02	
30			50	20.0	1.6	12.5	III		.86	[a]2.08						1.03	
31			50	21.0	1.7	12.3	III		1.68	[a]2.13							
32		↓	50	20.0	1.8	11.1	III		.88	[a]2.10							
33		Stream total	50	20.0	1.8	11.1	III		0.85	[a]2.10	[a]1.75		[a]0.67				
34		temperature	50	20.0	1.8	11.1	III		.80	[a]2.01	[a]1.72						
35		during combus-	50	20.0	1.9	10.5	III			[a]2.19	[a]1.74						
36		tion, chromel-	50	20.0	1.5	13.3	III			[a]2.19	[a]1.75						
37		alumel rake	50	18.0	1.9	9.5	II	0.04		[a]2.07		[a]0.82			0.73		
38			50	32.0	3.2	10.0	II	0.07		[a]2.04	[a]1.74	[a]0.90					[a]1.00
39			50	24.0	2.1	11.4	II	.04		[a]2.16	[a]1.79	[a].75	[a]0.45				[a].78
40			50	24.0	2.1	11.4	II	.03		[a]2.10	[a]1.80	[a].52	[a].50		0.70		
41			50	25.0	2.6	9.6	I	[a]0	[a]0.35	[a]2.13	[a]1.80	[a]1.14					
42		↓	50	25.0	2.5	10.0	I	[a]0	[a].44	[a]1.95	[a]1.72	[a].93					
43		Stream total	50	22.0	1.8	12.2	II	[a]0.06	[a]0.48	[a]2.04	[a]1.78	[a]0.93					
44		temperature	50	32.0	3.2	10.0	II	[a].03	[a].85	[a]2.04	[a]1.72	[a].94	0.60	0.61	0.67	0.72	
45		during combus-	50	35.0	3.7	9.5	II	[a].06	[a].50	[a]1.95	[a]1.75	[a].88	.51	.50			
46		tion, plati-	50	25.0	2.9	8.6	III	[a].07	[a].83	[a]1.83	[a]1.68	[a].89	.46	.39			
47		num - platinum + 13% rhodium rake	50	25.0	2.9	8.6	I	[a].11	[a].65	[a]2.04	[a]1.73	[a].93	.58	.66			
48		Stream static-	50	25.0	3.1	8.1	I			[a]1.86	[a]1.50	[a]0.88	0.65	0.63			
49		pressure change	50	25.0	4.1	6.1	III			[a]1.86	[a]1.50	[a].82	.35				
50	↓	below plate during combustion	50	25.0	3.0	8.3	II			[a]2.00	[a]2.02	[a]1.00	.65	.74			

[a]Measured with strain-gage-type pressure transducer.
[b]Runs 10 and 14 burned at two offcenter fuel orifices only (plug at center orifice).

COMBUSTION-RUN DATA

Static-pressure increase, in. Hg, at static pressure tap -																		Run
11	12	13	14	15	17	18	19	20	21	22	23	24	25	26	27	28	29	30	
0.84	0.41				[a]2.85	[a]3.21													1
			0.33		[a]1.67	[a]1.89													2
[a]1.03	.88		.75		[a]3.14	[a]3.18													3
[a].51	.28		.27		[a]2.56	[a]2.66													4
[a].55	.28		.41		[a]2.58	[a]3.01													5
0.31							[a]0.75	1.14	[a]1.35	1.44	[a]1.61	1.61						[a]3.80	6
1.66							[a]1.60	1.77	[a]1.76	1.99	[a]2.10	2.06						[a]4.05	7
1.66							[a]1.68	1.92	[a]1.93	2.24	[a]2.23	2.33						[a]4.35	8
							[a]1.65	2.38	[a]1.93	2.20	[a]2.18	2.26						[a]4.24	9
.67								1.36	[a]1.48	1.53	[a]1.66	1.59						[a]3.55	[b]10
1.32							[a]1.45	1.81	[a]1.86	2.04	[a]2.21	2.05						[a]4.10	11
1.74							[a]1.79	2.29	[a]2.17	2.21	[a]2.35	2.25						[a]4.32	12
1.33								1.77	[a]1.92	2.03	[a]2.18	2.08						[a]4.11	13
1.56							[a]1.64	1.77	[a]1.87	2.01	[a]1.96	1.86						[a]3.95	[b]14
2.14							[a]2.16	2.36	[a]2.48	2.56	[a]2.54	2.31						[a]4.27	15
[a]1.25		0.58		0.62				[a]1.91	2.02	2.19	2.25		2.10	2.07		2.18	[a]4.18	[a]4.35	16
[a]1.46			0.87	.99				[a]1.64	1.73	1.85	1.84		1.73	1.70	1.82	1.79	[a]3.91	[a]3.87	17
		1.10	1.03	1.12				[a]1.87	1.97	2.08	2.07		1.99	1.94	2.07	2.06	[a]3.88	[a]4.03	18
	1.29	1.22	1.24	1.35					1.96	2.09	2.08		1.97	1.90	2.10	2.09			19
																		[a]3.99	20
	1.02	.93	1.08	1.03					1.85	1.96	2.01		1.89	1.90	1.97	2.01		[a]4.05	21
	1.52	1.34	1.34	1.51															22
	1.42	1.40	1.31	1.54															23
	1.54	1.56	1.53	1.60															24
1.57	.85	1.00	1.03	.78			1.51	1.56	[a]1.89										25
1.45	.80	.93	.83	.91			1.47	1.67	[a]1.77										26
1.42	0.86	0.94	0.83	0.76			1.51	1.68	[a]1.74										27
1.46	.77	.97	.94	.78			1.47	1.70	[a]1.77										28
1.36							1.40		1.71	1.74	1.77		1.74	1.81	1.78	1.87			29
							1.50		1.77	1.80	1.82		1.81	1.82	1.85	1.88			30
							1.46	[a]1.58	1.76	1.77	1.82		1.79	1.85	1.85	1.86			31
							1.48	[a]1.57	1.74	1.78	1.82		1.83	1.87	1.83	1.85			32
							1.49	[a]1.60	1.72	1.76	1.82		1.79	1.86	1.83	1.81			33
							1.45		1.69	1.75	1.80		1.78	1.83	1.78	1.87			34
							1.44	[a]1.67	1.79	1.80	1.85		1.80	1.87	1.86	1.90			35
							1.47		1.77	1.80	1.86		1.88	1.83	1.87	1.90			36
				0.83			1.31		1.65										37
				0.78					1.64										38
				.84					1.73										39
1.09							1.38	[a]1.57	1.75										40
							1.46	[a]1.58									[a]4.01		41
																	[a]3.78		42
									[a]1.57										43
	0.51	0.67	0.47	0.67				1.46	[a]1.41										44
		.50	.28	.58															45
		.60		.48				1.27	1.36	1.41	1.43						[a]3.56		46
		.52		.53															47
		.64		.64															48
		.41		.40				0.37	0.45	0.67	0.55								49
		.57		.59															50

TABLE III. - TUNNEL TEST-SECTION CONDITIONS PRIOR TO COMBUSTION RUNS

Run	Model	Tunnel total pressure, P_0, in. Hg	Tunnel total temperature, T_0, °R	Dew point, °F	Mean Mach number below model, M	Mean static pressure, p_0	Mean static temperature, t, °R	Ignitor (fig. 5)
1	Short	46.95	564	-56	2.45	2.97	256	I
2	flat	47.72	564	-70	↓	3.02	256	I
3	plate	46.79	564	-64		2.96	256	I
4	↓	47.50	555	-65		3.01	252	I
5		47.65	558	-65		3.01	254	I
6	Extended	47.71	564	-49	2.46	2.97	255	II
7	flat	47.73	560	-44	↓	2.97	253	II
8	plate	47.86	560	-50		2.98	253	II
9	↑	46.74	566	-50		2.91	256	II
10		47.26	560	-48		2.94	253	II
11		47.19	562	-44		2.94	254	II
12		47.29	554	-26		2.95	251	II
13		47.80	555	-52		2.98	251	II
14		47.52	556	-48		2.96	252	II
15		47.40	557	-48		2.95	252	II
16		47.30	557	-50		2.95	252	II
17		47.57	555	-42		2.96	251	II
18		47.43	560	-60		2.95	253	II
19		47.63	560	-65		2.97	253	II
20		47.24	559	-45		2.94	253	II
21		47.42	563	-45		2.95	255	II
22		47.85	566	-56		2.98	256	II
23		47.01	564	-56		2.93	255	II
24		47.29	574	---		2.95	260	II
25		48.80	520	-61		3.04	235	III
26		48.80	566	-60		3.04	256	III
27		48.65	553	-50		3.03	250	III
28		48.26	552	-55		3.01	250	III
29		47.39	559	-78		2.95	253	III
30		47.56	562	-55		2.96	254	III
31		47.35	558	-48		2.95	252	III
32		47.75	562	-48		2.97	254	III
33		47.34	562	-43		2.95	254	III
34		47.40	558	-47		2.95	252	III
35		47.35	563	-49		2.95	255	III
36		47.49	560	-41		2.96	253	III
37		46.95	559	-45		2.92	253	III
38		47.16	563	-47		2.94	255	III
39		47.60	561	-60		2.97	254	III
40		47.49	563	-60		2.96	255	III
41		47.64	558	-53		2.97	252	III
42		47.83	566	-53		2.98	256	III
43		47.64	556	-60		2.97	252	III
44		47.60	558	-42		2.97	252	III
45		48.06	563	-34		2.99	255	III
46		47.85	556	-52		2.98	252	III
47		47.85	562	-45		2.98	254	III
48		47.71	561	-25		2.97	254	III
49		47.48	562	-18		2.96	254	III
50	↓	47.93	559	-28	↓	2.99	253	III

TABLE IV. - INDICATED TOTAL TEMPERATURES DURING COMBUSTION

(a) Measurements in stream adjacent to flat-plate surface

Run	Thermocouple											
	Chromel-alumel						Platinum - platinum plus 13 percent rhodium					
	Distance from flat-plate surface, in.											
	1/4	3/4	1 1/4	1 3/4	2 1/4	2 3/4	1/4	3/4	1 1/4	1 3/4	2 1/4	2 3/4
	Temperature, °R											
Rake station I, 5.25 in. from fuel orifice												
41	2810	>3010	1040	580	560							
42	2810	3010	640	700	570							
47							3160	2790	660			
Rake station II, 15.5 in. from fuel orifice												
37	2090	2450	2090	2240	1720	740						
38	2600	2740	2590	2190	1400	620						
39	2700	2370	2290	1940	1820	850						
40	2640	2400	2360	2110	1940	890						
43								3240	2410	2060	1350	580
44							2870	3470	3230	2400	1430	560
45							2880	3370	2710	2030	1060	630
Rake station III, 20.0 in. from fuel orifice												
33	1860	2240	>2310	2280	1550	540						
34	1910	2110	2510	2390	1490	560						
35	1850	1980	2260	2440	1560	560						
36	1780	2630	2160	2310	1550	560						
46							2460	2790	2540	2020	1250	680

(b) Wake measurements, 28.5 in. from fuel orifice

Run	Distance from plane of flat-plate surface, in.					
	-1/4	1/4	1/2	1	1 1/4	1 3/4
	Temperature, °R					
6	700		830		910	
7	1490		1450		660	
13		1830		880		540
16		1730		1600		760
18		1420		810		
19		1260		680		
20		1410		840		
21		1570		910		

[redacted]

TABLE V. - INDICATED TOTAL-PRESSURE CHANGES DUE TO COMBUSTION

Rake station	Run	Distance from flat-plate surface, in.						
		1/4	3/4	$1\frac{1}{4}$	$1\frac{3}{4}$	$2\frac{1}{4}$	$2\frac{3}{4}$	$3\frac{1}{4}$
		Pressure change, in. Hg						
I	22	-19.0	-18.6	-3.5, -10.5	6.25			
	23	-20.0	-18.4	-7.8, -11.7	6.25			
	24	-18.55	-18.0	-2.2, -7.4	6.02	6.53	6.14	
II	25	-19.1	-19.1	-17.95	-16.7	-16.6	-8.0	
	26	-19.1	-19.1	-17.45	-16.45	-14.7	3.8, -8.0	
	27	-19.1	-19.0	-18.67	-17.95	-15.8	2.98, -4.02	7.8
	28	-19.1	-18.7	-17.95	-17.93	-15.95	2.13, -3.7	7.3
III	29	-19.4	-19.6	-19.4	-19.1	-16.95	7.8	7.8
	30	-19.4	-19.45	-18.8	-19.0	-15.6	7.95	7.4
	31	-19.7	-18.6	-19.4	-18.6	-15.9	8.03	7.64
	32	-19.8	-18.0	-19.4	-18.5	-15.7	7.95	7.50

4138

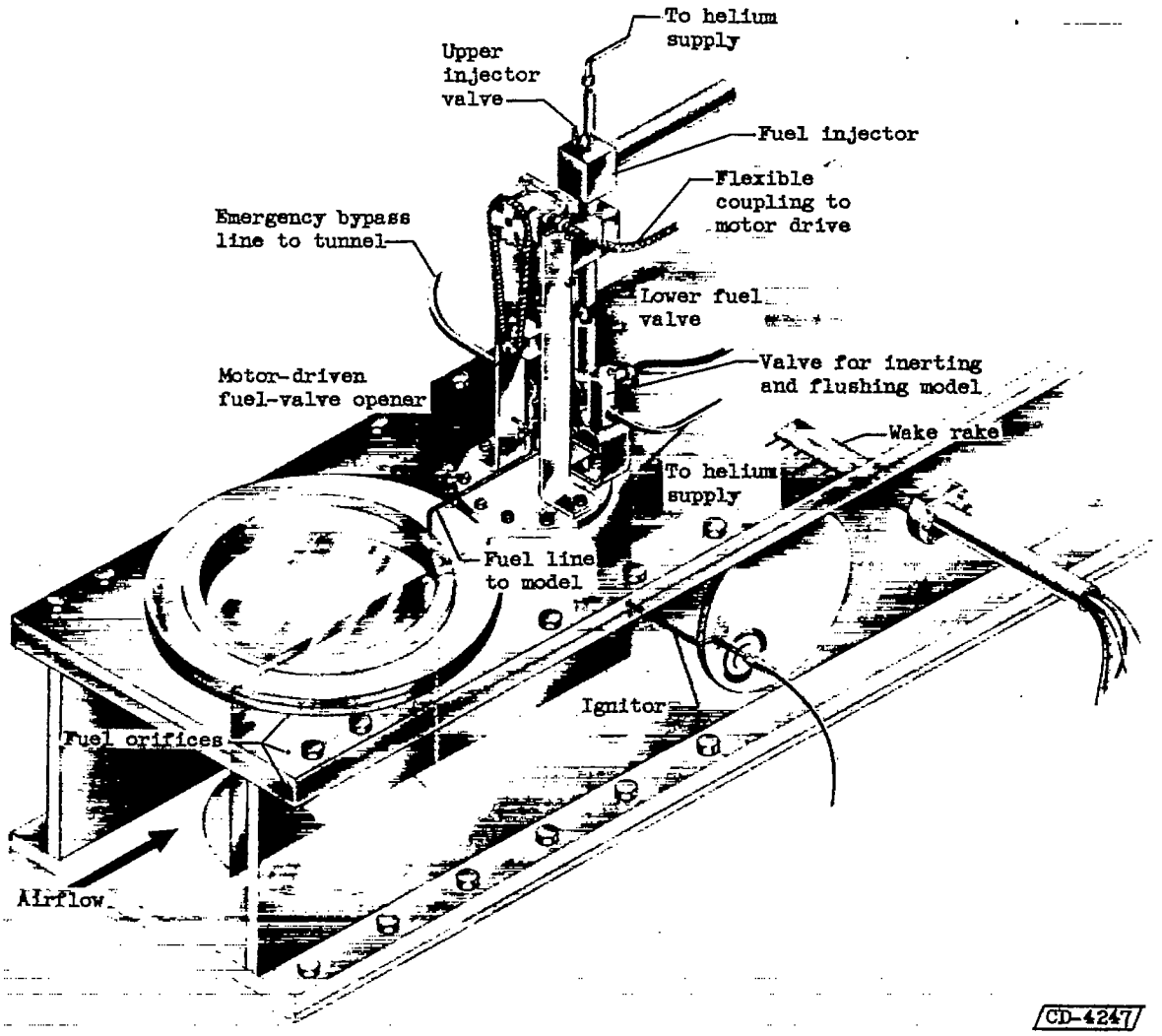

Figure 1. - Flat-plate-model installation in 1- by 1-foot test section.

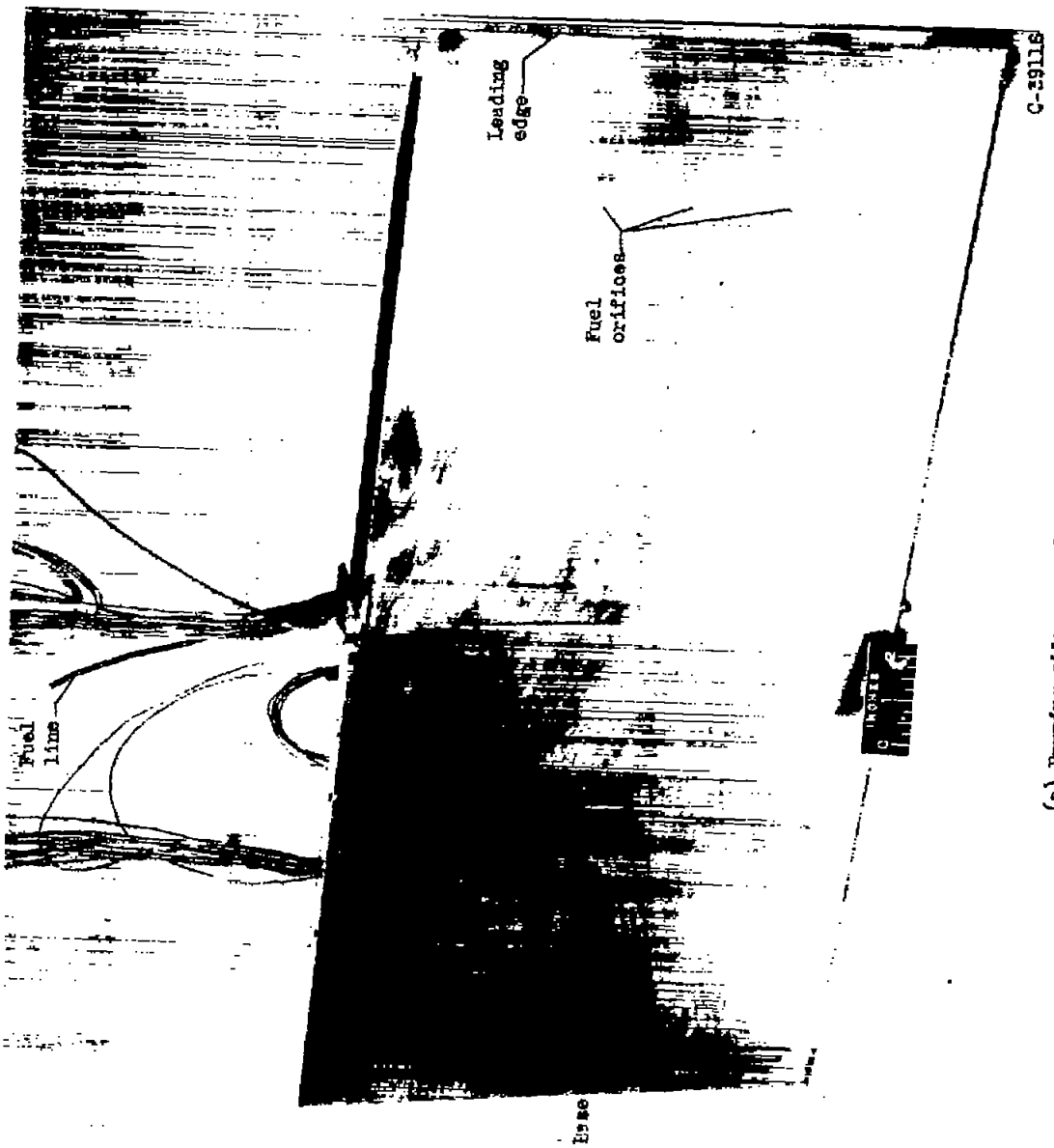

(a) Burning side, or reference surface.

Figure 2. - Extended flat-plate model.

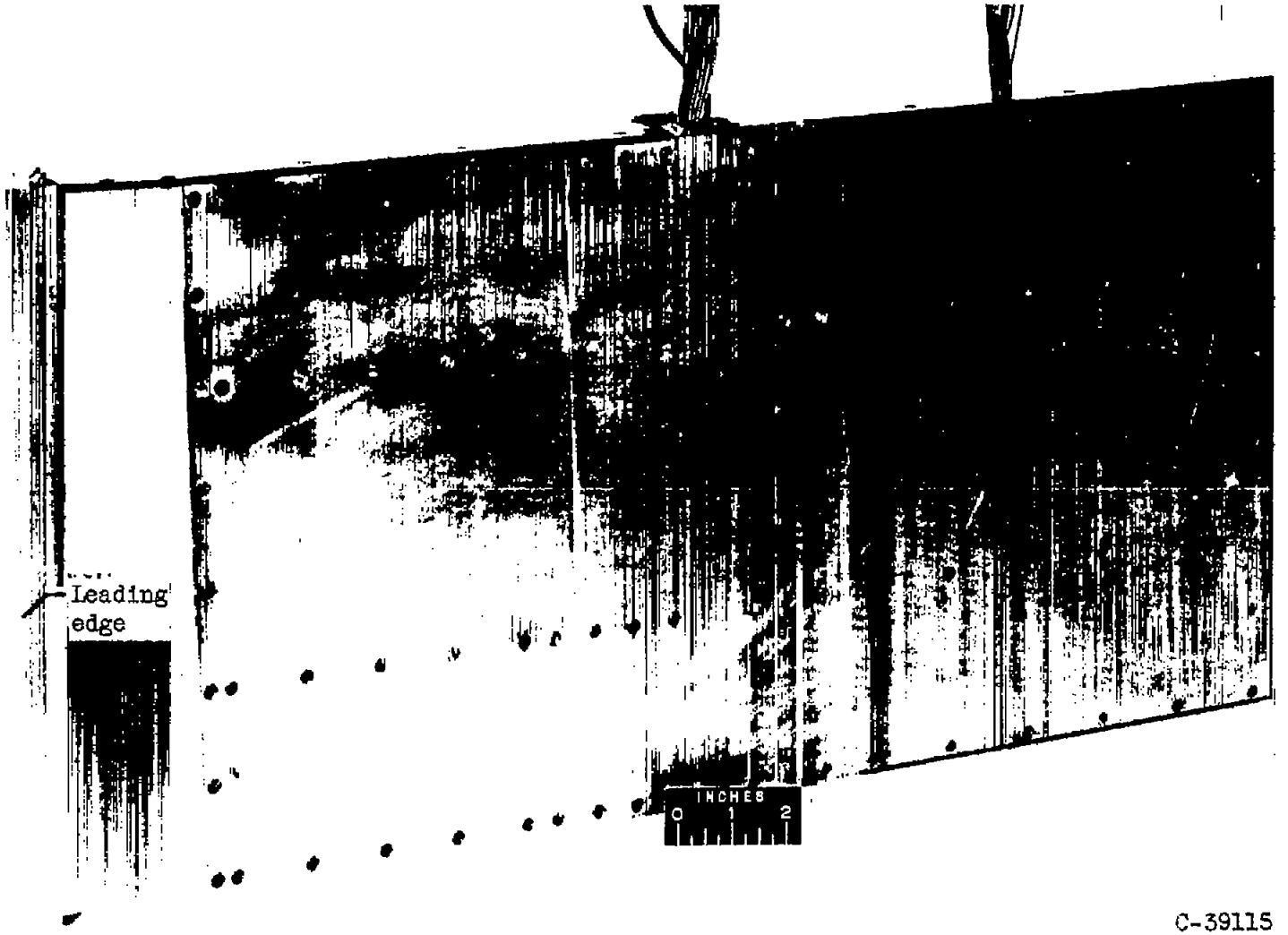

C-39115

(b) Nonburning side.

Figure 2. - Concluded. Extended flat-plate model.

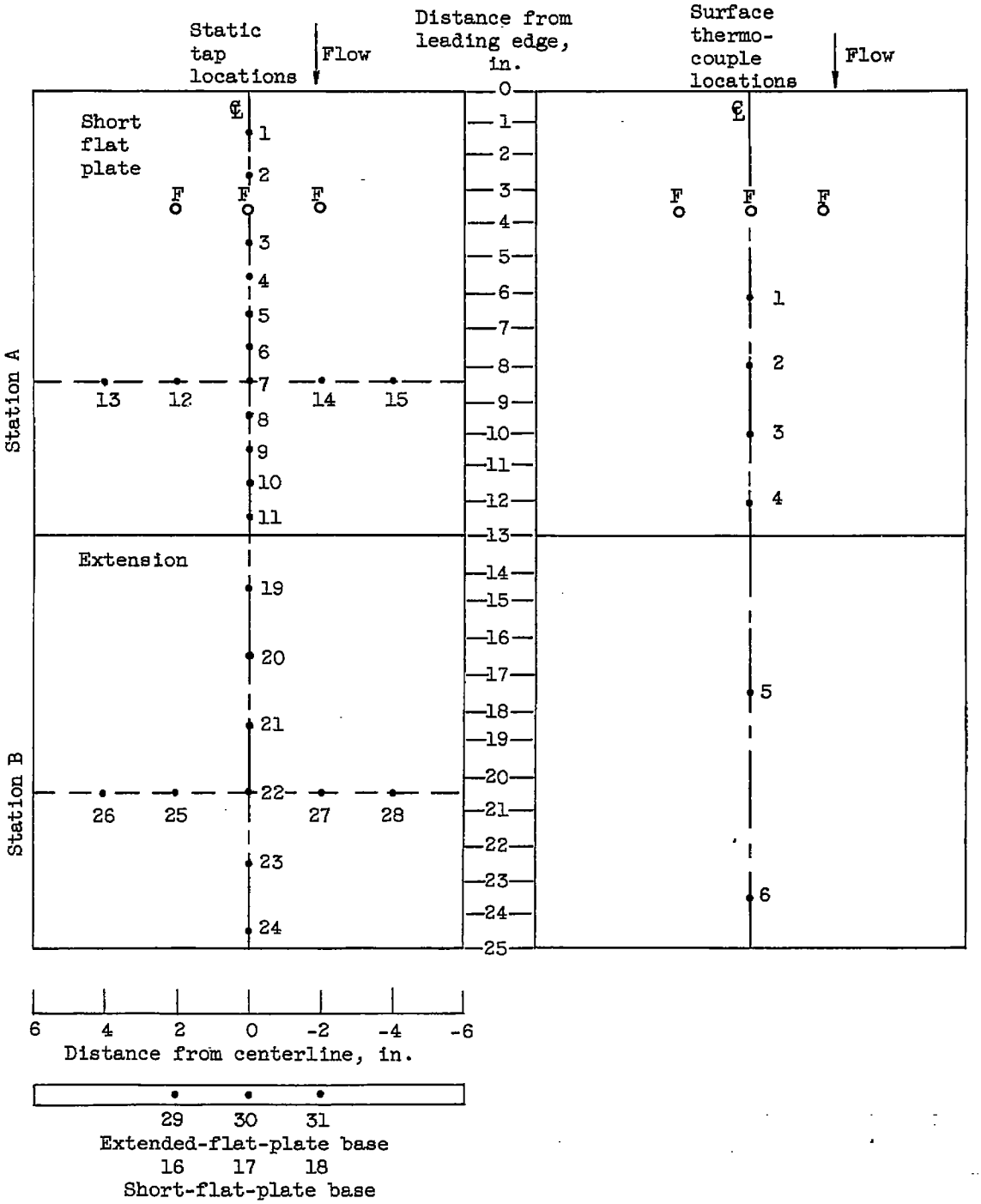

Figure 3. - Location of fuel orifices F, static-pressure taps, and thermocouple junctions in flat-plate-model surface.

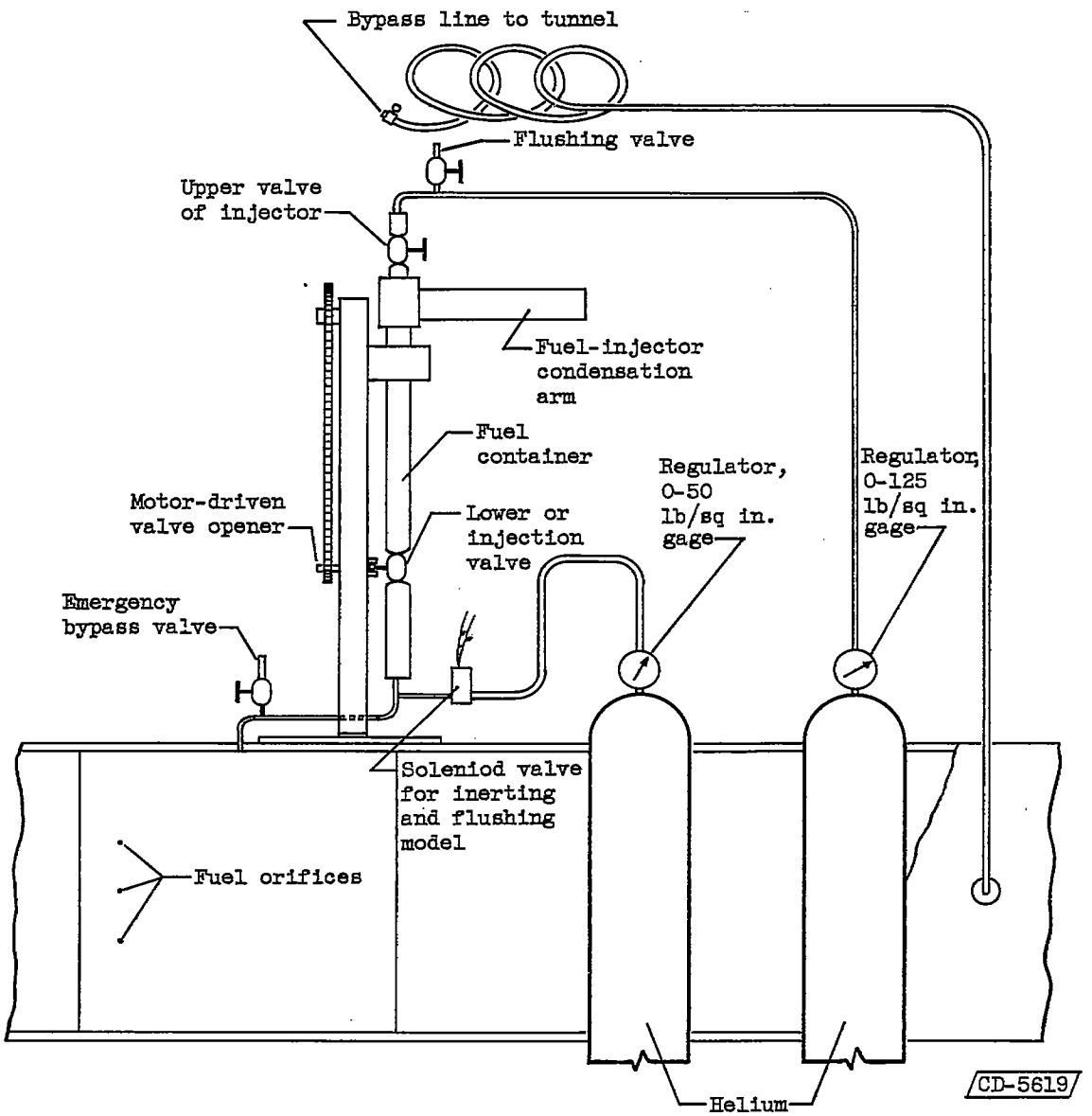

(a) Schematic sketch.

Figure 4. - Fuel-injection system.

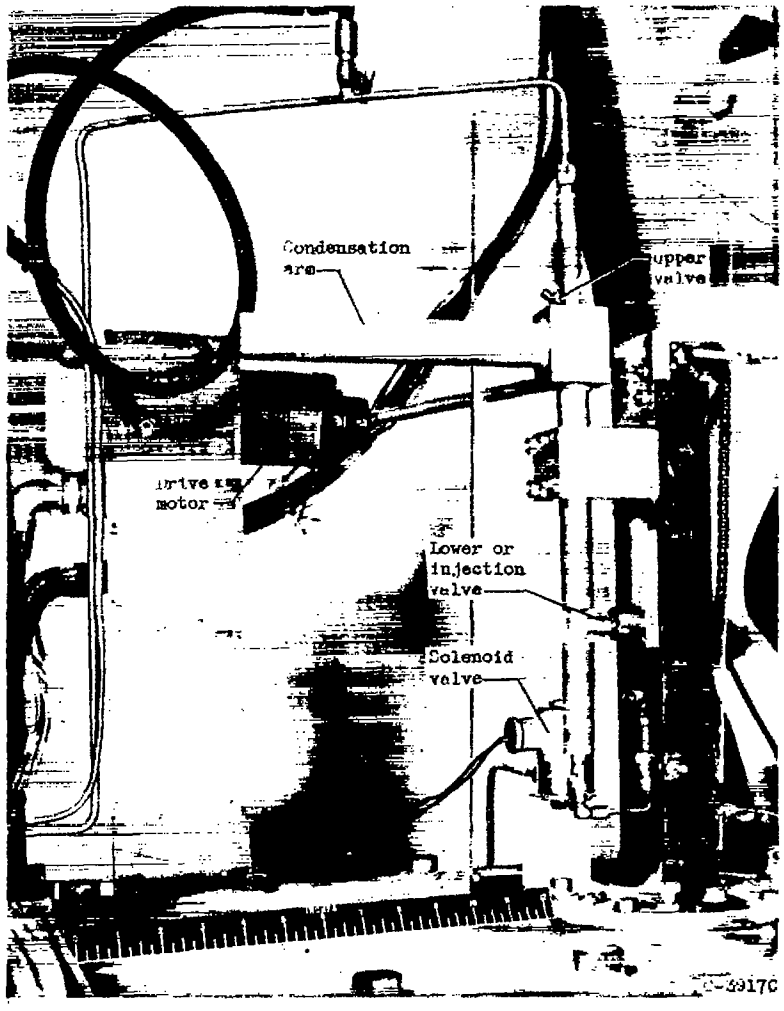

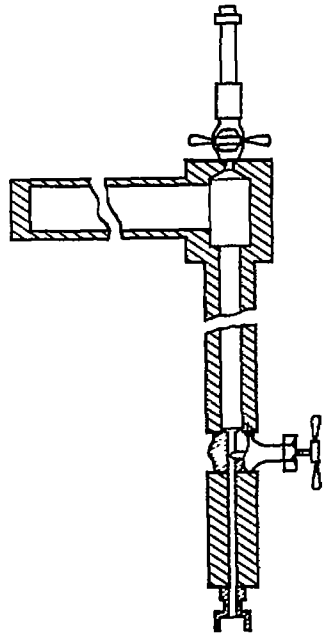

(b) Valve-type fuel injector.

Figure 4. - Continued. Fuel-injection system.

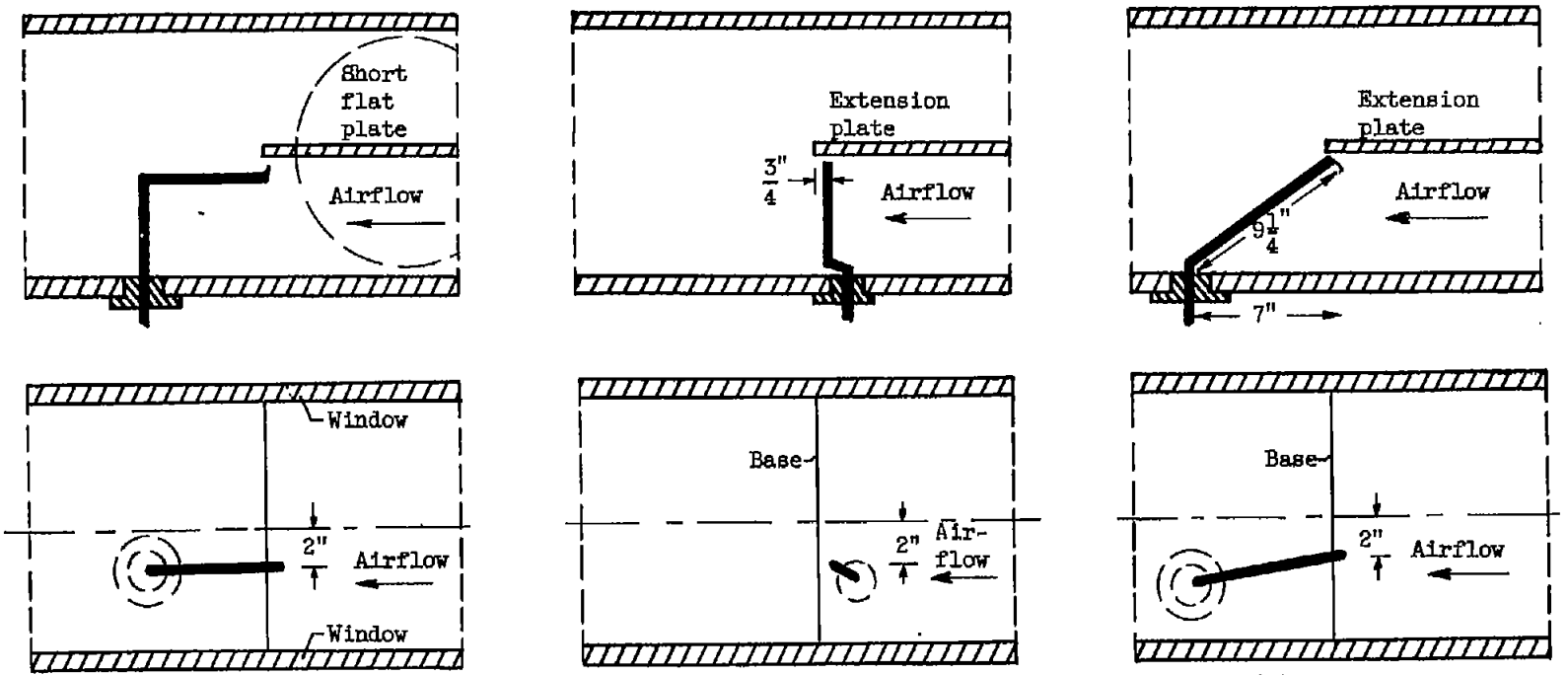

(a) Ignitor I. (b) Ignitor II. (c) Ignitor III.

Figure 5. - Ignitor configurations employed.

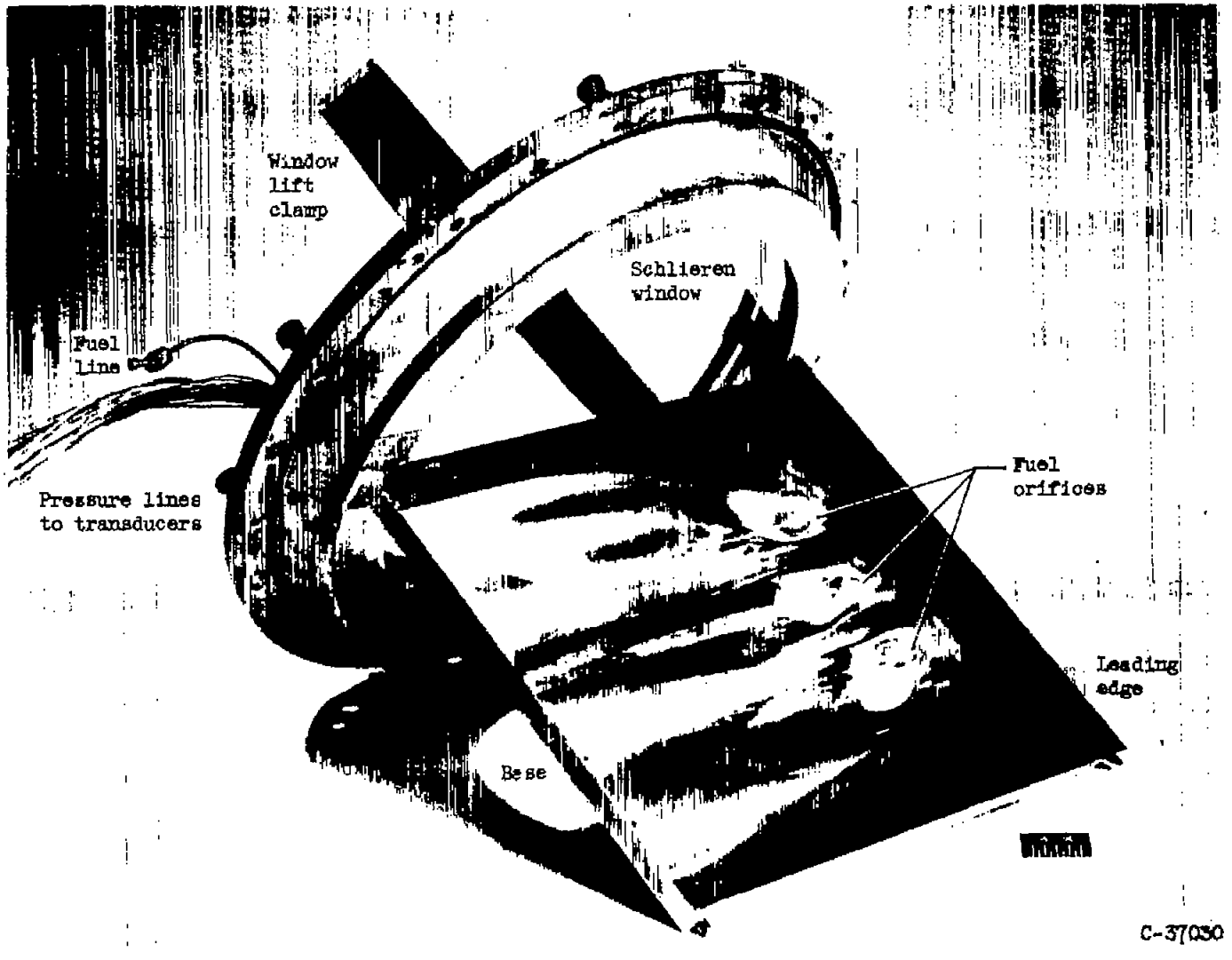

Figure 6. - Short-flat-plate model attached to schlieren window retaining ring. Ash deposit on surface resulted from combustion run.

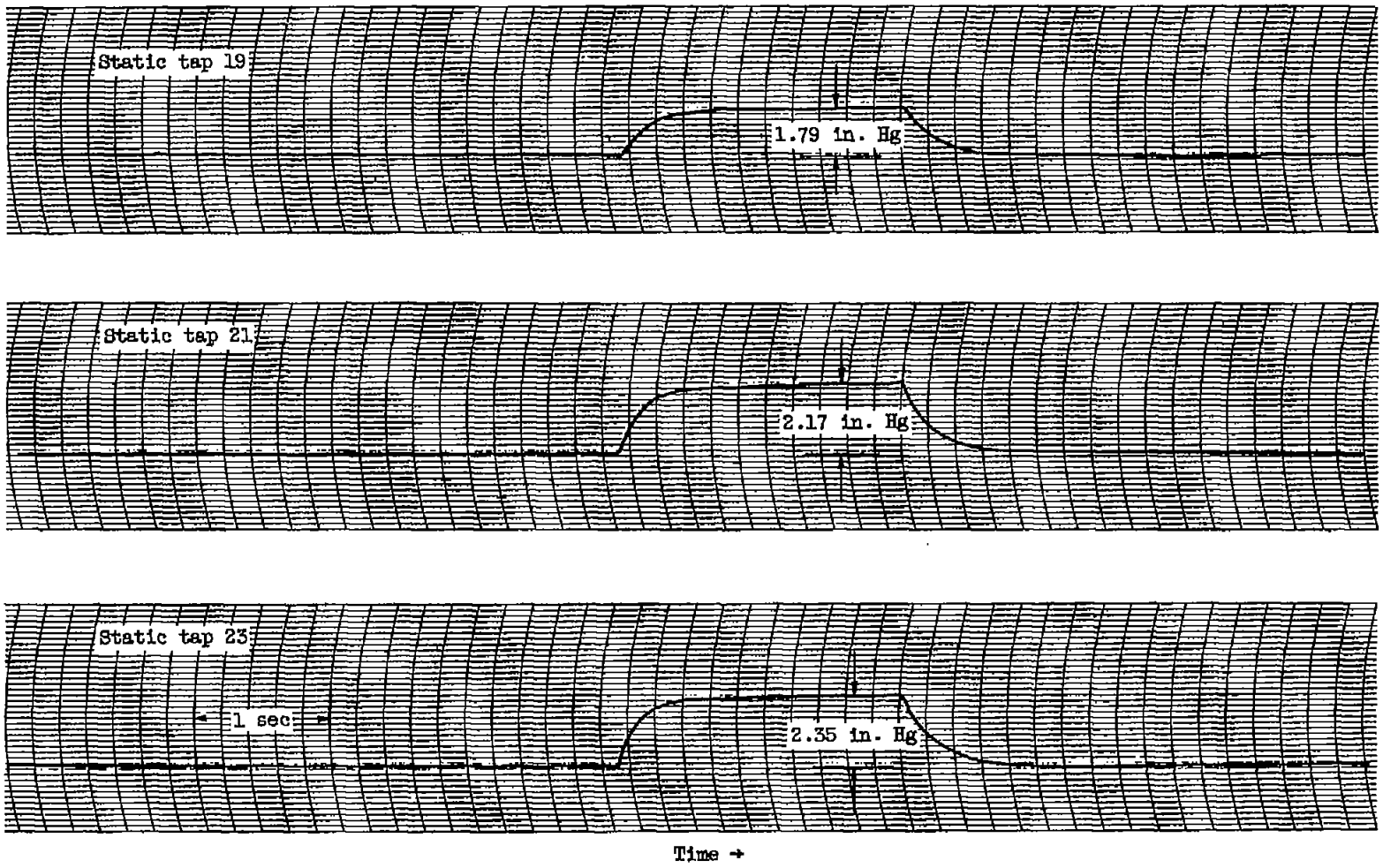

(a) Strain-gage; run 12, table II.

Figure 7. - Traces of static-pressure changes from strain-gage and six-capsule differential-pressure-transducer records.

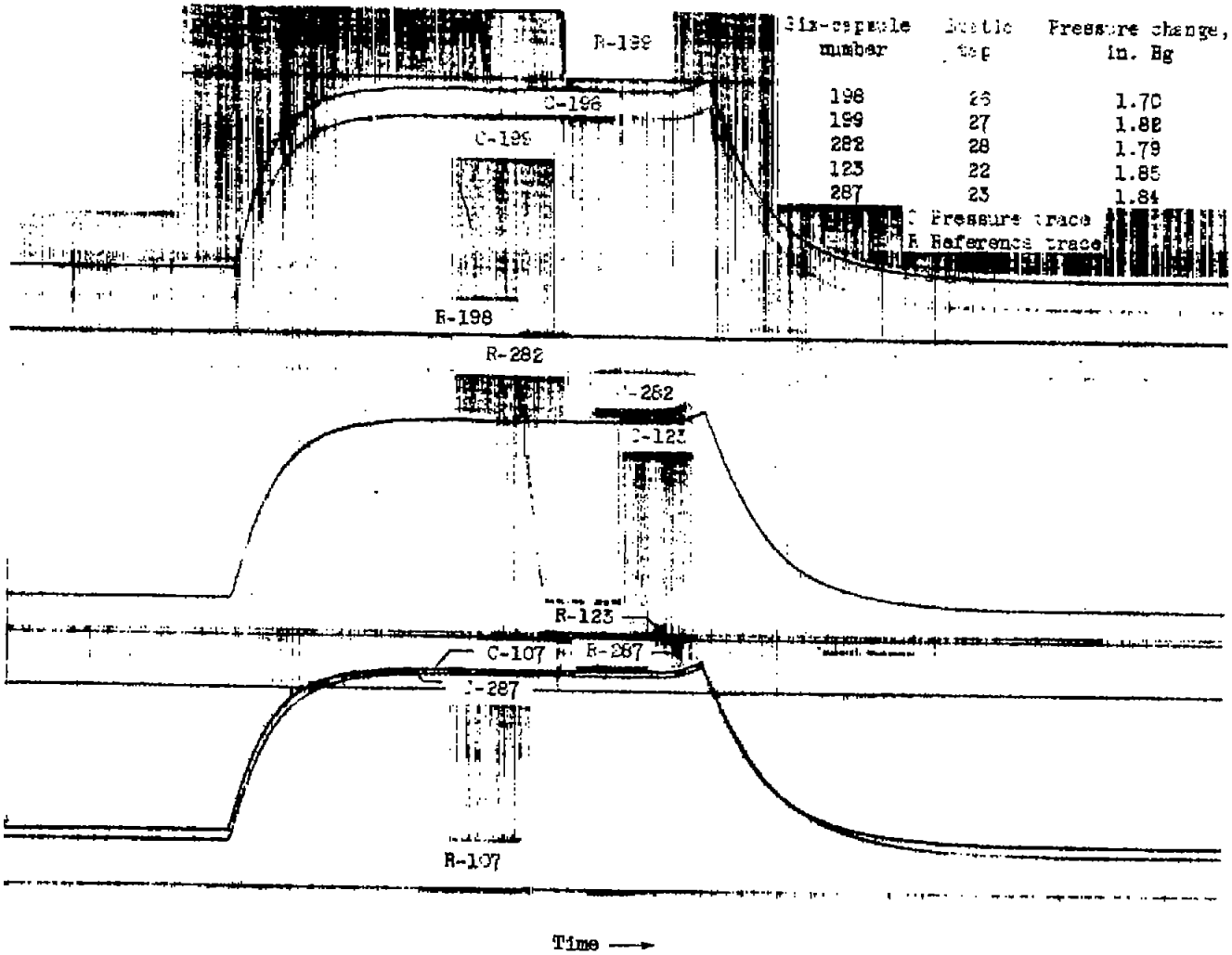

(b) Six-capsule; run 17 of table II.

Figure 7. - Concluded. Traces of static-pressure changes from strain-gage and six-capsule differential-pressure-transducer records.

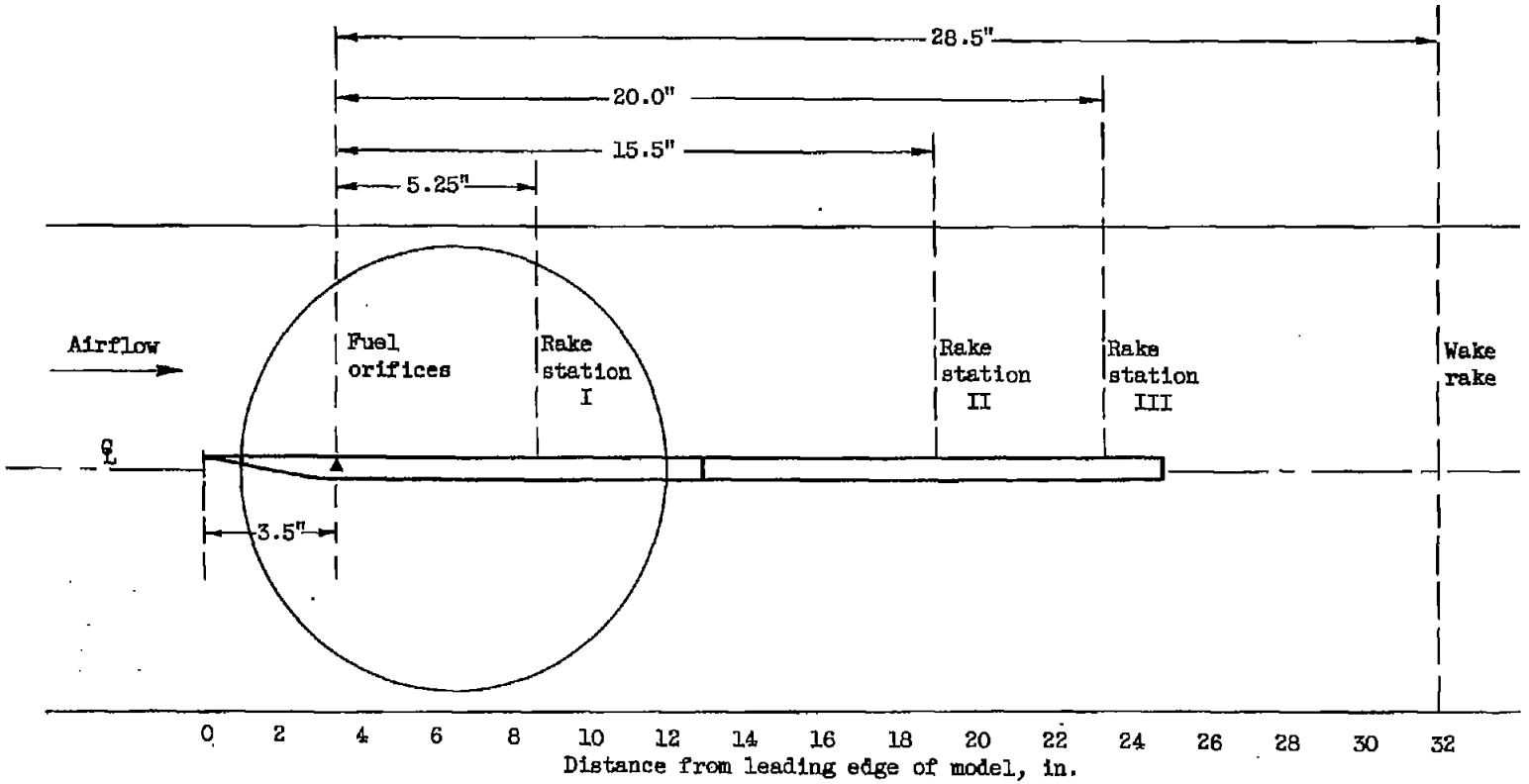

Figure 8. - Location of stream measuring stations in centerline plane perpendicular to model surface.

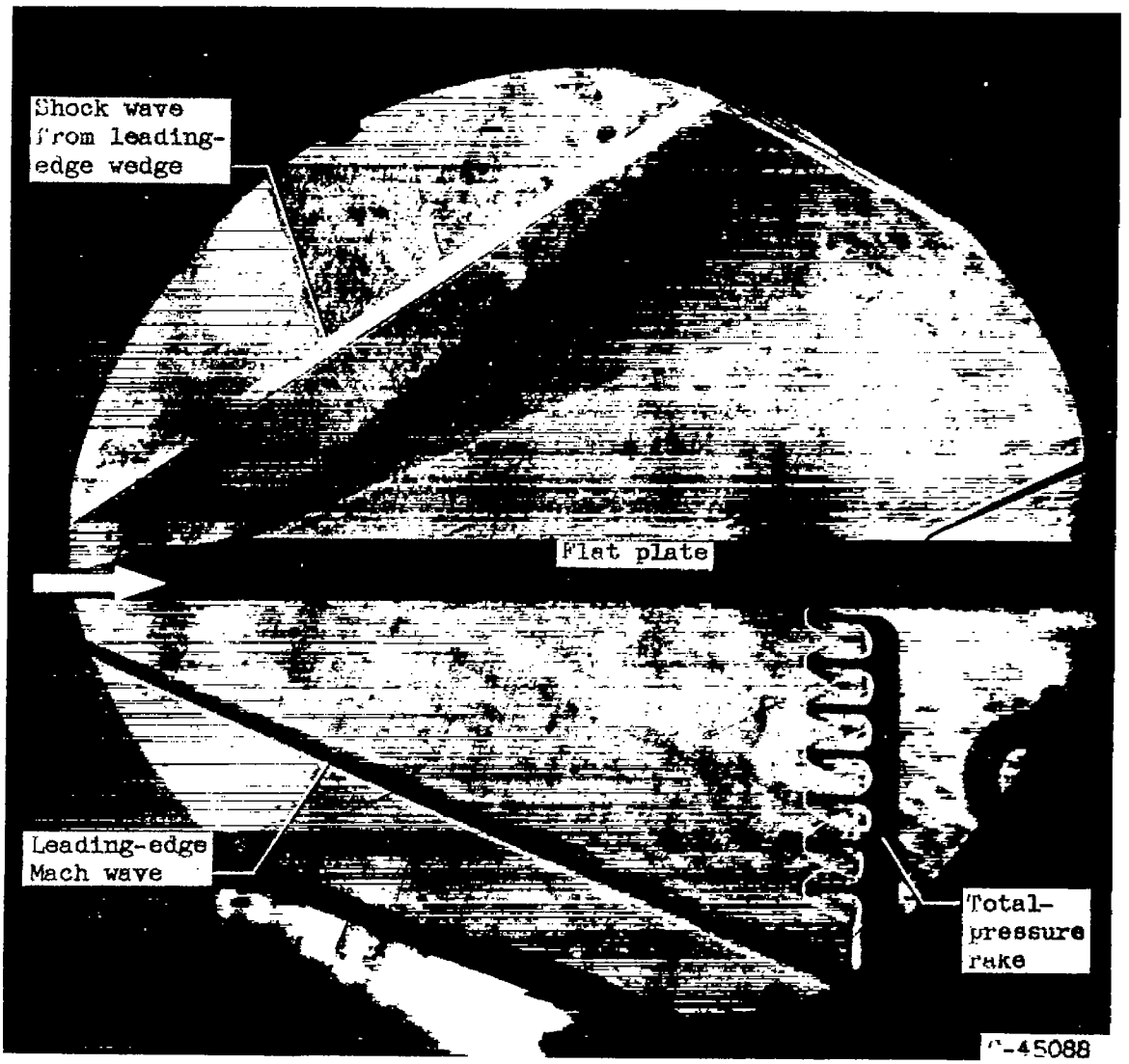

Figure 9. - Schlieren photograph of total-pressure rake at station I (upstream station).

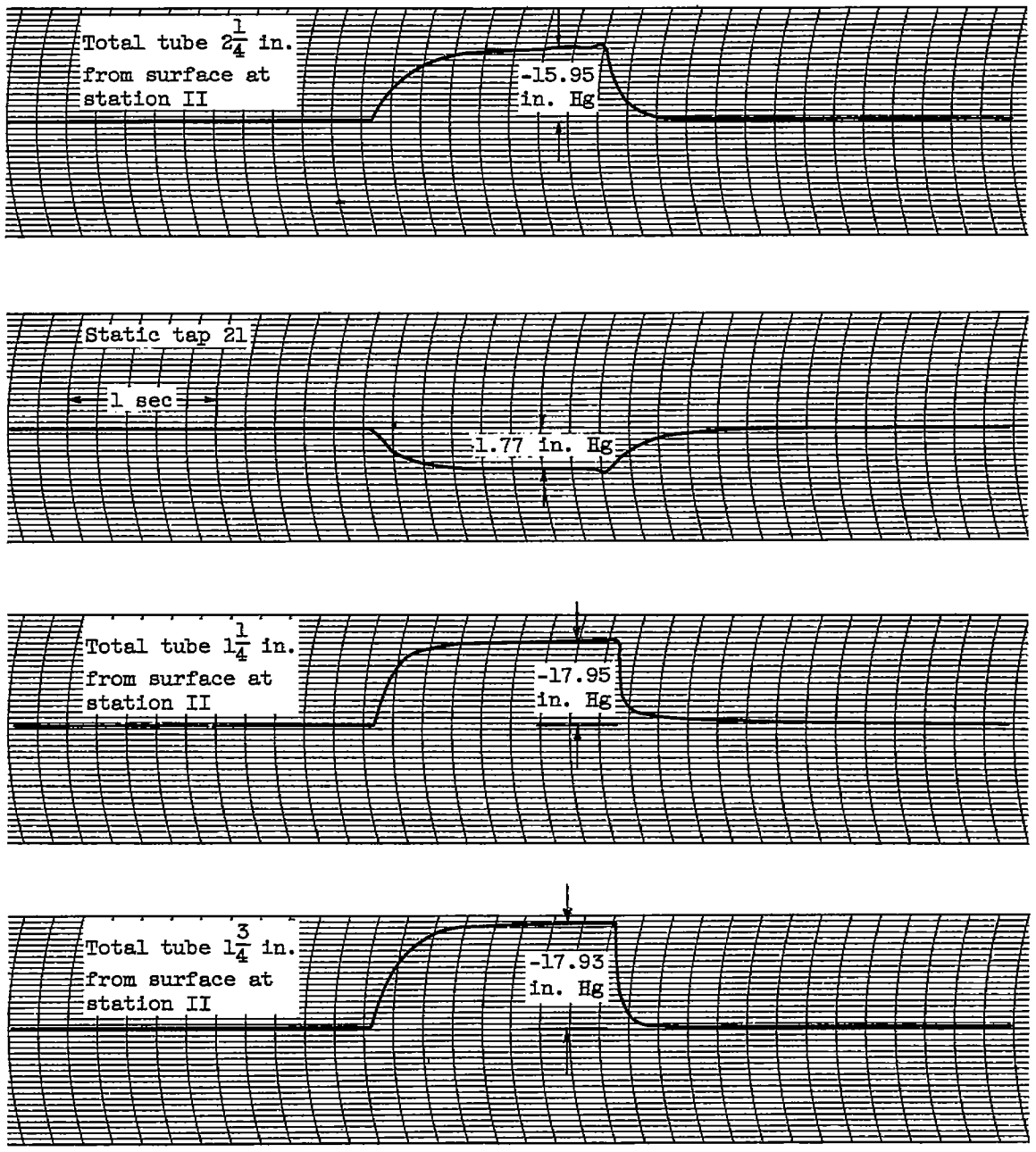

Figure 10. - Traces of indicated pressure changes from strain-gage-type pressure-transducer record for total-pressure rake during run 28 of table II. Shown for comparison is trace of one static-pressure change from same run.

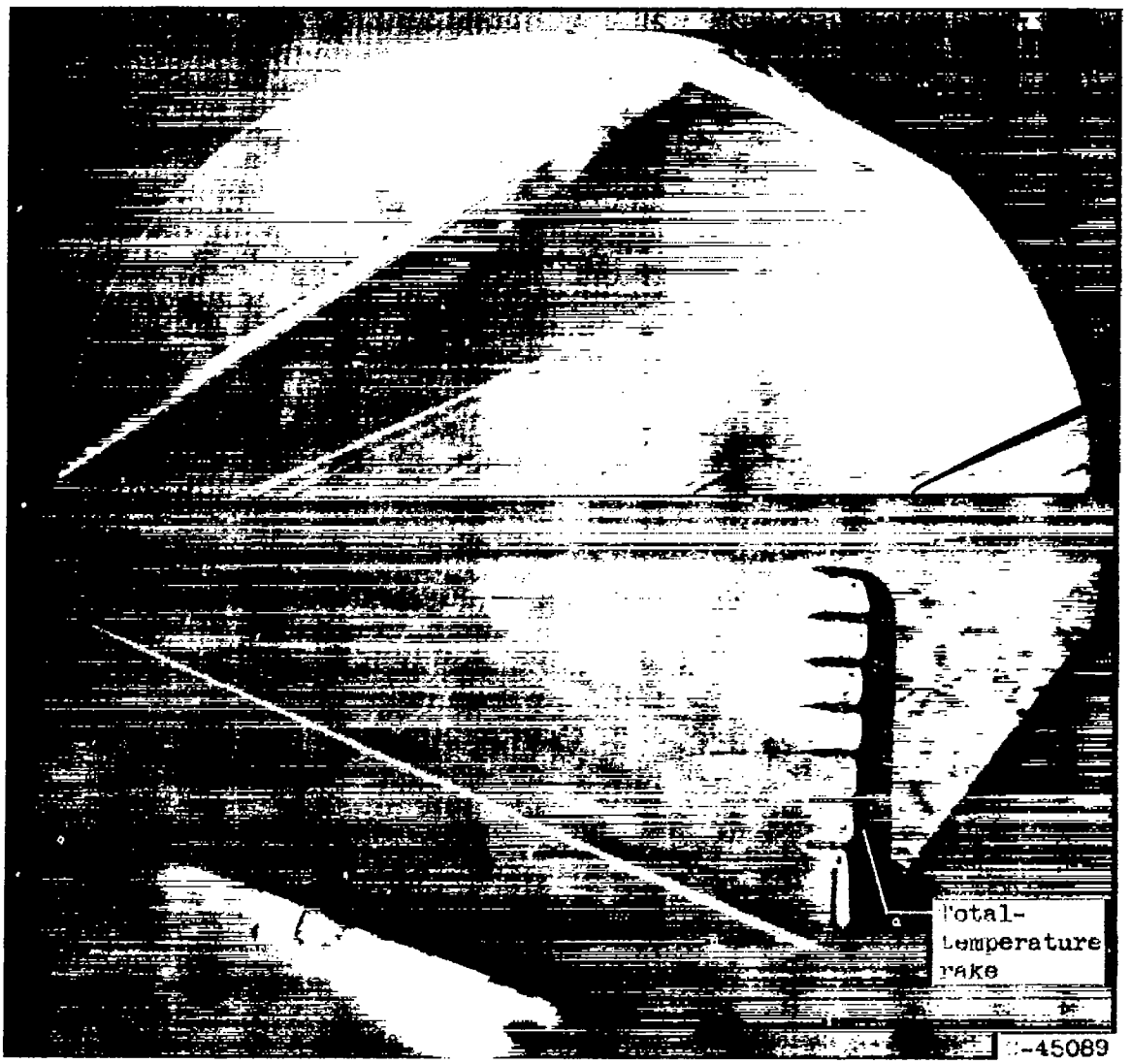

Figure 11. - Schlieren photograph of thermocouple rake in stream at station 1.

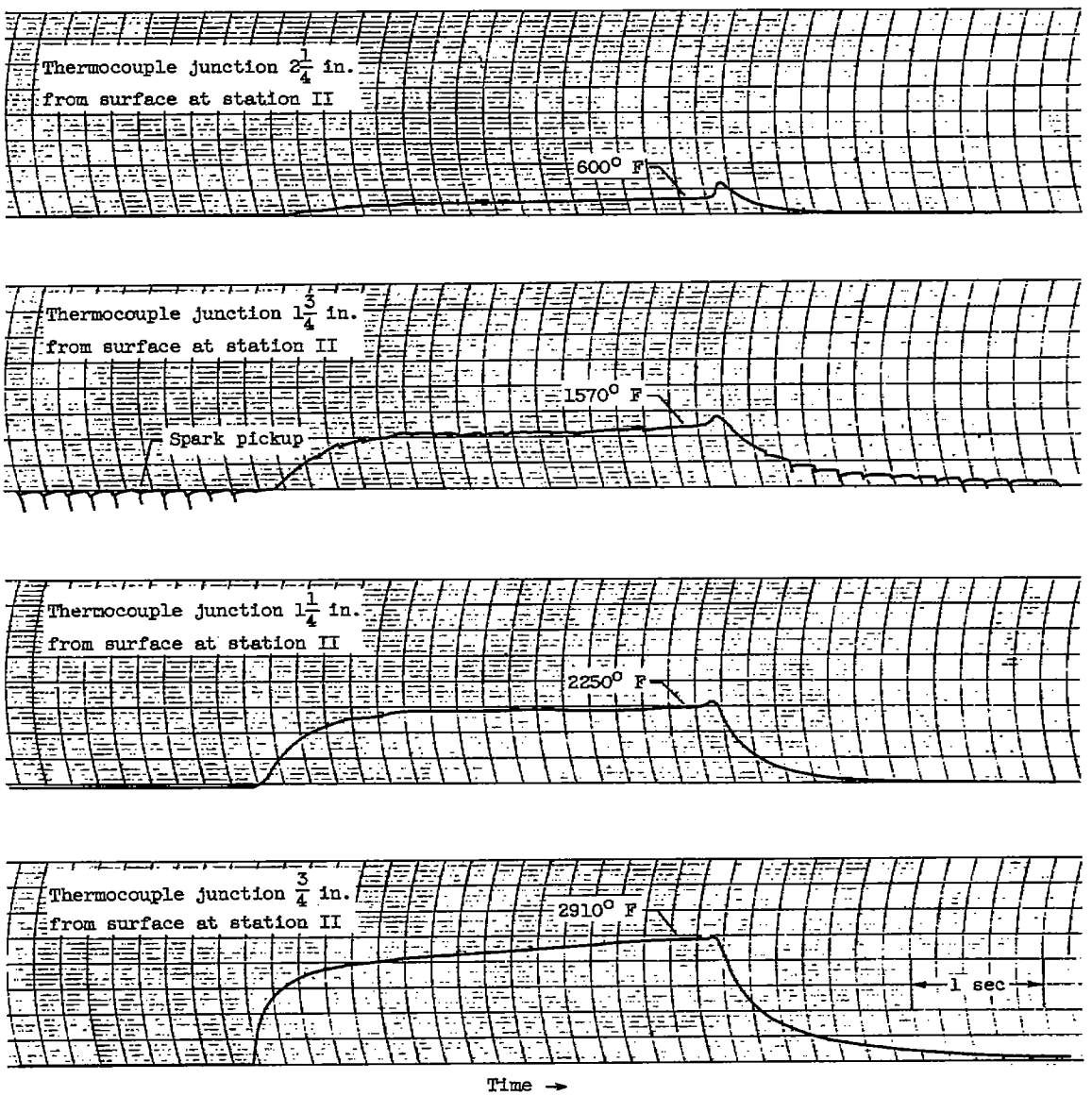

Figure 12. - Sample indicated temperature traces obtained during combustion from total-temperature-rake recorder. (Run 45 of table II; platinum - platinum plus 13 percent rhodium thermocouples.)

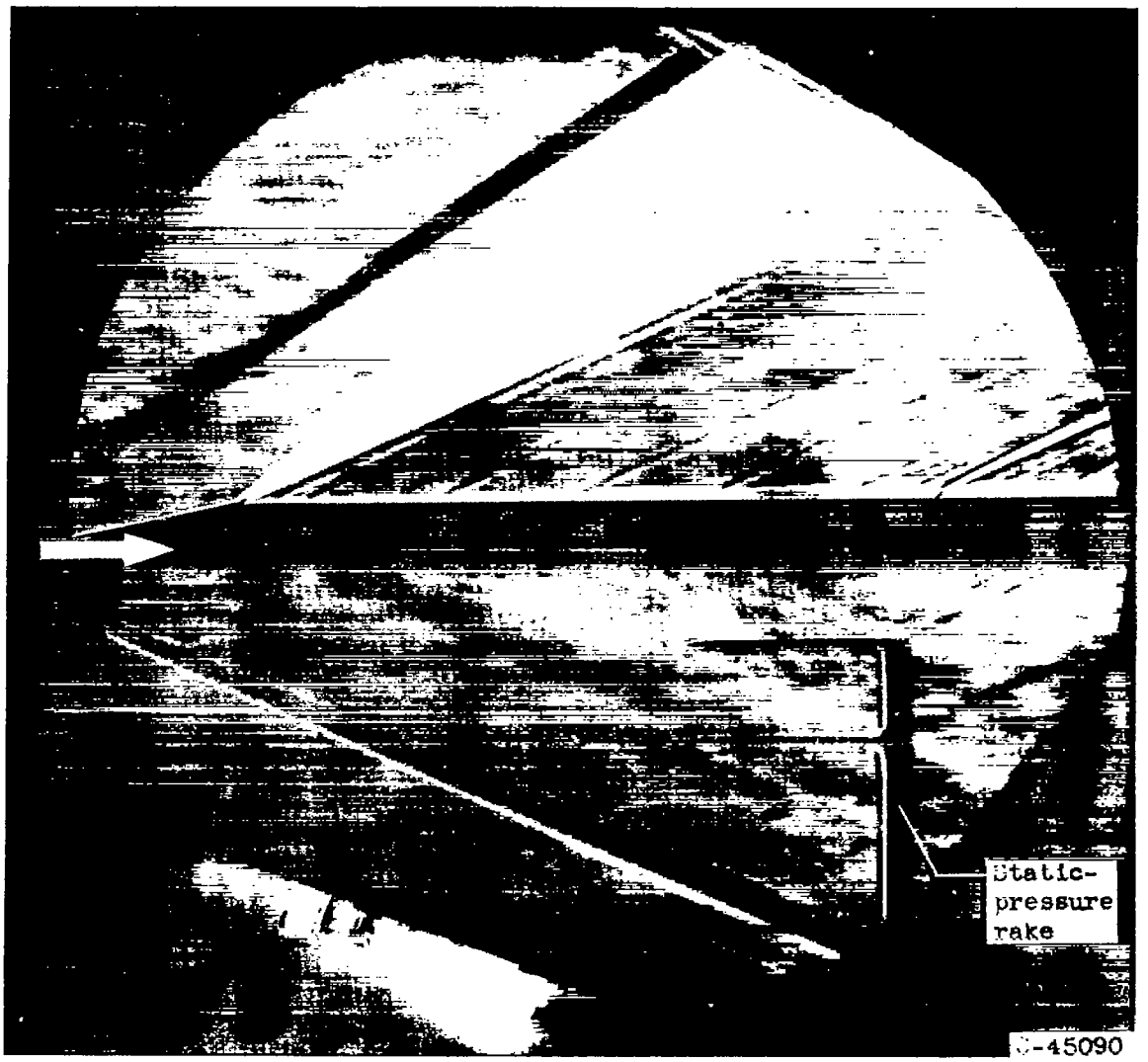

Figure 13. - Schlieren photograph of static-pressure rake in stream.

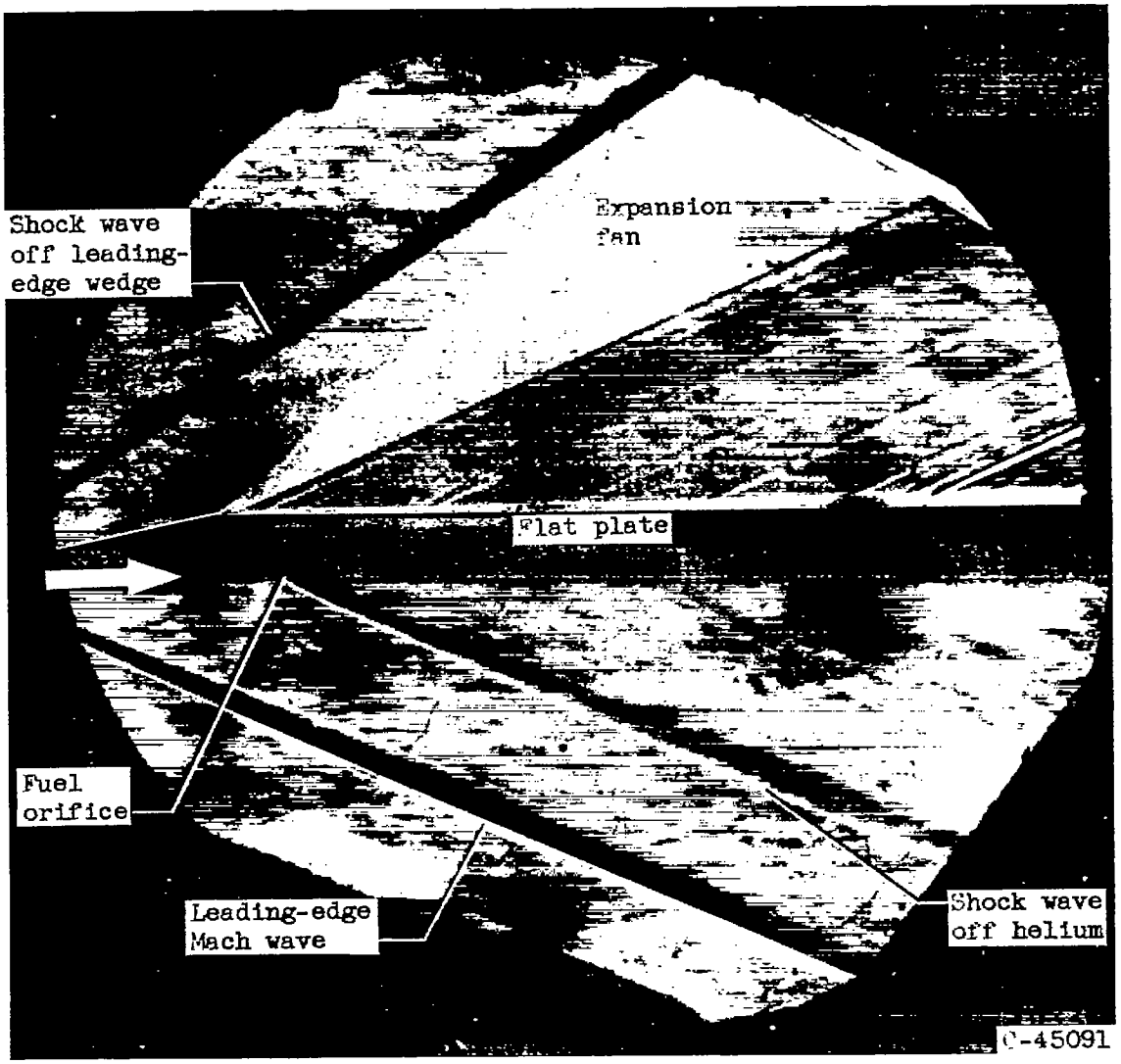

(a) Prior to combustion. Inerting helium is streaming out fuel orifices causing weak shock system.

Figure 14. - Combination open-shutter and schlieren flash photographs of combustion runs.

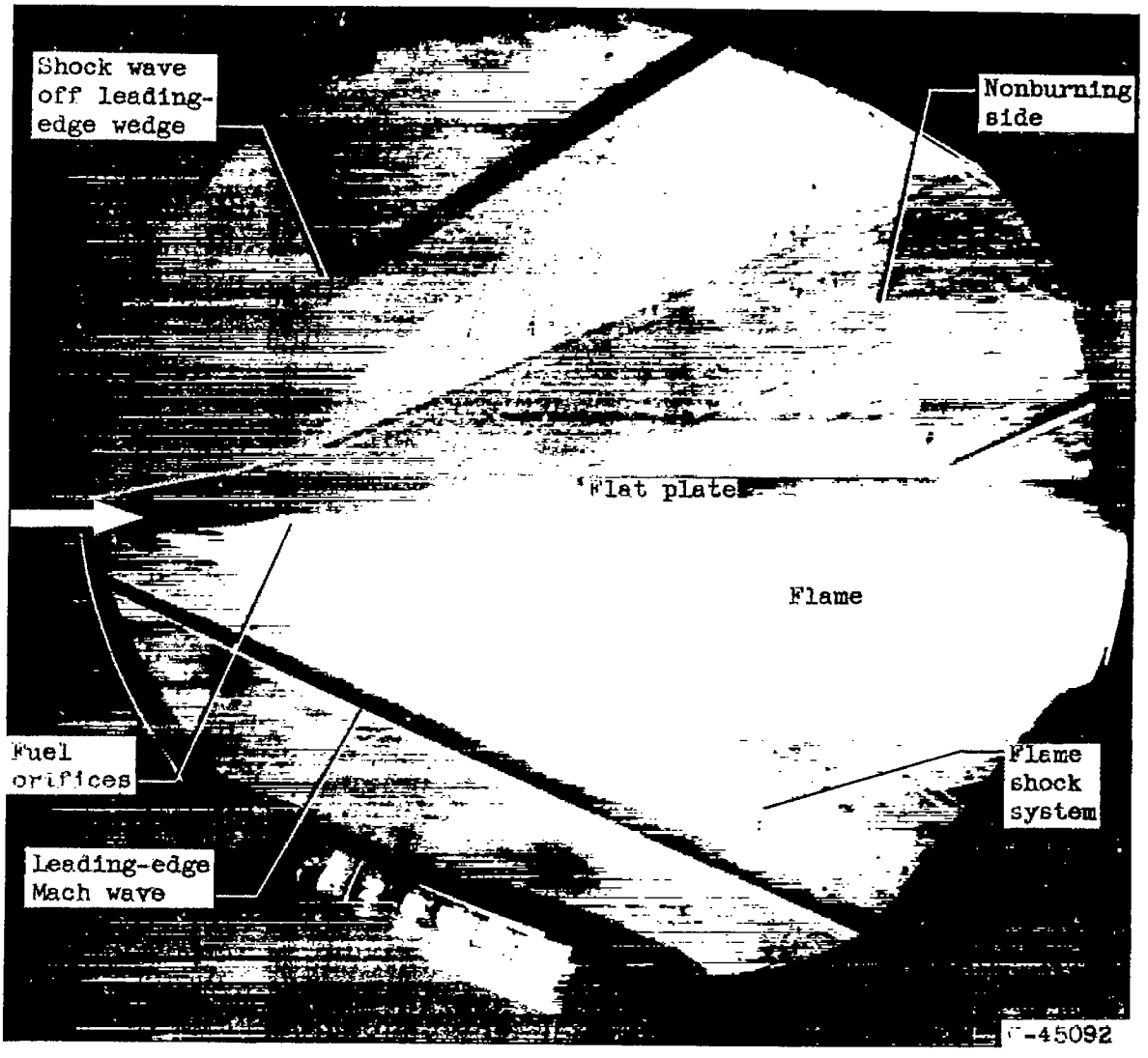

(b) Combustion run 31 (table II).

Figure 14. - Continued. Combination open-shutter and schlieren flash photographs of combustion runs.

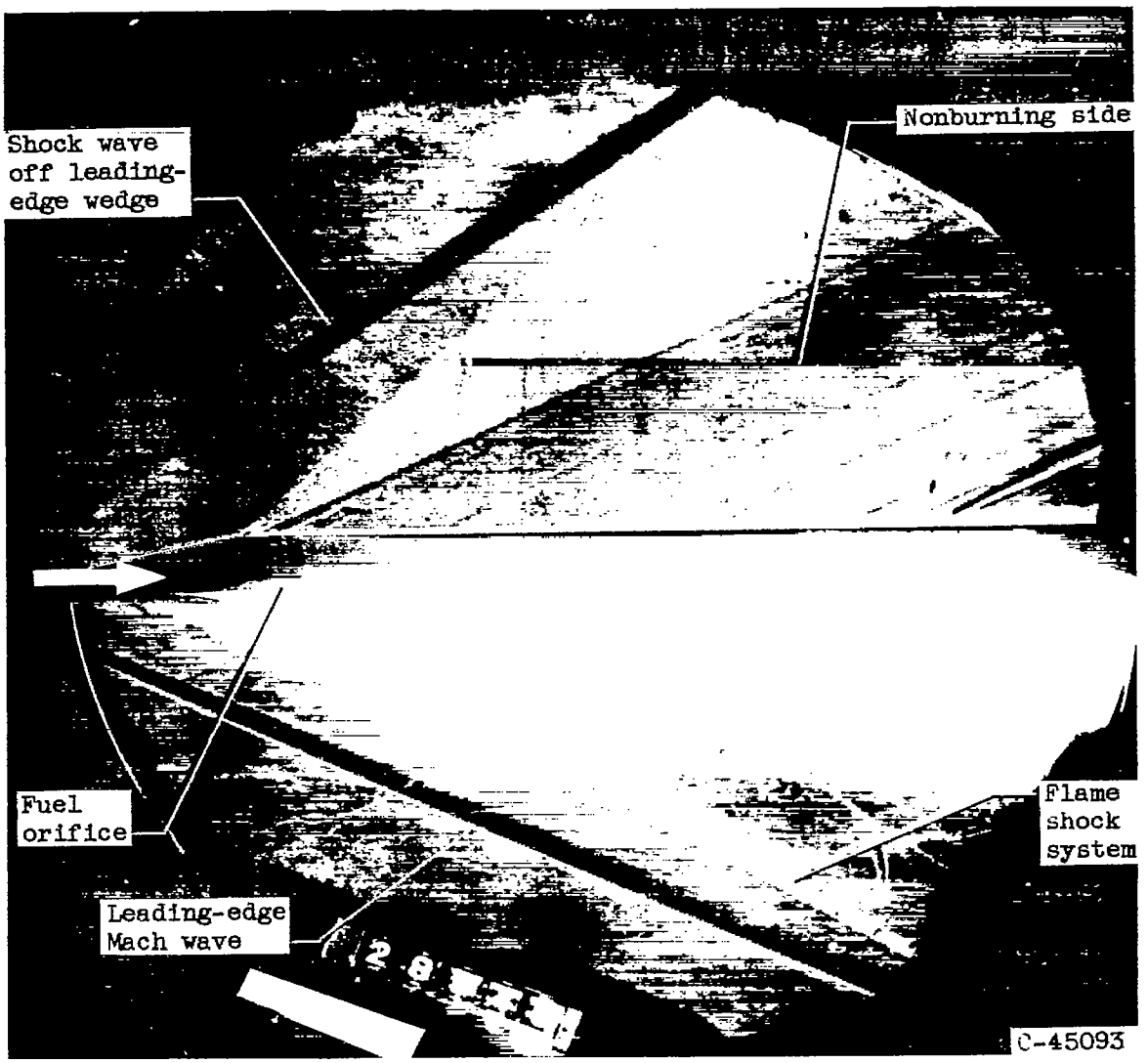

(c) Combustion run 32 (table II).

Figure 14. - Concluded. Combination open-shutter and schlieren flash photographs of combustion runs.

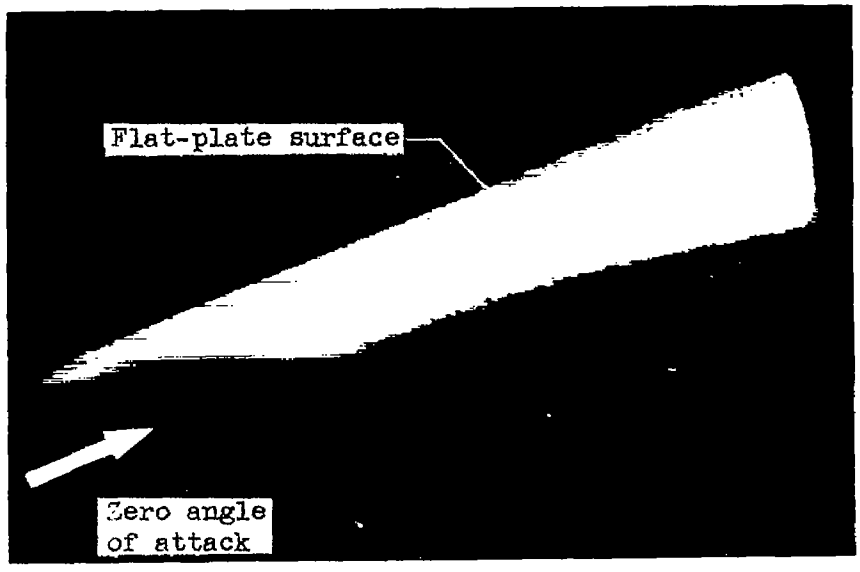

Frame 1

Frame 2

(a) Selected direct high-speed motion-picture frames. Stage II, frames 1 to 4; stage III, frames 5 to 10.

Figure 15. - Main (stage II) and end (stage III) stages of combustion in stream adjacent to flat-plate model. (Run 18, table II.)

Frame 3

Frame 4

(a) Continued. Selected direct high-speed motion-picture frames. Stage II, frames 1 to 4; stage III, frames 5 to 10.

Figure 15. - Continued. Main (stage II) and end (stage III) stages of combustion in stream adjacent to flat-plate model. (Run 18, table II.)

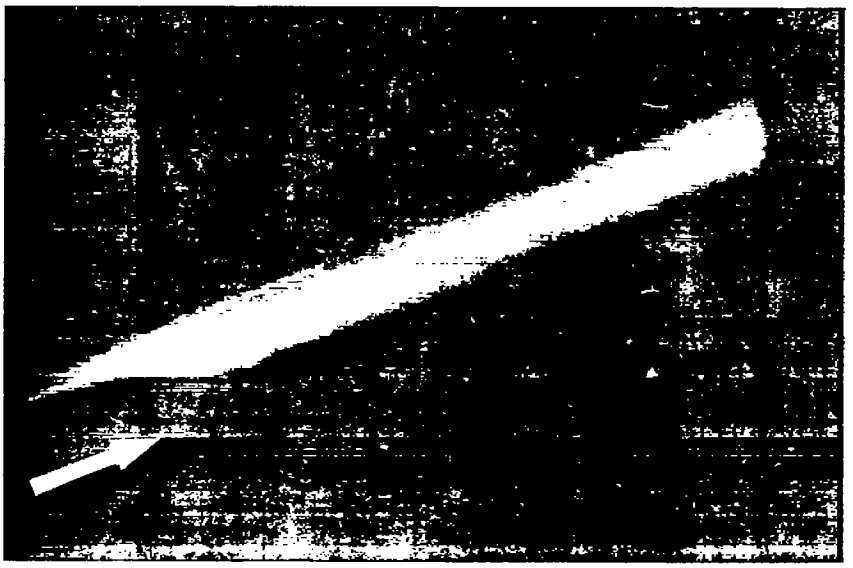

Frame 5

Frame 6

(a) Continued. Selected direct high-speed motion-picture frames. Stage II, frames 1 to 4; stage III, frames 5 to 10.

Figure 15. - Continued. Main (stage II) and end (stage III) stages of combustion in stream adjacent to flat-plate model. (Run 18, table II.)

Frame 7

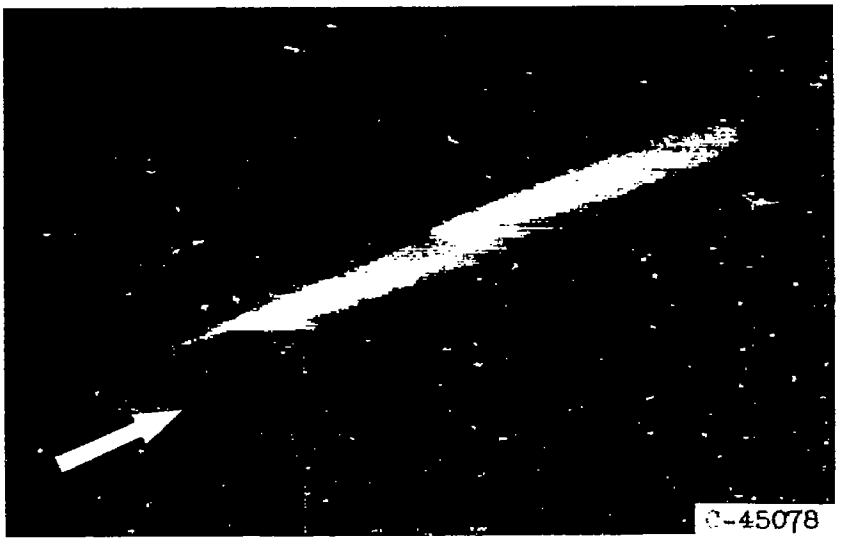

Frame 8

(a) Continued. Selected direct high-speed motion-picture frames. Stage II, frames 1 to 4; stage III, frames 5 to 10.

Figure 15. - Continued. Main (stage II) and end (stage III) stages of combustion in stream adjacent to flat-plate model. (Run 18, table II.)

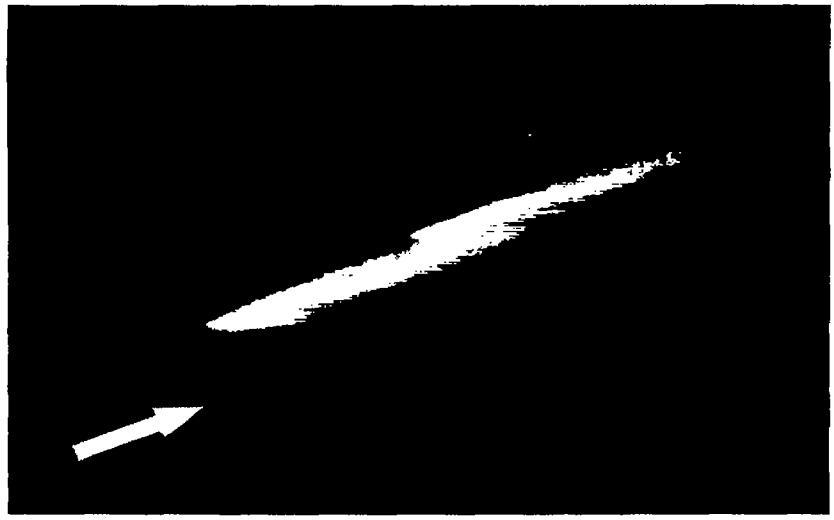

Frame 9

Frame 10

(a) Concluded. Selected direct high-speed motion-picture frames. Stage II, frames 1 to 4; stage III, frames 5 to 10.

Figure 15. - Continued. Main (stage II) and end (stage III) stages of combustion in stream adjacent to flat-plate model. (Run 18, table II.)

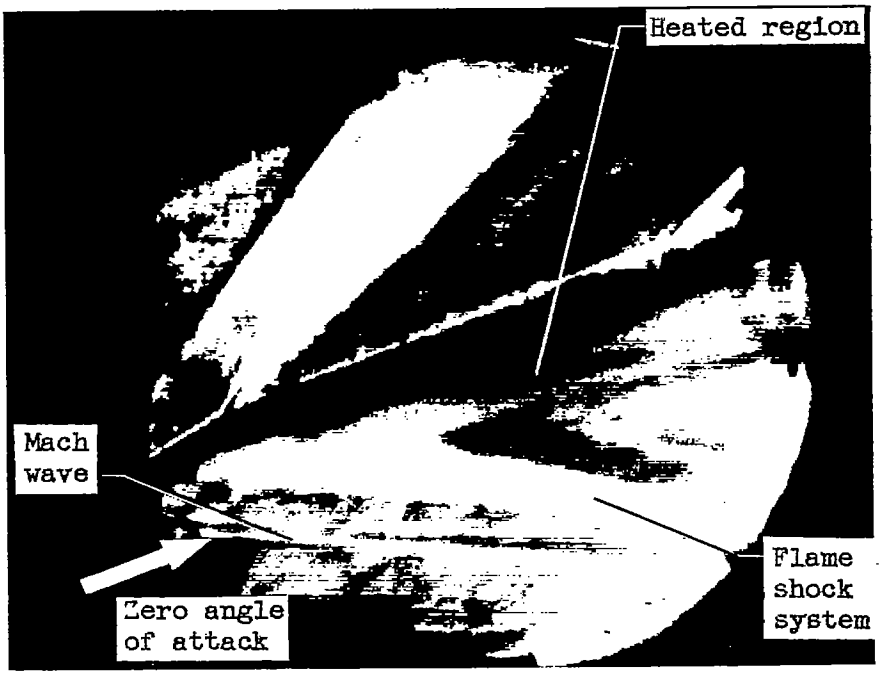

Frame 1

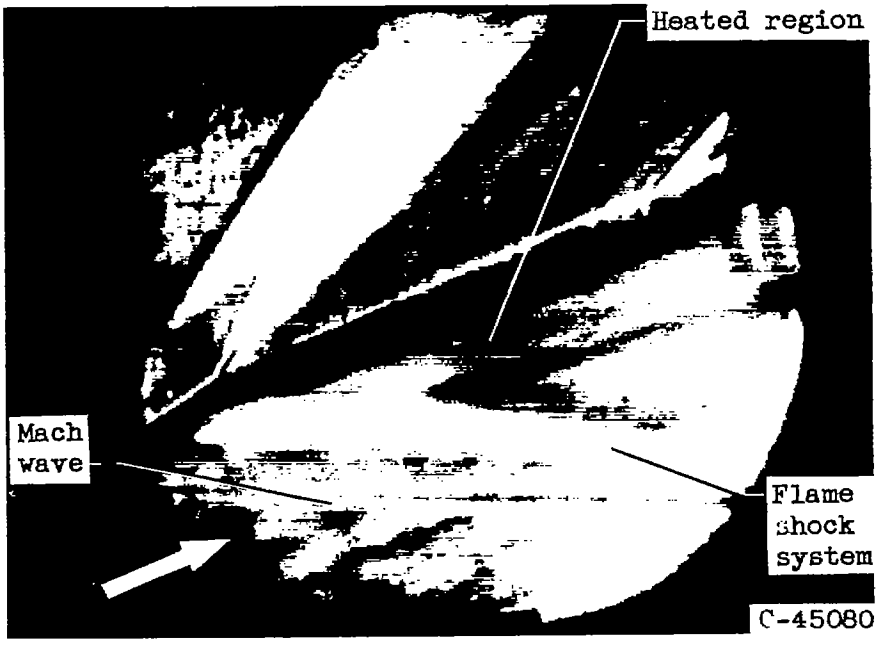

Frame 2

(b) Selected schlieren high-speed motion-picture frames. Stage II, frames 1 and 2; stage III, frames 3 to 8.

Figure 15. - Continued. Main (stage II) and end (stage III) stages of combustion in stream adjacent to flat-plate model. (Run 18, table II.)

Frame 3

Frame 4

(b) Continued. Selected schlieren high-speed motion-picture frames. Stage II, frames 1 and 2; stage III, frames 3 to 8.

Figure 15. - Continued. Main (stage II) and end (stage III) stages of combustion in stream adjacent to flat-plate model. (Run 18, table II.)

Frame 5

Frame 6

(b) Continued. Selected schlieren high-speed motion-picture frames. Stage II, frames 1 and 2; stage III, frames 3 to 8.

Figure 15. - Continued. Main (stage II) and end (stage III) stages of combustion in stream adjacent to flat-plate model. (Run 18, table II.)

Frame 7

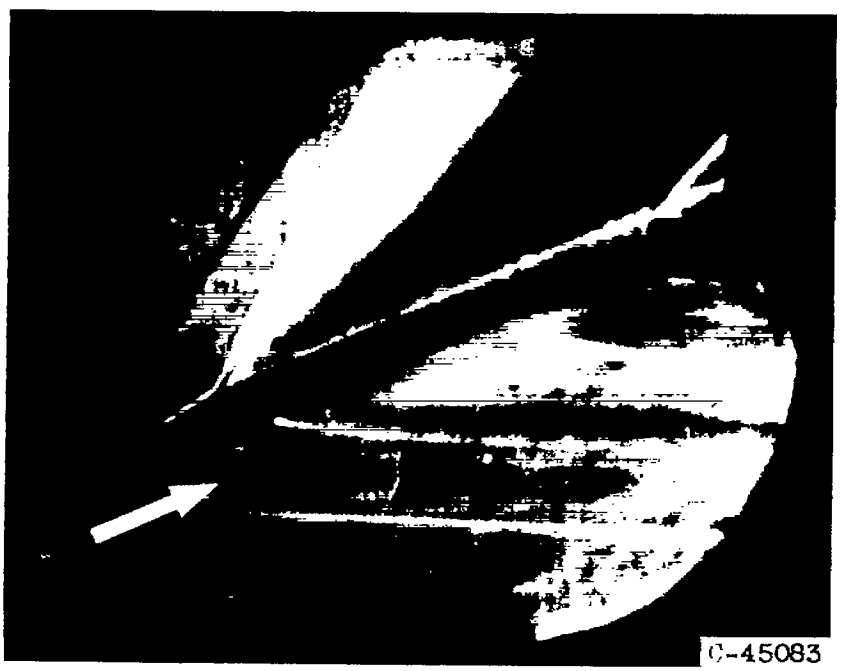

Frame 8

(b) Concluded. Selected schlieren high-speed motion-picture frames. Stage II, frames 1 and 2; stage III, frames 3 to 8.

Figure 15. - Concluded. Main (stage II) and end (stage III) stages of combustion in stream adjacent to flat-plate model. (Run 18, table II.)

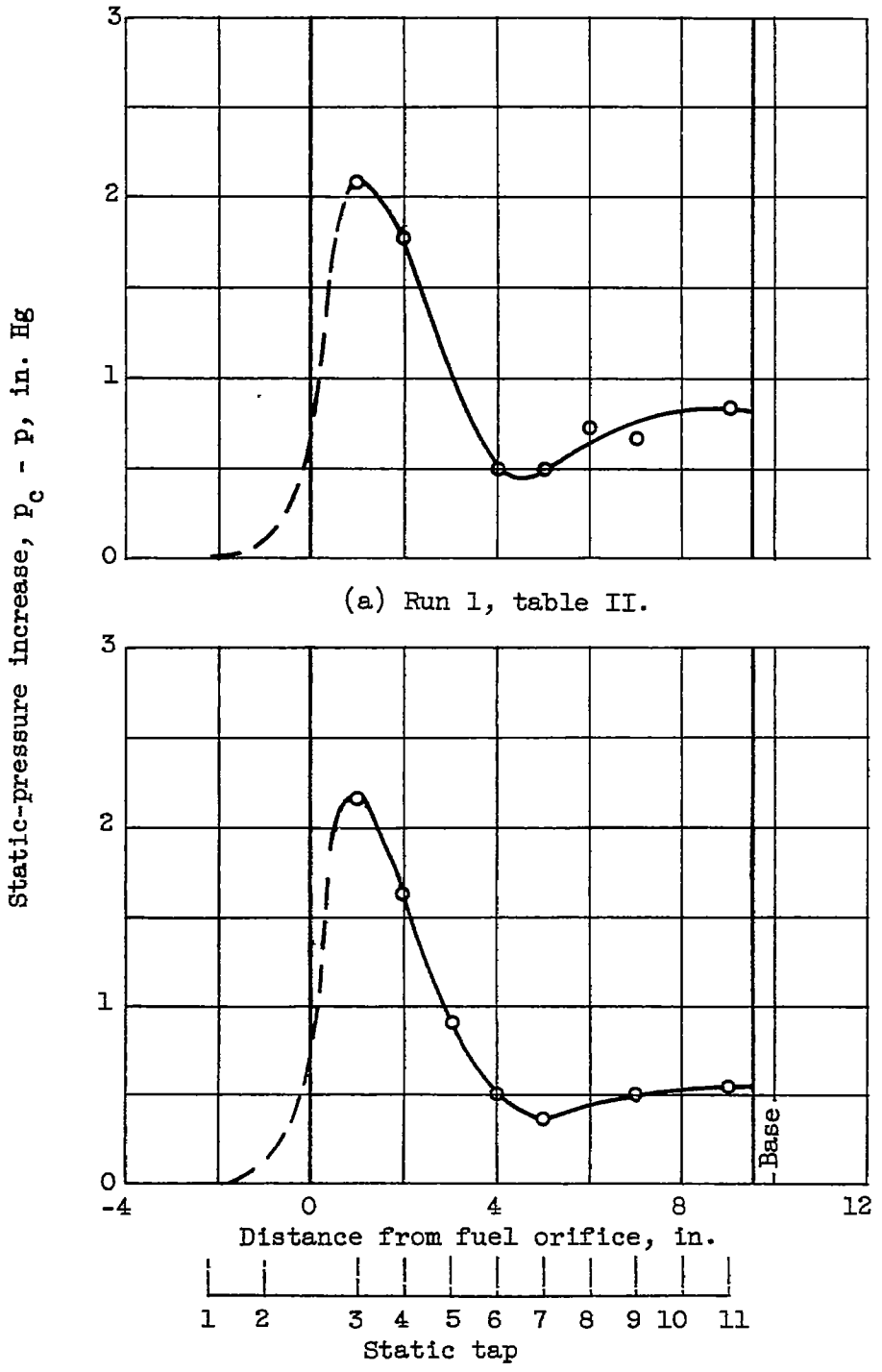

(a) Run 1, table II.

(b) Run 5, table II.

Figure 16. - Chordwise distribution of static-pressure increase on short-flat-plate surface due to combustion.

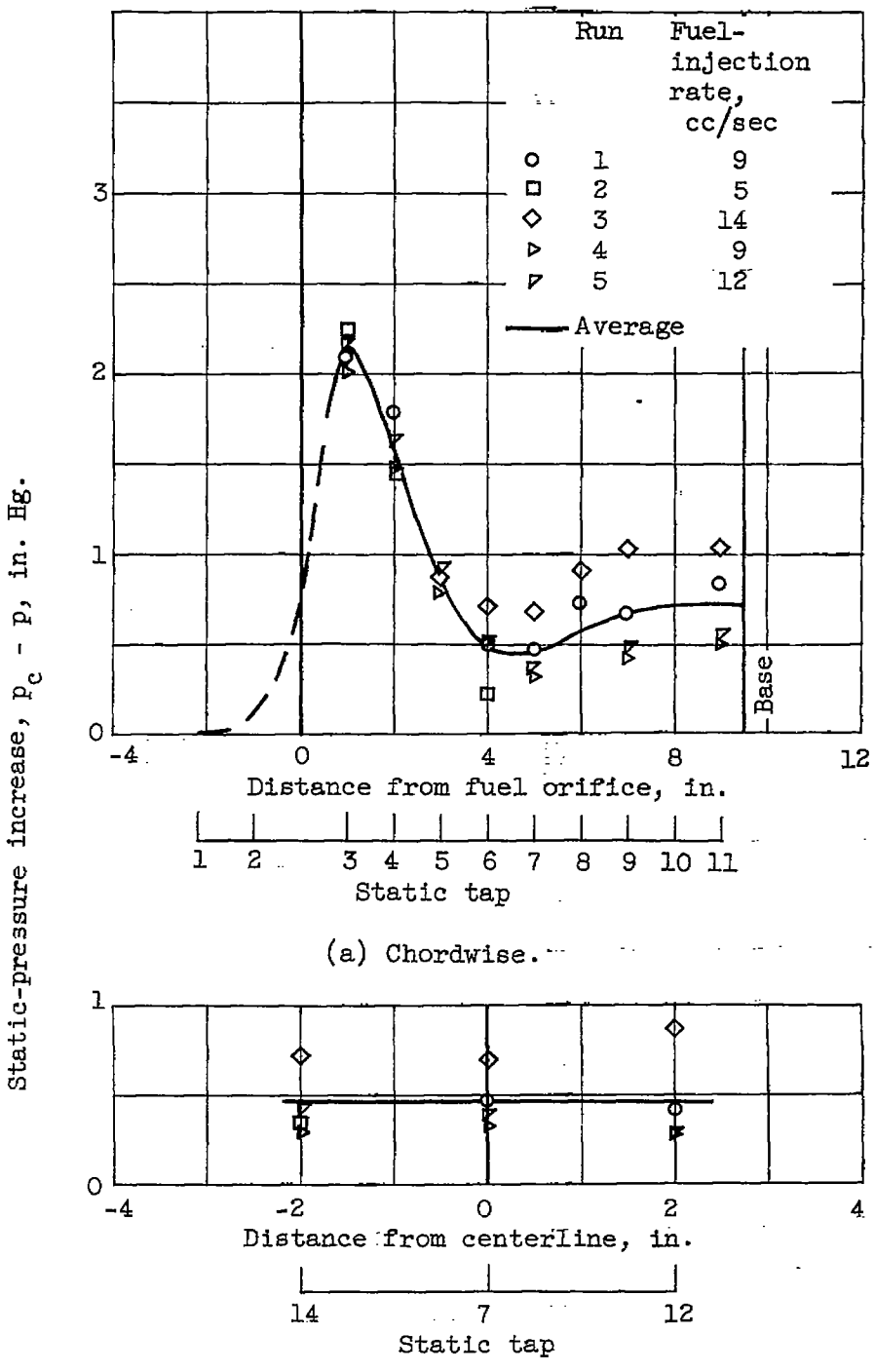

(a) Chordwise.

(b) Spanwise (station A).

Figure 17. - Static-pressure increases due to combustion on short-flat-plate surface (runs 1 to 5, table II).

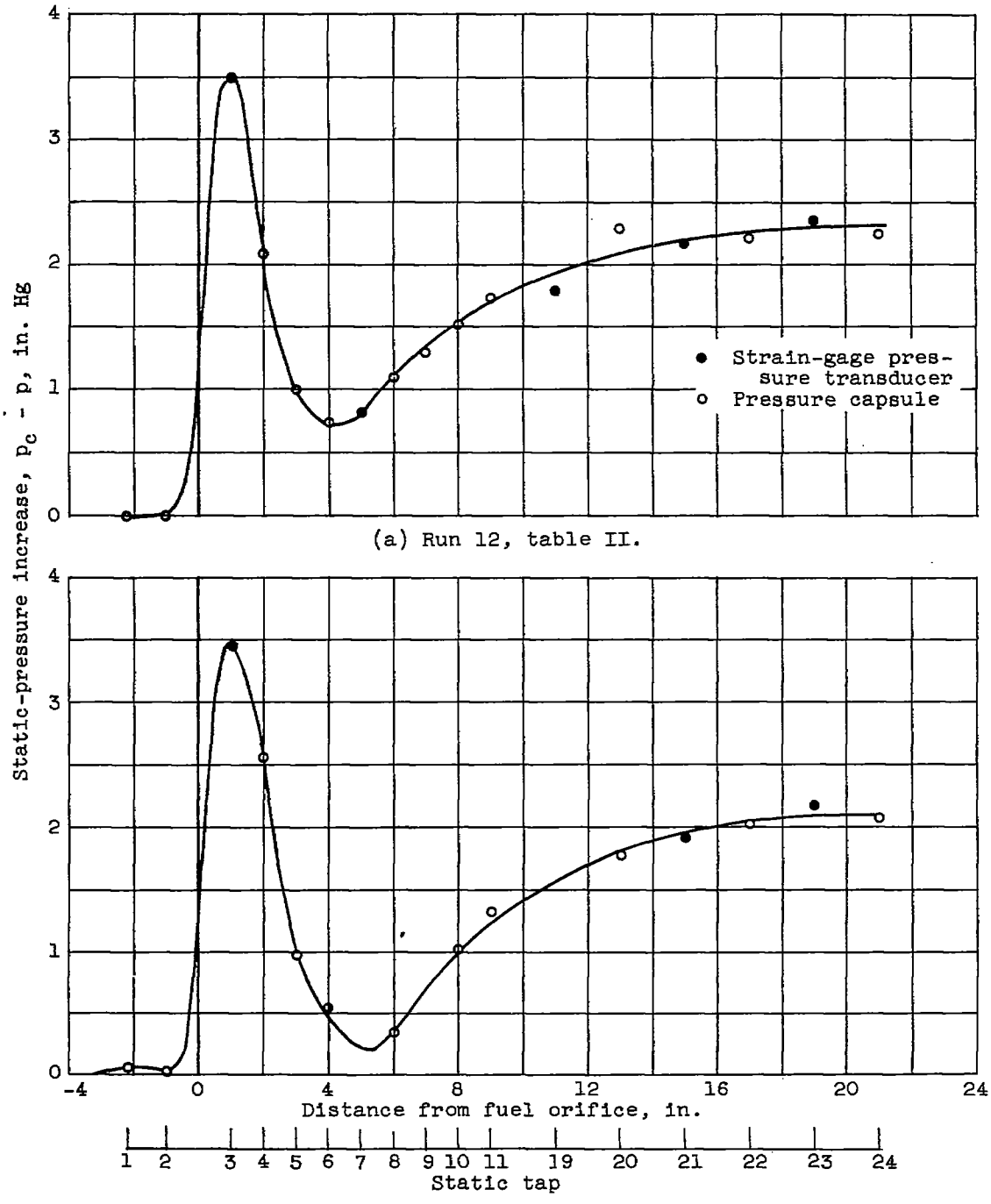

(a) Run 12, table II.

(b) Run 13, table II.

Figure 18. - Static-pressure increases due to combustion on extended-flat-plate surface.

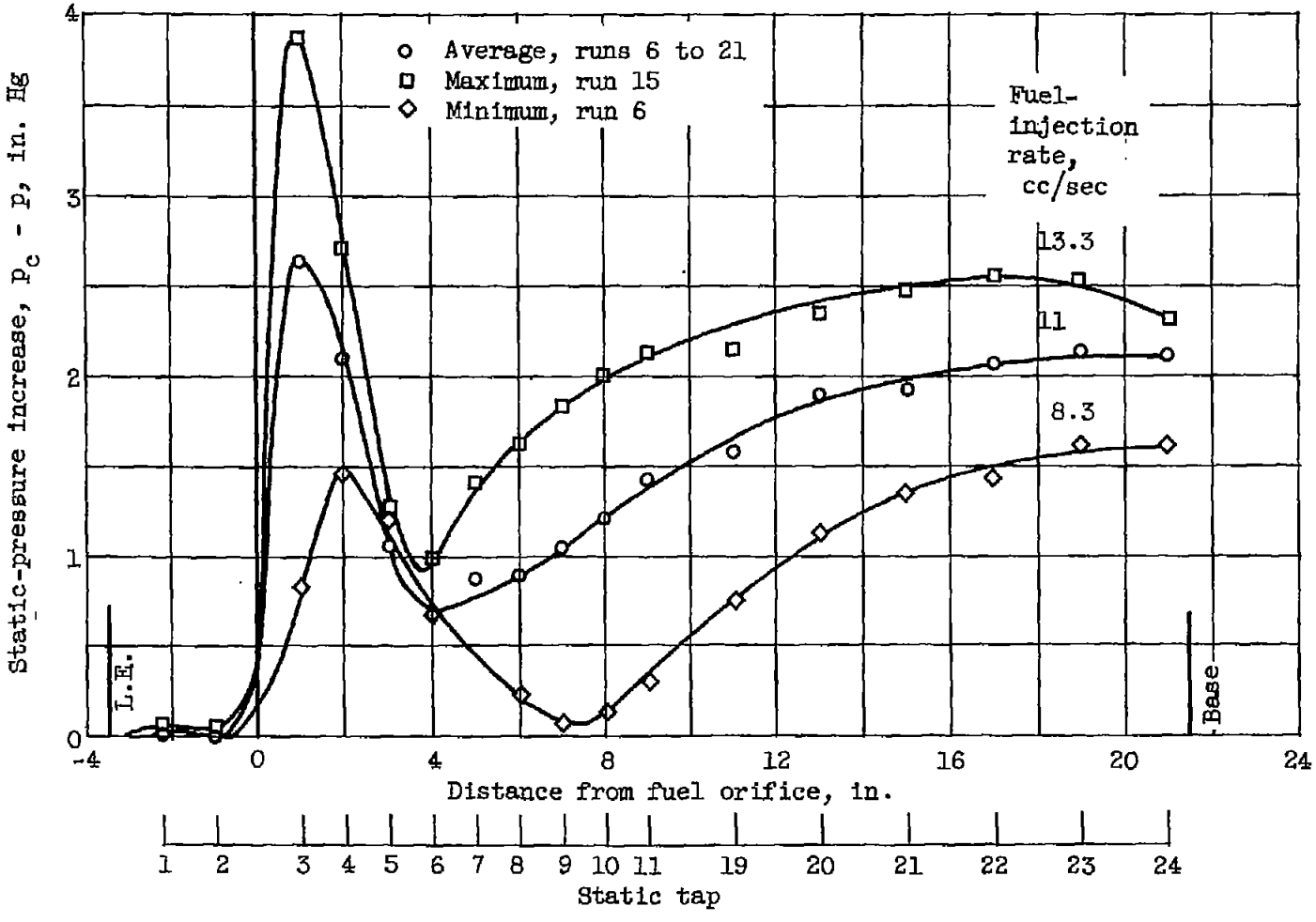

Figure 19. - Average, maximum, and minimum chordwise static-pressure increases due to combustion (table II).

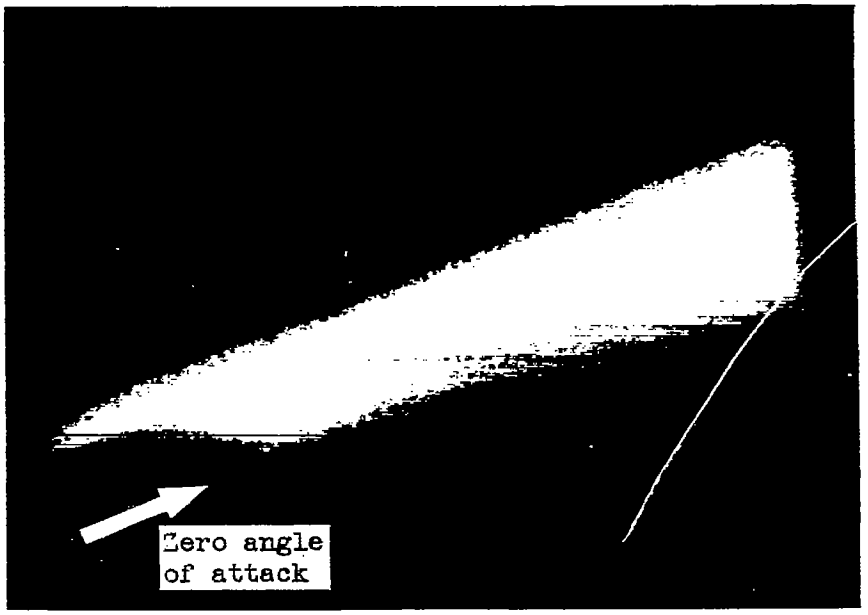

Frame 1

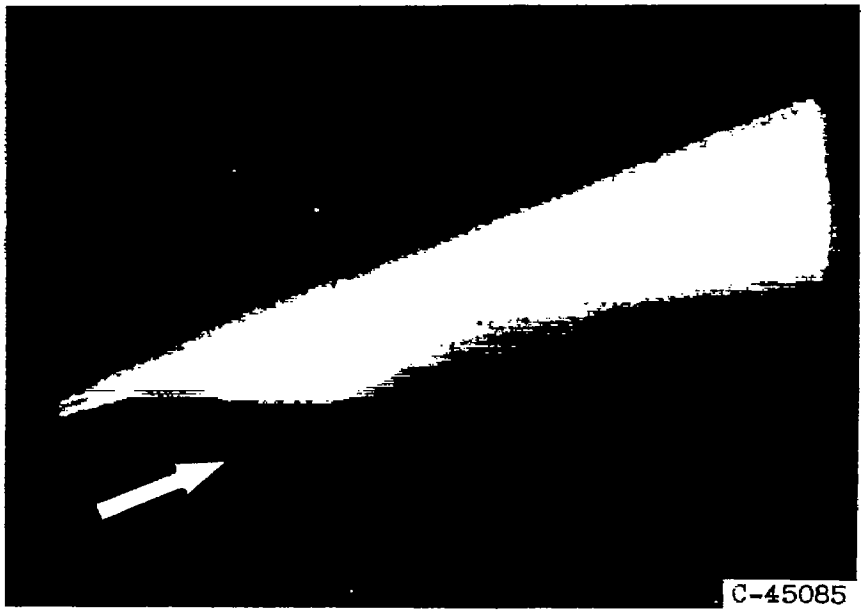

Frame 2

(a) Direct.

Figure 20. - Direct and schlieren photographs from maximum-pressure-increase run (run 15, table II).

Frame 1

Frame 2

(b) Schlieren.

Figure 20. - Concluded. Direct and schlieren photographs from maximum-pressure-increase run (run 15, table II).

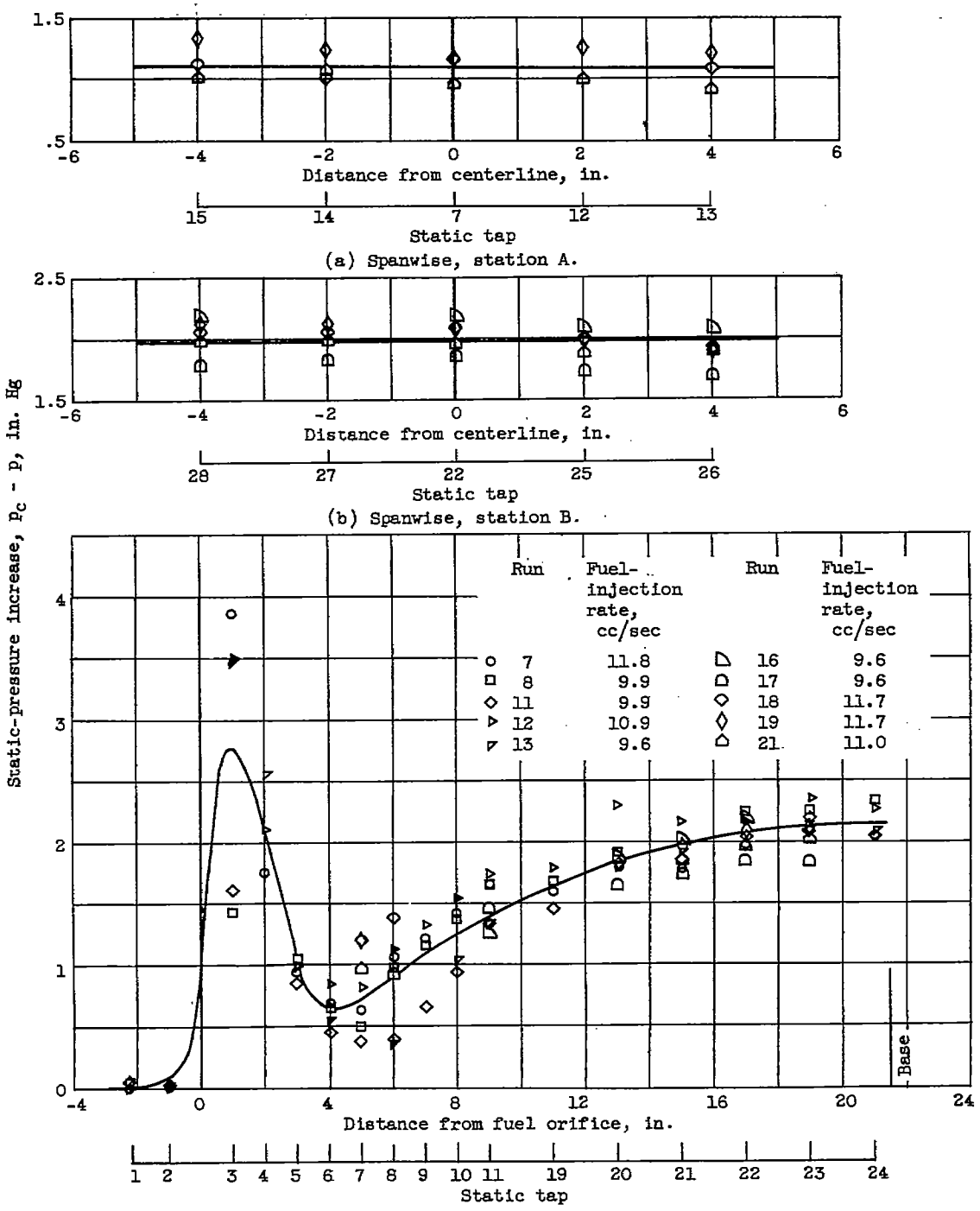

Figure 21. - Static-pressure increases due to combustion measured during runs with fuel-flow rates between 9.6 and 11.8 cubic centimeters per second. Average pressure change for these runs is shown by faired curve.

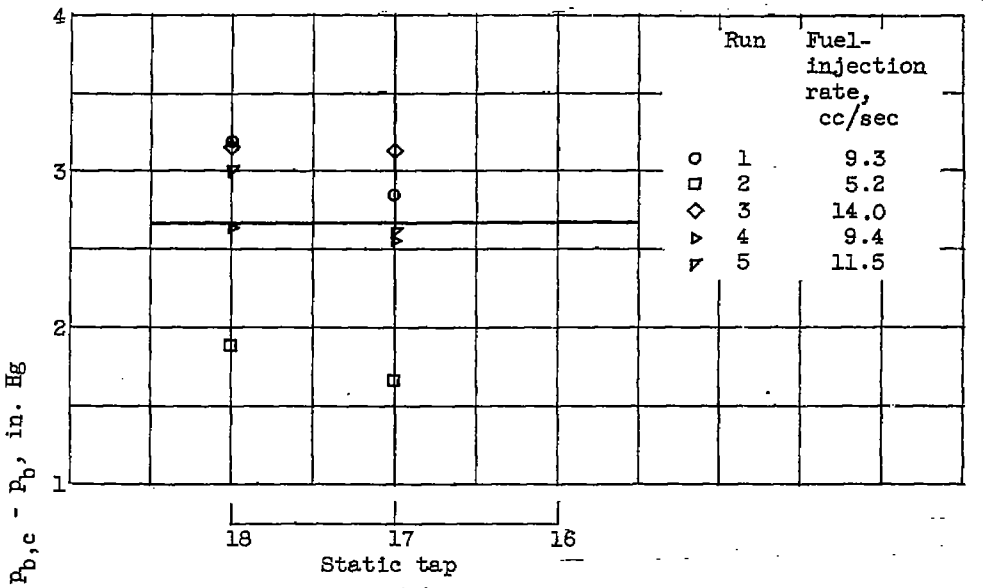

(a) Short flat plate.

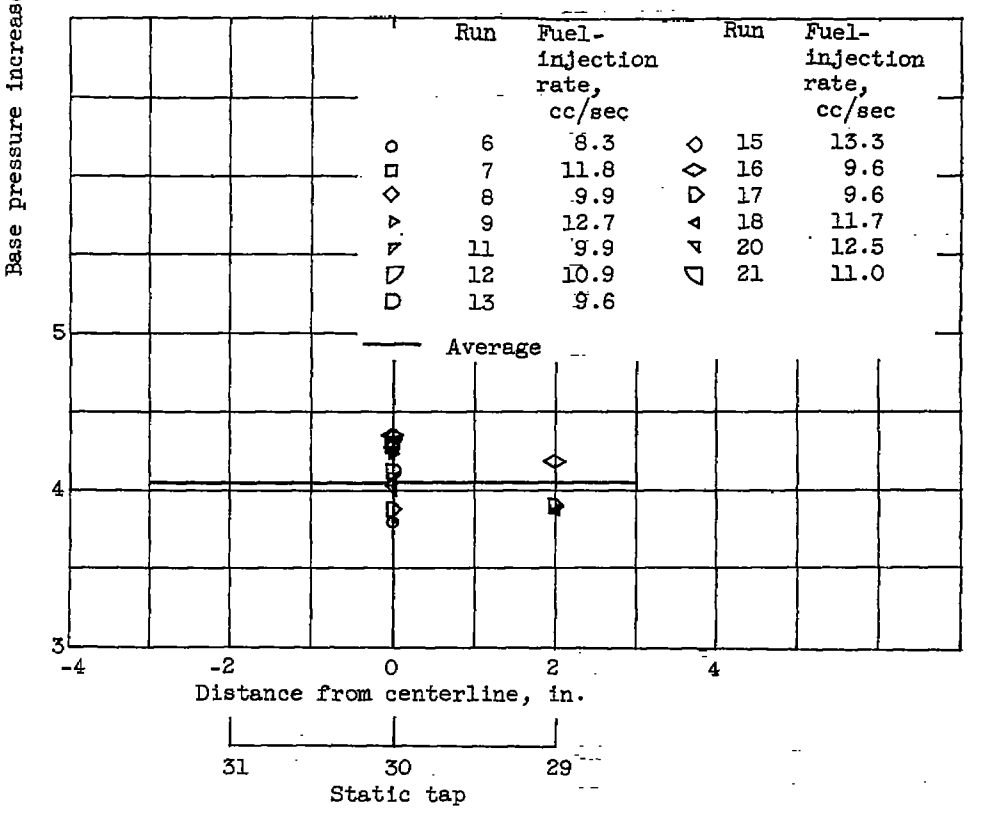

(b) Extended flat plate.

Figure 22. - Base pressure increases due to combustion.

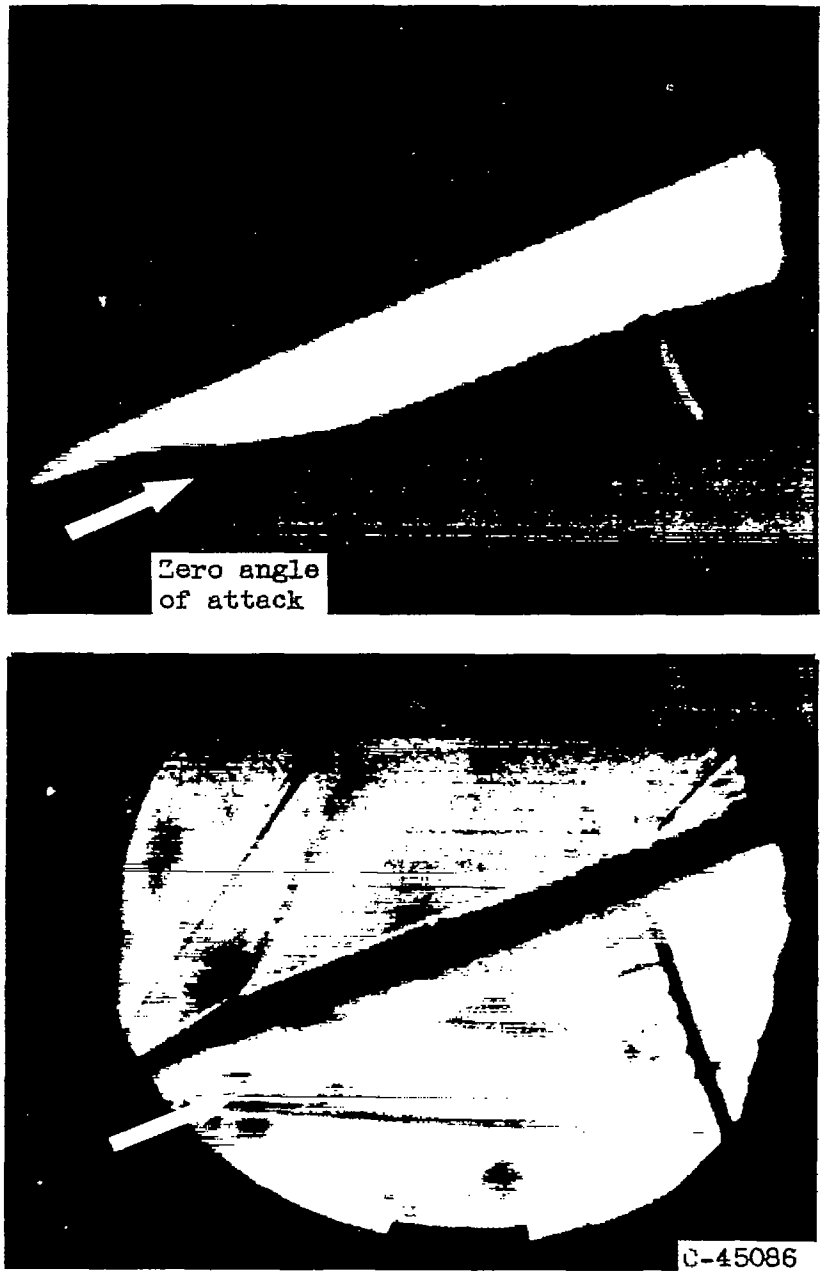

(a) Total-temperature rake.

Figure 23. - Selected frames from direct and schlieren high-speed motion pictures of stream probes at station I during combustion.

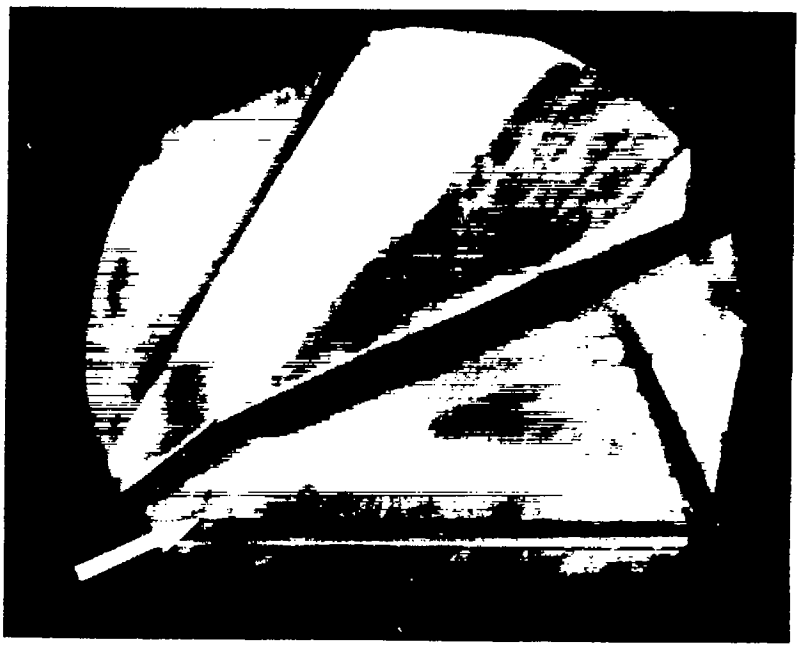

Frame 1

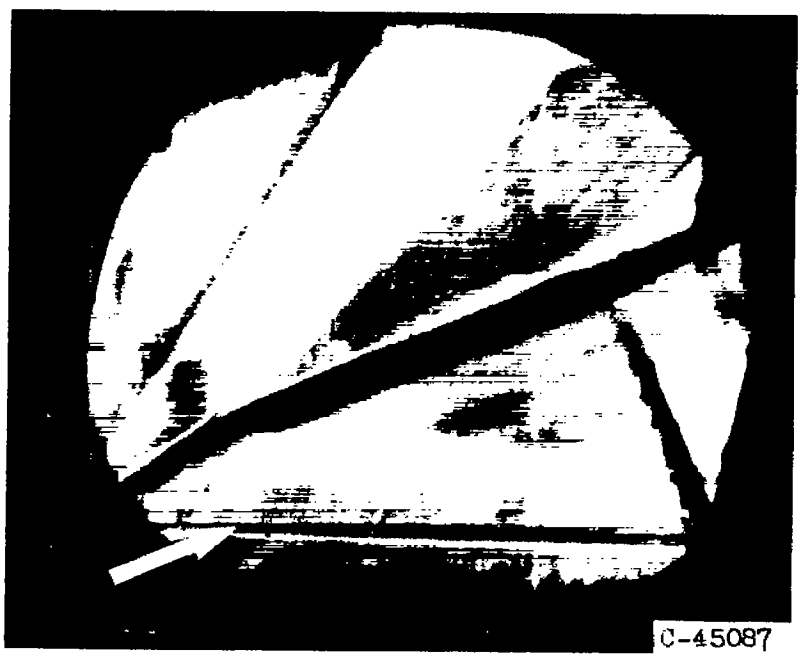

Frame 2

(b) Total-pressure rake.

Figure 23. - Concluded. Selected frames from direct and schlieren high-speed motion pictures of stream probes at station I during combustion.

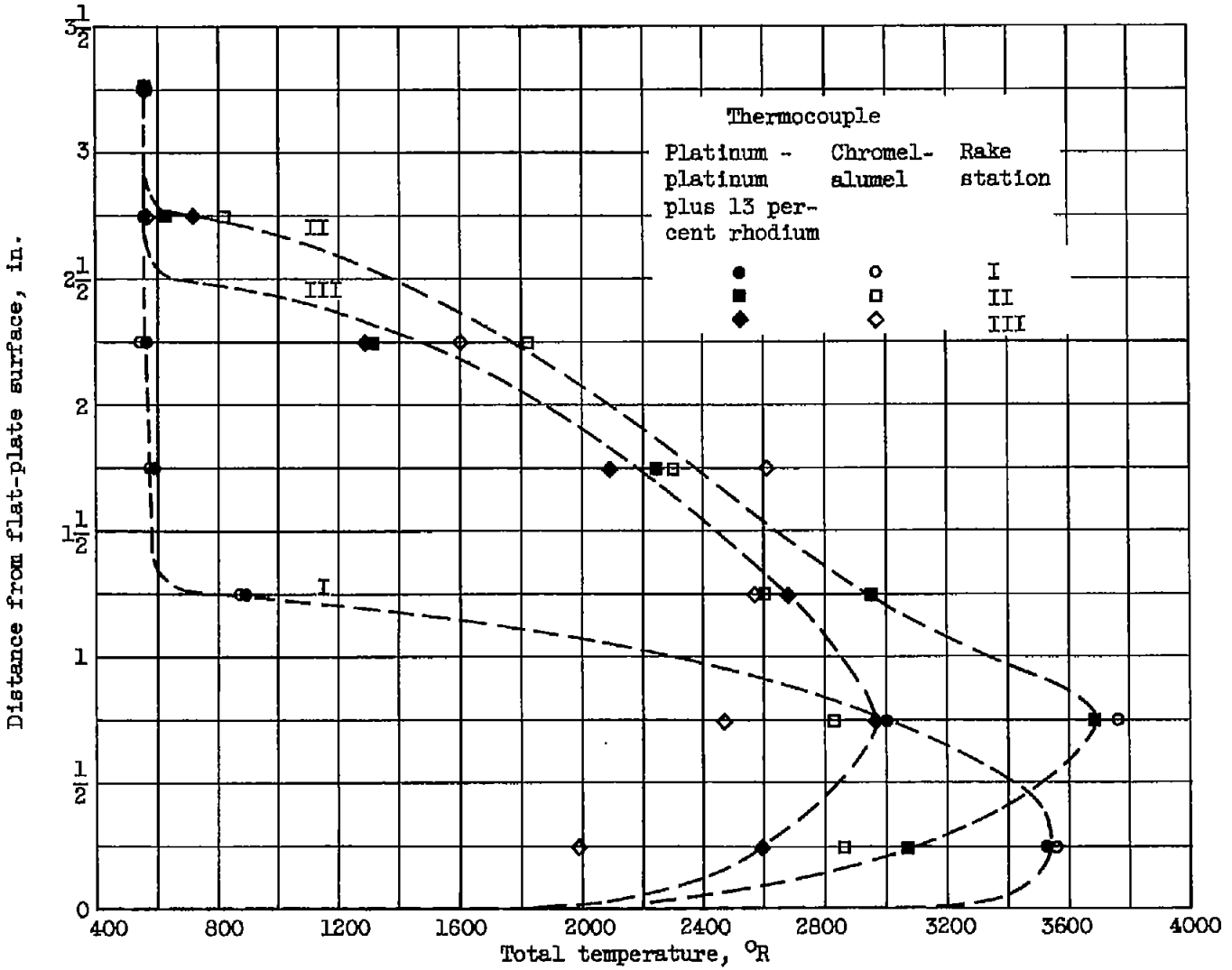

Figure 24. - Average total temperatures during combustion at three rake stations in stream adjacent to flat-plate surface.

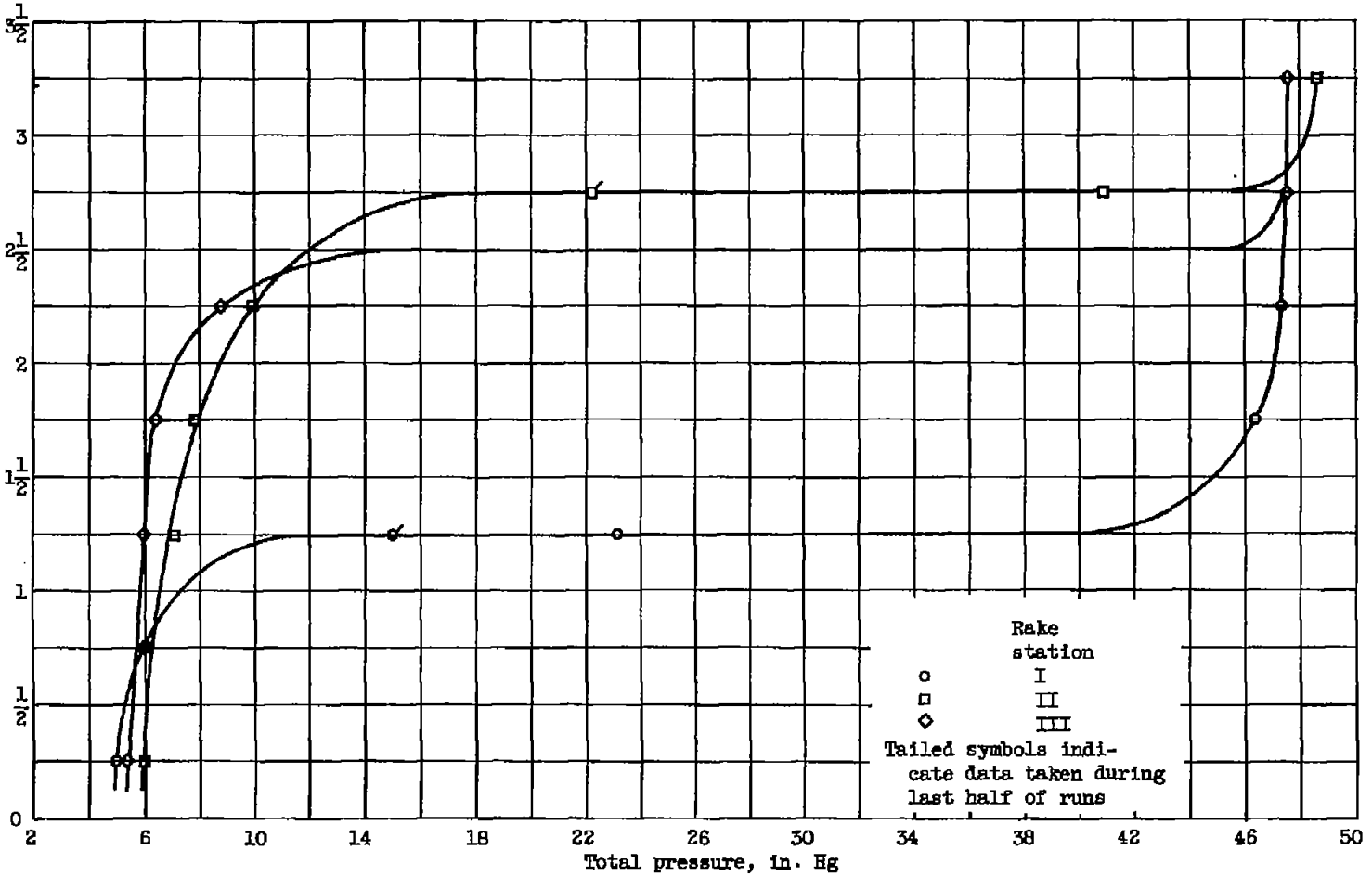

Figure 25. - Average total pressures during combustion at three rake stations in stream adjacent to flat-plate surface.

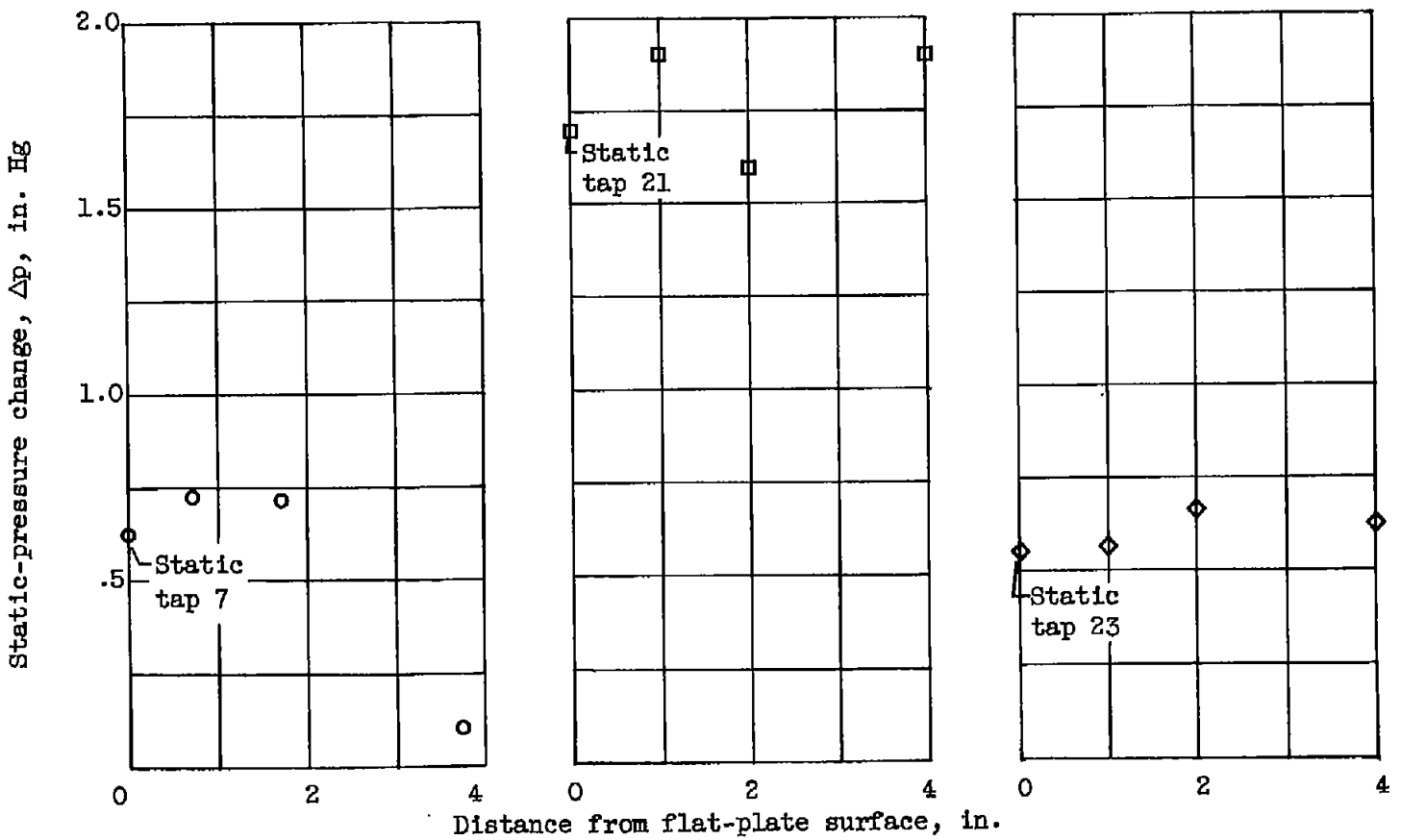

(a) Rake station I, run 48. (b) Rake station II, run 50. (c) Rake station III, run 49.

Figure 26. - Stream static-pressure changes due to combustion measured with static-pressure rake.

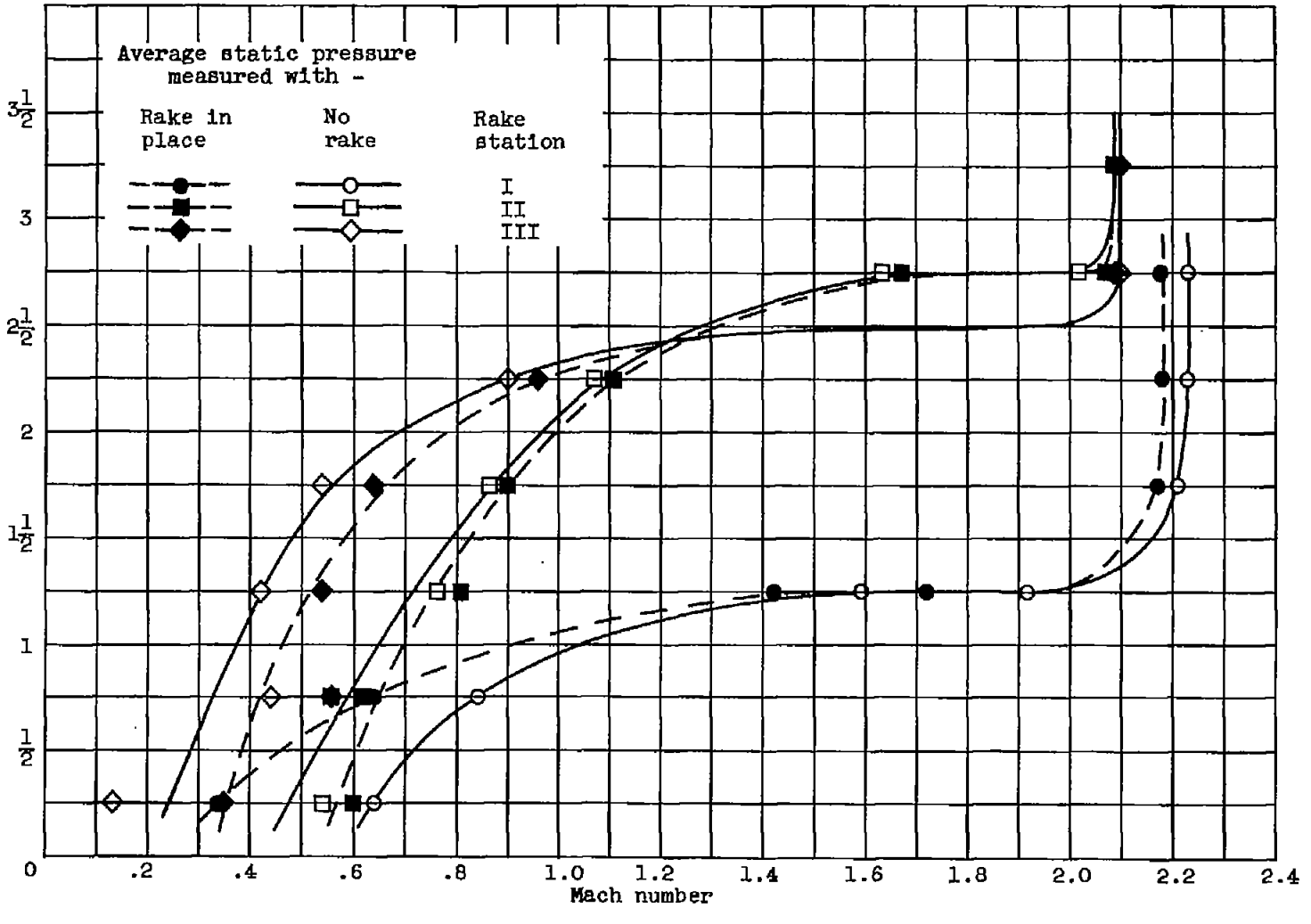

Figure 27. - Estimate of local Mach number in stream during combustion at stations I, II, and III as computed from stream data by simplified calculations.

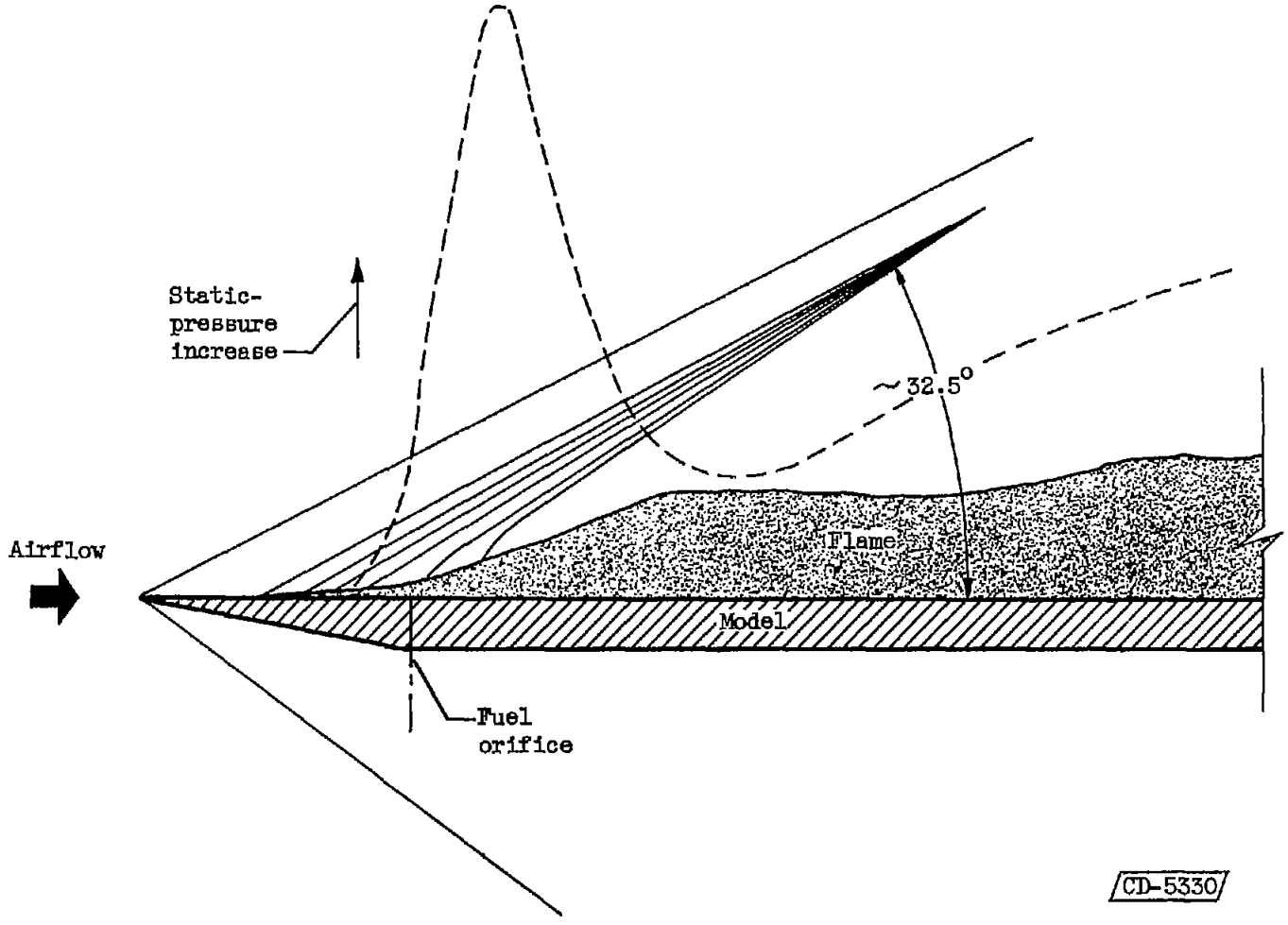

Figure 28. - Two-dimensional sketch (for centerline plane perpendicular to model flat-plate surface) of typical flame shape and associated shock waves adjacent to upstream portion of extended flat plate. Typical chordwise-pressure-increase pattern in this area is superimposed for comparison.

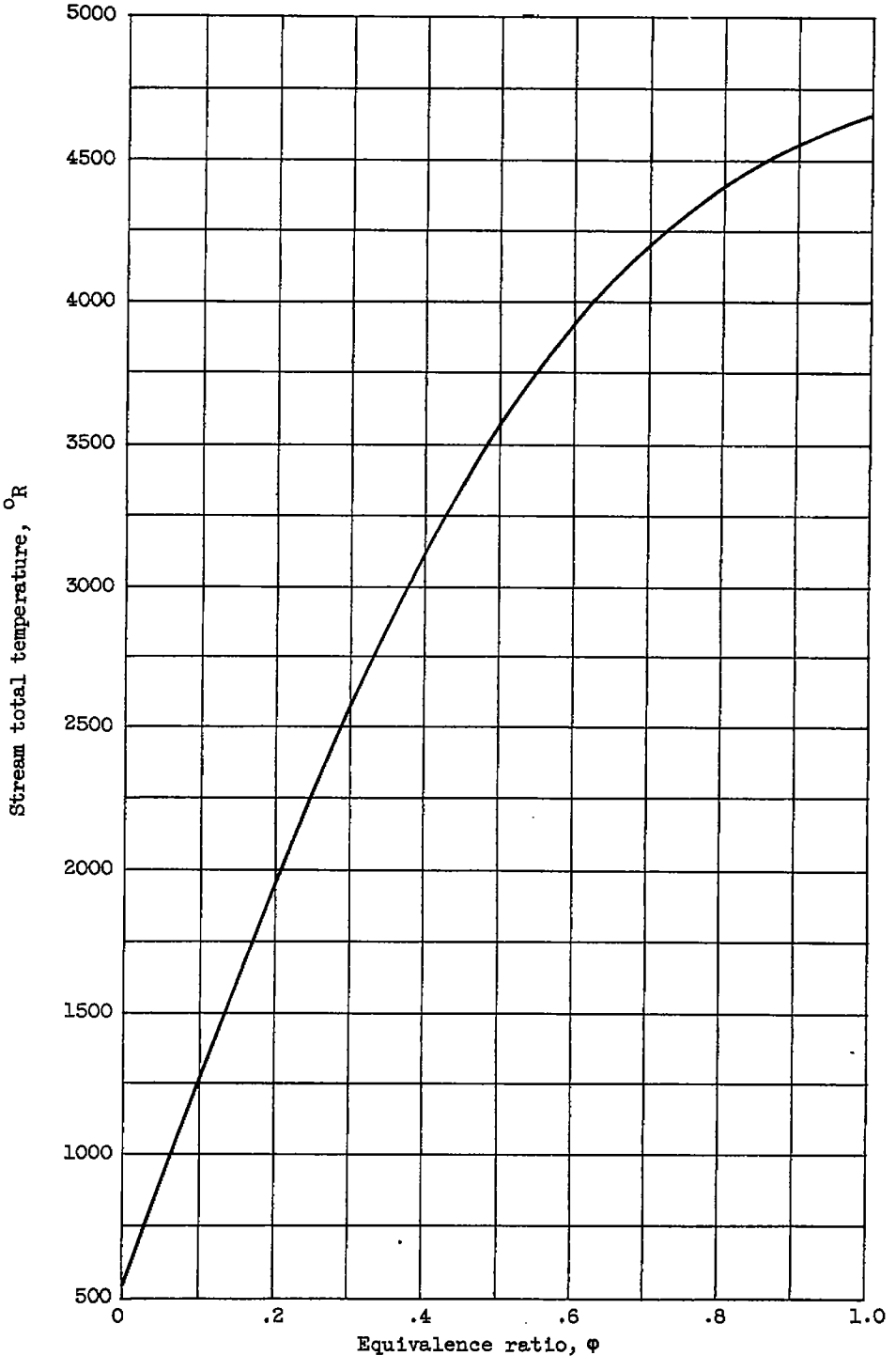

Figure 29. - Calculated (appendix D) stream total temperature assuming complete combustion as function of fuel-air equivalence ratio.

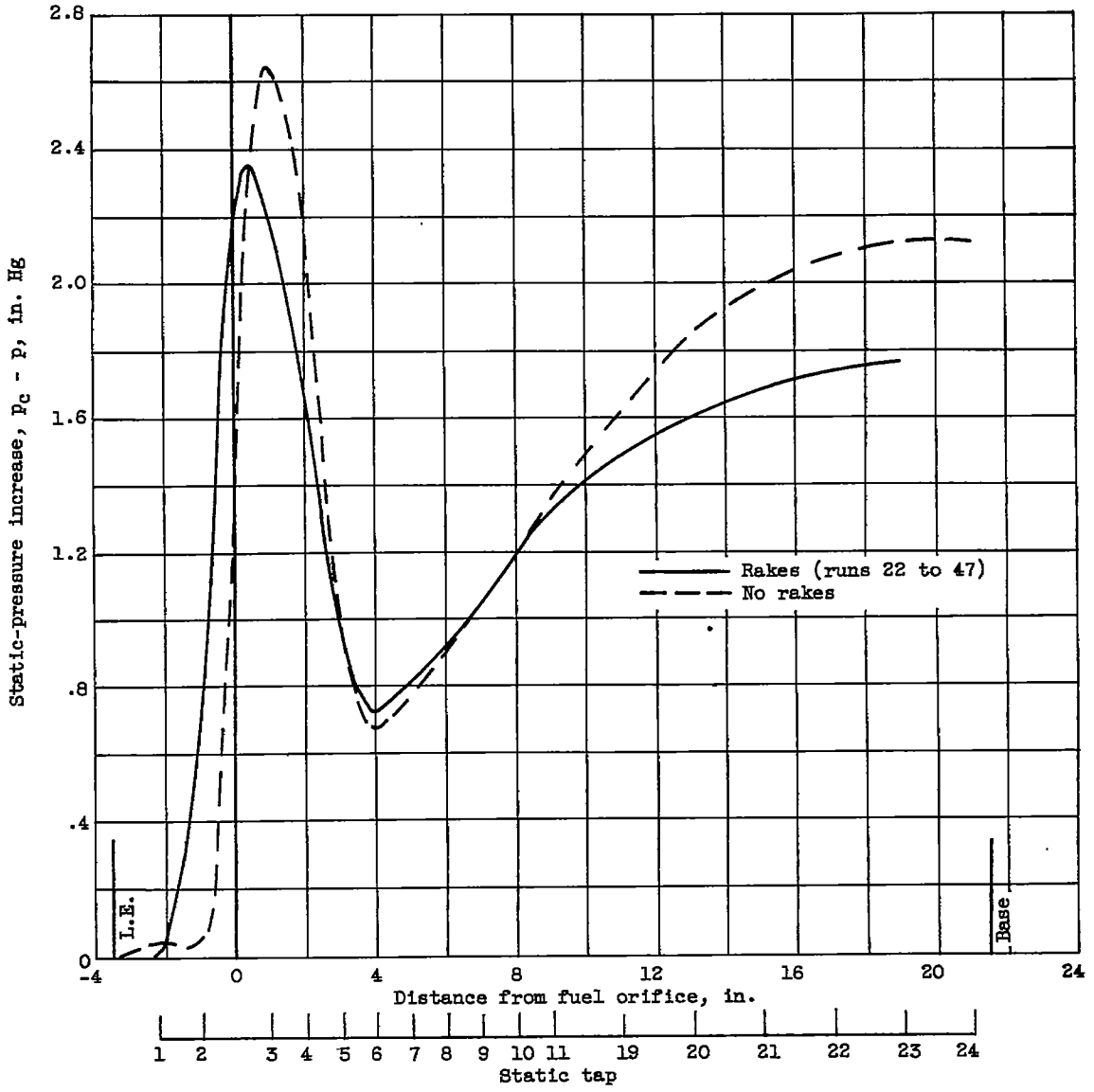

Figure 30. - Comparison of average of all static-pressure increases due to combustion measured with rakes in stream with average with no rakes.

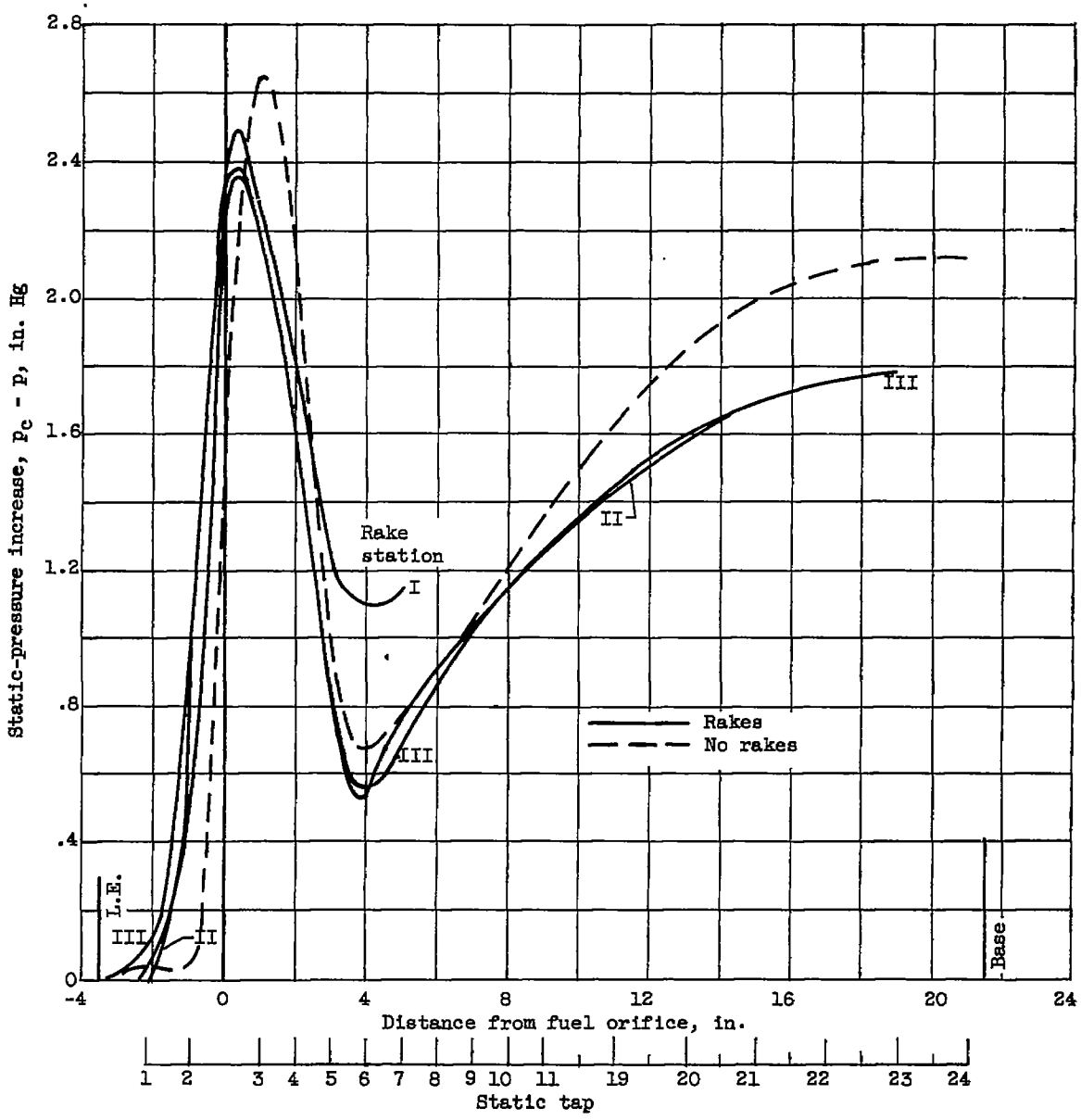

Figure 31. - Comparison of average of all static-pressure increases due to combustion measured upstream of all rakes at stations I, II, and III with average with no rakes.

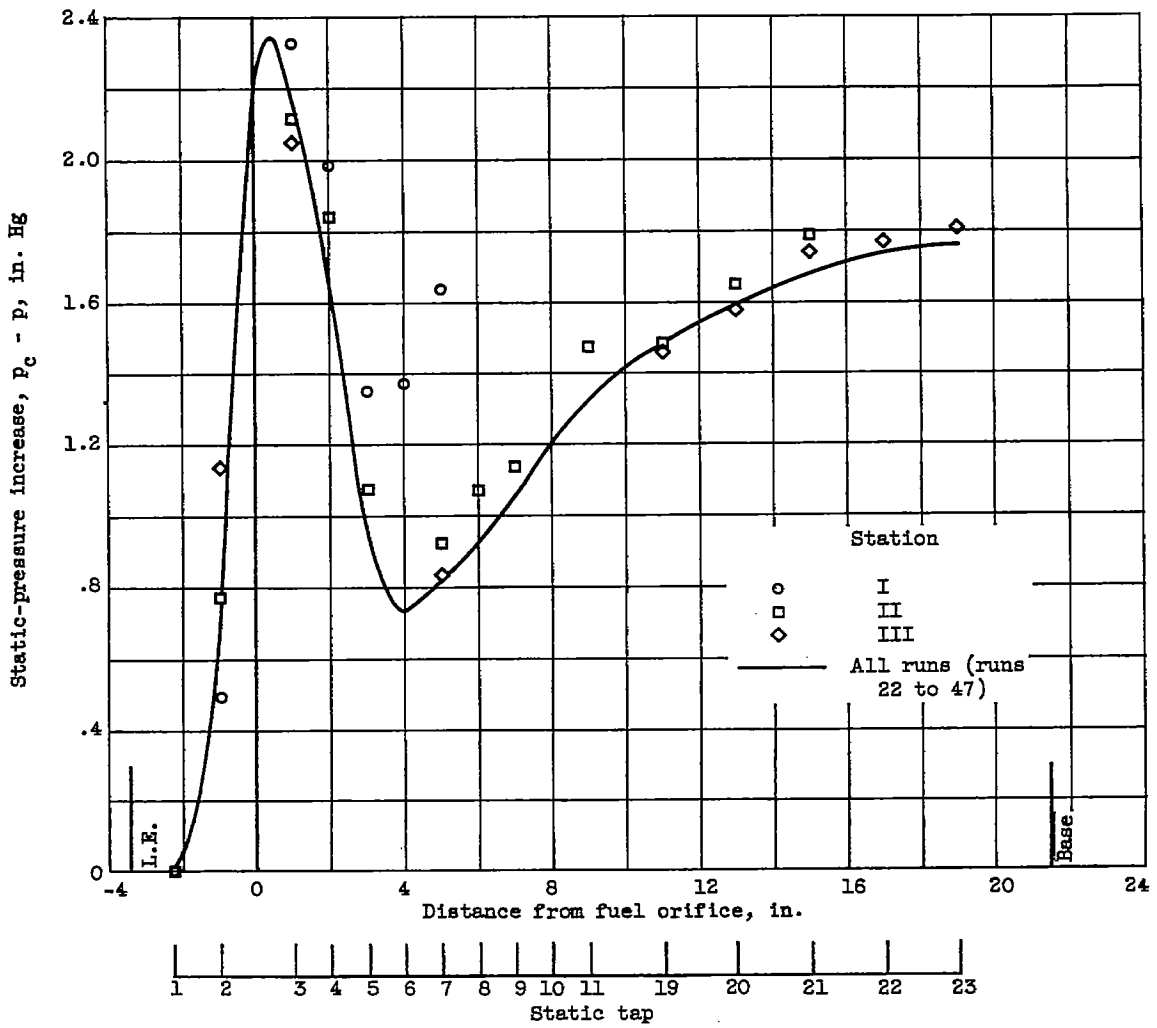

Figure 32. - Comparison of average of all static-pressure increases due to combustion measured upstream of total-pressure rakes at stations I, II, and III with average for all runs with rakes in stream.

NACA - Langley Field, Va.